



PONTIFICIA UNIVERSIDAD CATÓLICA DE CHILE
FACULTAD DE FÍSICA
INSTITUTO DE FÍSICA

Geometrical Approach for Quantum Control: The Qubit Case

BY

MAURO JAVIER MENDIZÁBAL PICO

Tesis presentada a la Facultad de Física de la Pontificia Universidad Católica de Chile,
para optar al grado académico de Magíster en Física.

SUPERVISORS : Dr. Guiseppe De Nittis. Pontificia Universidad Católica de Chile
: Dr. Dominique Spehner. Universidad de Concepción

CORRECTOR : Dr. Jerónimo Maze

May, 2021

Santiago, Chile

©2021, Mauro Mendizábal

Declaration

The work described in this thesis was undertaken between 2019 and 2020 while the author was a researcher master student under the supervision of Professor Guiseppe De Nitts and Professor Dominique Spehner, in the Institute of Physics at the Pontificia Universidad Católica de Chile. This work has not been submitted for any other degree at the Pontificia Universidad Católica de Chile or any other university.

©2021, Mauro Mendizábal

Se autoriza la reproducción total o parcial, con fines académicos, por cualquier medio o procedimiento, incluyendo la cita bibliográfica del documento.

To my parents, my family, my Chilean family, my love, friends ...

To Rammstein, Bella Ciao, J. Peterson and The Avengers ...

Not to COVID.

L'homme c'est rien — l'oeuvre c'est tout.

Acknowledgements

I am grateful to my research group: my tutors. Thanks to Prof. De Nittis for your time, support and for your assistant in this quest. In addition, for introducing me to the topic of Quantum Information and its geometry. This has evolved in me a great interest in the Quantum Computing revolution. To Prof. Spehner, thank you, for this amazing topic and your assistant, too. As a group, we always get further! This work could be a small contribution for the science community but for me, it was a life change.

A special thanks to my parents who supports me and are always giving me their best vibes.

Thanks to my Chilean family: Anita, Dani and Cami. It was not my home but it felt like I was part of the family.

In this whole process, I met Joha who not only is a wonderful woman but also a strong personality.

Thanks to my friends. You will be in my hearth, specially the Chilean ones.

Thanks to Secretaría Nacional de Educación Superior, Ciencia, Tecnología e Innovación, SENESCYT and its "Programa de Becas Internacionales posgrado 2018".

Contents

1	Introduction	9
1.1	How to control a two level quantum system, the qubit	11
1.2	Steering an state: the most common methods so far	15
1.3	GRAPE optimization	16
1.3.1	GRAPE algorithm	19
1.3.2	GRAPE in action	20
1.4	CRAB Algorithm	22
1.4.1	CRAB in action	23
1.5	Krotov's method	23
1.5.1	Krotov in action	25
1.6	Geometry of Quantum states	26
1.6.1	States viewing from Physics and Maths	26
1.6.2	The Bures metric	29
1.6.3	The Bures tensor metric	32
1.6.4	Geodesic of the density matrices set	35
2	Methodology	36
2.1	Model	38
2.1.1	The objective function $\cos \alpha$ and its maximum	43
2.1.2	State to state transfer: pure states procedure	49
2.1.3	State to state transfer for mixed states	50

2.1.4	State to state transfer: mixed states procedure	53
2.2	Using a most general Hamiltonian	53
3	Results and discussion	57
3.1	Experiments for pure states	57
3.2	Experiments for pure states with a general Hamiltonian	63
3.3	Experiments with mixed states	68
3.4	Improvements	69
3.5	Analysis and comparison with other models	76
3.6	Future activities	80
4	Conclusions	82
Bibliography		85
A	Mathematical aid	86
A.1	Singular Value Decomposition <i>SVD</i>	86
A.2	Polar decomposition	87
B	Physical aid	89
B.1	Index and relative states	89
B.2	Where does the geodesic of Quantum states come from ?	90

List of Tables

List of Figures

1.1	Control amplitude of GRAPE algorithm	17
1.2	Transition from $ 0\rangle$ to $ x_+\rangle$ using GRAPE	21
1.3	Transition from $ \psi\rangle = \cos(\pi/8) 0\rangle + \sin(\pi/8) 1\rangle$ to $ y_+\rangle$ using GRAPE Python package	22
1.4	Transition from $ 0\rangle$ to $ y_+\rangle$ using CRAB method in Python package	23
1.5	Transition from $ \psi\rangle = \cos(\pi/8) 0\rangle + \sin(\pi/8) 1\rangle$ to $ y_-\rangle$ using Krotov Python package	26
1.6	Transition from $ \psi\rangle = \cos(\pi/8) 0\rangle + \sin(\pi/8) 1\rangle$ to $ x_-\rangle$ using Krotov Python package	27
1.7	Mixture representation of a tangent vector	33
2.1	Schematic representation of our methodology on the Bloch sphere	37
3.1	Transition from $ \psi_1\rangle = \cos \frac{\pi}{8} 0\rangle + \sin \frac{\pi}{8} 1\rangle$ to $= x_+\rangle$	59
3.2	Transition from $ \psi_1\rangle = \cos \frac{\pi}{8} 0\rangle + \sin \frac{\pi}{8} 1\rangle$ to $ y_+\rangle$	60
3.3	Transition from $ y_+\rangle$ to $ \phi_2\rangle = \cos \frac{\pi}{8} 0\rangle + \sin \frac{\pi}{8} 1\rangle$	61
3.4	Transition from $ \psi_1\rangle = \cos \frac{\pi}{8} 0\rangle + \sin \frac{\pi}{8} 1\rangle$ to $ y_-\rangle$	62
3.5	Transition from: $ \psi_1\rangle = 0\rangle$ to $ x_+\rangle$	63
3.6	Transition with a clockwise rotation with small value of Δt	64
3.7	Transition from: $ \psi_1\rangle = \cos \frac{\pi}{8} 0\rangle + \sin \frac{\pi}{8} 1\rangle$ to $ x_+\rangle$ using the Hamiltonian with n_x and n_y constants.	65

3.8 Transition from: $ \psi_1\rangle = \cos \frac{\pi}{8} 0\rangle + \sin \frac{\pi}{8} 1\rangle$ to $ \phi_2\rangle = y_+\rangle$ using (2.3) with n_x, n_y constants	66
3.9 Transition from: $ \psi_1\rangle = \cos \frac{\pi}{8} 0\rangle + \sin \frac{\pi}{8} 1\rangle$ to $ \phi_2\rangle = y_-\rangle$ using (2.3) with n_x, n_y unknowns constants	66
3.10 Transition from: $ \psi_1\rangle = 0\rangle$ to $ \phi_2\rangle = x_+\rangle$ using 2.3 with n_x, n_y unknowns constants	67
3.11 Transition of two mixed states: experiment a	69
3.12 Transition of two mixed states: experiment b	70
3.13 Transition from: $ \psi_1\rangle = \cos \frac{\pi}{8} 0\rangle + \sin \frac{\pi}{8} 1\rangle$ to $ \phi_2\rangle = y_-\rangle$ using 2.3 with n_x, n_y unknowns constants and the hybrid algorithm	73
3.14 Transition from $ \psi_1\rangle = \cos \frac{\pi}{8} 0\rangle + \sin \frac{\pi}{8} 1\rangle$ to $ y_+\rangle$, using $n_z \neq 0$ in (2.3)	75
3.15 Transition from $ \psi_1\rangle = \cos \frac{\pi}{8} 0\rangle + \sin \frac{\pi}{8} 1\rangle$ to $ y_+\rangle$, using n_z and t_{op}	76
3.16 Transition from $ x_+\rangle$ to $ y_+\rangle$ and the opposite	77
3.17 Transition from $ \psi_1\rangle = 0\rangle$ to $ \phi_2\rangle = y_-\rangle$: half π pulse, using CRAB algorithm.	78
3.18 Transition from $ \psi_1\rangle = 0\rangle$ to $ \phi_2\rangle = y_-\rangle$; half π pulse: using GRAPE algorithm.	79
3.19 Transition from $ \psi_1\rangle = 0\rangle$ to $ \phi_2\rangle = y_-\rangle$; half π pulse: using our Hybrid algorithm algorithm.	80

Resumen

En esta tesis presentamos un modelo de control cuántico para transiciones de estados puros y mixtos, aplicado a un qubit. El modelo está basado en la geometría del espacio de los estados cuánticos dada por la métrica de Bures y la ecuación de Liouville-von Neumann, la cuál contiene información sobre los parámetros de los campos de control. Además, hacemos una revisión y simulación de los modelos o algoritmos de control cuántico que están bien establecidos en el área de control cuántico. Hemos llegado a concluir que nuestro trabajo supera a los modelos CRAB y GRAPE cuando se desea llegar al estado final en menos pasos; es decir, haciendo evolucionar al estado inicial lo menos posible, cumpliendo con un rango de valor de infidelidad deseado.

Abstract

We present a method in quantum control for quantum state transitions for pure and mixed states of a qubit. Our method is based on the geometry of the density matrices manifold given by the Bures metric and the Liouville-von Neumann equation. In this work, we review and simulate the models CRAB, GRAPE and Krotov and compare them with our model. We can show that our model outperforms GRAPE and CRAB, if one is interested in arriving to the final state with a small amount of steps given by the evolution operator of the initial state while keeping a low value of infidelity.

Chapter 1

Introduction

Quantum control has gained a considerable interest since 1970 and nowadays more with the emerging of the Quantum Computing revolution (Brif et al. 2010). Quantum control is the art of steering a known initial quantum state to a known final one (Cong 2014). If one searches for methods and theory of steering quantum states, there are numerous ways and algorithms doing it (Cong 2014; Goerz et al. 2019; Machnes et al. 2018; Caneva et al. 2011). In this context, we propose in this thesis a cunning solution to the problem of steering which concerns the geometry of the density matrix manifold.

In a general sense, we want to study the trajectories in the manifold of density matrices. A natural way to get a trajectory is by the Hamiltonian evolution of an initial state. On the other hand, the set of density matrices with Bures metric is a Riemannian manifold. Thus, there is a geodesic equation between two quantum states. The aim of this work consists of finding a Hamiltonian or a set of Hamiltonians which accomplishes two things: steers the initial state to the final one and approximates the path of the geodesic between the two states.

To motivate the reader we want to present a brief introduction of our proposal of steering an initial state to a final one in general terms. This is done just to give a hint that our model can be promising and it can challenge well established models or algorithms in the quantum control community like CRAB, GRAPE and Krotov. Without being highly

specific of our methodology, at first it needs a Hamiltonian $H = H_0 + H_c$ of the hole system with its unitary evolution operator U . The Hamiltonian H consists of two parts: H_0 which is the Hamiltonian of the system without any perturbation and H_c which is the Hamiltonian that has the control fields parameters. These parameters are very important and they form a set of real unknown constants given by $n = \{n_x, n_y, n_z, \dots\}$ and Δt . The set n can be expanded or diminished depending on the transition that one wants as we will see in § 3. One will see that the set n gives the “direction” on the Bloch sphere where the final state is located and Δt gives the “forward” evolution on the Bloch sphere to reach the final state. Thus, $H = H(n_x, n_y, \dots, \Delta t)$ and $U = U(n_x, n_y, \dots, \Delta t)$. As one will see, these ideas are not seen in well establish models like CRAB, GRAPE and Krotov; however, we can explain a bit more how to get the unknown parameters.

The parameters n_x , n_y , and n_z , that we had used in our model, come from the optimization of the function $\cos \alpha$ given by (2.1) which concerns the derivative of the geodesic equation (1.76) and the Liouville-von Neumann equation which contains the Hamiltonian and within it the control parameters. The Δt can have a fixed value at first according to the algorithms reviewed; however we find a feasible idea that it can be gauged according to the fidelity which is a function that measures how “equal” or “similar” are two states. This can be seen in section 3.4 of § 3 with the “hybrid model”.

In addition, this work is completed by several graphs and charts in order to explain what we have done and to contrast with other methodologies or algorithms. We hope that the reader enjoy our work and believe as we do that our model in the future will be a well establish quantum control algorithm of steering quantum states.

Having said the field of our investigation, our objectives and a brief resume of our proposal to solve the steering problem, we want to conclude this introduction by stating how this work is presented. This thesis is structured as follows. In the introduction, we revisit how to steer an initial state to a final one and some important methods and algorithms. Also, we give the mathematical framework that we need in order to study trajectories of quantum states. Next, we present our methodology where we are going

to use concepts of the geometry of the quantum state manifold to solve the problem of steering using the geodesic of this manifold. Following the methodology, we have results and discussion and finally we end up this work with conclusions and what we need to work in the future.

1.1 How to control a two level quantum system, the qubit

After the theoretical and experimental study of separating the geometrical phase from the dynamical phase in neutron spin experiments (Wagh & Chand Rakhecha 1990; Wagh & Rakhecha 1993; Wagh et al. 1997), the authors (Wagh & Rakhecha 2001) proposed that any evolution of a two level quantum system can be implemented by any member of the following infinite set of Hermitian Hamiltonians expressed in terms of Pauli matrices $\vec{\sigma}$ as:

$$H = \frac{\hbar}{2} \vec{\sigma} \cdot \{ \vec{\gamma} \times \dot{\vec{\gamma}} + w(t) \vec{\gamma} \}, \quad (1.1)$$

where $w(t)$ is an arbitrary real function of time and $\vec{\gamma}$ is the direction of the magnetic field. In this Hamiltonian set, the first term which contains $(\vec{\gamma} \times \dot{\vec{\gamma}})$ are the Hamiltonians that generate geometric phases and the last term which contains $w(t)\vec{\gamma}$ are Hamiltonians that generate the dynamical phase.

In (Bohm et al. 2003), it is known that the geometric phase appears on eigenstates of the Hamiltonian when the parameter $\hat{\gamma} = \frac{\vec{\gamma}}{|\vec{\gamma}|}$ traverses a closed path on the parameter space which in this case is given by the direction of the magnetic field that geometrically can be represented as points on the sphere S^2 :

$$S^2 = \{ \hat{\gamma} \in \mathbf{R}^3 : |\hat{\gamma}| = 1 \}, . \quad (1.2)$$

In a close path represented as $\mathbf{C} : \gamma(0) \rightarrow \gamma(t) \rightarrow \gamma(T) = \gamma(0)$, where T is the period of the close path, the Hamiltonian H that depends on $\gamma(t)$, its eigenvalues ¹ represented as

¹supposed to be discrete

$E_n(\gamma(t))$ and the projection operators that can be represented as $|n, \gamma(t)\rangle \langle n, \gamma(t)|$ at $\gamma(0)$ are the same as $\gamma(T)$. In equations this will be:

$$\begin{aligned} H(\gamma(0)) &= H(\gamma(T)) \\ E_n(\gamma(0)) &= E_n(\gamma(T)) \\ |n, \gamma(0)\rangle \langle n, \gamma(0)| &= |n, \gamma(T)\rangle \langle n, \gamma(T)|. \end{aligned} \tag{1.3}$$

But for eigenstates given by $|n, \gamma(t)\rangle$ in general we must have

$$|n, \gamma(0)\rangle = e^{i\epsilon_n(\gamma)} |n, \gamma(T)\rangle, \tag{1.4}$$

where $e^{i\epsilon_n(\gamma)}$ is a phase factor. This is because eigenvectors are defined only up a phase factor. The important fact about this phase² is that it contains information about the geometry of the parameter space. In this work, we are working with trajectories that starts in an initial state given by $|\psi_1\rangle$ and evolves it until it reaches a final state given by $|\phi_2\rangle$ with $|\psi_1\rangle \neq |\phi_2\rangle$. Thus, we can neglect in (1.1) the part that generate geometric phases. As a complement, (Aguiar Pinto et al. 2009) made a theoretical study of a two level quantum system interacting with a classical electromagnetic field, similar as our case, where they showed that if the classical electromagnetic field is real, one can not see the geometrical phase. On the other hand, in the same research appears that working with a complex classical electromagnetic field, the eigenstates acquire a geometric phase along a close loop in the parameter space (1.2).

Giving the above explanation, the first term of the set (1.1) can be eliminated for trajectories that the initial state is different form the final state, given the following generator of evolution for a two level quantum system

$$H = \frac{1}{2} w(t) \vec{\sigma} \cdot \vec{\gamma}, \tag{1.5}$$

with $\hbar = 1$, $\vec{\gamma} = (\gamma_x, \gamma_y, \gamma_z)$ is the magnetic field direction.

²that appears after close path on the parameter space

Following the above Hamiltonian, in (Cong 2014) a qubit, which is a single spin 1/2 particle, is controlled doing the following. The quantum system called the controlled system, consisting of a qubit in a fixed magnetic field B_0 in the $z-axis$ and a control magnetic field³ on the $x - y$ plane given by

$$\begin{aligned} B_x &= A \cos(wt + \phi) \\ B_y &= -A \sin(wt + \phi). \end{aligned} \tag{1.6}$$

The Hamiltonian H of the system is the sum of a free Hamiltonian $H_0 = -\frac{\gamma B_0 \hbar}{2} \sigma_z$ and a control Hamiltonian $H_c = \frac{\hbar \gamma}{2} (B_x \sigma_x + B_y \sigma_y)$ with γ the magnetic ratio of the particle, thus

$$\begin{aligned} H_0 &= -\frac{\hbar}{2} w_0 \sigma_z \\ H_c(t) &= -\frac{\hbar \Omega}{2} (e^{-i(wt+\phi)} \sigma_- + e^{i(wt+\phi)} \sigma_+), \end{aligned} \tag{1.7}$$

where $w_0 = \gamma B_0$ is the natural frequency or eigenfrequency of the system and $\Omega = \gamma A$ is the Rabi frequency of the particle, $\sigma_- = \begin{bmatrix} 0 & 0 \\ 1 & 0 \end{bmatrix}$ and $\sigma_+ = \begin{bmatrix} 0 & 1 \\ 0 & 0 \end{bmatrix}$.

In matrix form we end up with,

$$H = H_0 + H_c = -\frac{\hbar}{2} \begin{bmatrix} w_0 & \Omega e^{i(wt+\phi)} \\ \Omega e^{-i(wt+\phi)} & -w_0 \end{bmatrix}. \tag{1.8}$$

Going into the frame of the control field, using the transformation $U_c = e^{-iwt\sigma_z/2}$, the Hamiltonian becomes

$$H_{eff} = U_c H U_c^\dagger + i\hbar \dot{U}_c U_c^\dagger, \tag{1.9}$$

thus

³complex

$$H_{eff} = \frac{(w_0 - w)\hbar}{2}\sigma_z - \frac{\Omega\hbar}{2}\sigma_x \cos\phi + \frac{\Omega\hbar}{2}\sigma_y \sin\phi = \frac{\hbar}{2} \begin{bmatrix} w - w_0 & -\Omega e^{i\phi} \\ -\Omega e^{-i\phi} & -w + w_0 \end{bmatrix}. \quad (1.10)$$

The evolution operator associated to this Hamiltonian is given by $U_{eff} = e^{-\frac{i t}{\hbar} H_{eff}}$,

$$U_{eff}(t) = \begin{bmatrix} \cos(at) + \frac{i(w_0-w)}{2} \sin(at) & \frac{i\Omega}{2a} e^{i\phi} \sin(at) \\ \frac{i\Omega}{2a} e^{-i\phi} \sin(at) & \cos(at) - \frac{i(w_0-w)}{2} \sin(at) \end{bmatrix}. \quad (1.11)$$

where $a = \sqrt{\frac{(w_0-w)^2}{4} + \frac{\Omega^2}{4}}$ and the term $w - w_0$ is called “detuning”.

This was done using the Pauli matrix exponentiation given by

$$e^{ib(\hat{n}.\vec{\sigma})} = I \cos(b) + i \sin(b)(\hat{n}.\vec{\sigma}), \quad (1.12)$$

where $\vec{b} = b\hat{n}$ and $|\hat{n}| = 1$. In our case, $b = at$, $\hat{n} = 1/b \begin{bmatrix} -\frac{\Omega t}{2} \cos\phi \\ \frac{\Omega t}{2} \sin\phi \\ \frac{-t}{2}(w_0 - w) \end{bmatrix}$ and $\vec{\sigma} = \begin{bmatrix} \sigma_x \\ \sigma_y \\ \sigma_z \end{bmatrix}$.

In the resonant situation where $w = w_0$, we can get

$$U_{eff}(t) = \begin{bmatrix} \cos(\frac{\Omega t}{2}) & ie^{i\phi} \sin(\frac{\Omega t}{2}) \\ ie^{-i\phi} \sin(\frac{\Omega t}{2}) & \cos(\frac{\Omega t}{2}) \end{bmatrix}. \quad (1.13)$$

Returning to laboratory frame $U_c = e^{-iw_0 t \sigma_z t/2}$ and using

$$H = U_c^\dagger H' U_c - i\hbar U_c^\dagger \dot{U}_c, \quad (1.14)$$

which gives,

$$H = \frac{-\hbar w_0}{2}\sigma_z - \frac{\hbar\Omega}{2} \cos(w_0 t + \phi)\sigma_x + \frac{\hbar\Omega}{2} \sin(tw_0 + \phi)\sigma_y \quad (1.15)$$

and the evolution operator in laboratory frame is given by $U(t) = U_c^{-1} U_{eff}$

$$U(t) = \begin{bmatrix} e^{i\frac{tw_0}{2}} \cos\left(\frac{\Omega t}{2}\right) & ie^{i\frac{tw_0+2\phi}{2}} \sin\left(\frac{\Omega t}{2}\right) \\ ie^{-i\frac{(w_0t+2\phi)}{2}} \sin\left(\frac{\Omega t}{2}\right) & e^{-i\frac{tw_0}{2}} \cos\left(\frac{\Omega t}{2}\right) \end{bmatrix}. \quad (1.16)$$

Factoring this operator we get,

$$U(t) = \begin{bmatrix} e^{(iw_0t+\phi)/2} & 0 \\ 0 & e^{-i(w_0t+\phi)/2} \end{bmatrix} \begin{bmatrix} \cos \frac{\Omega t}{2} & i \sin \frac{\Omega t}{2} \\ i \sin \frac{\Omega t}{2} & \cos \frac{\Omega t}{2} \end{bmatrix} \begin{bmatrix} e^{-i\phi/2} & 0 \\ 0 & e^{i\phi/2} \end{bmatrix}, \quad (1.17)$$

where the first matrix rotates a point around the $z - axis$ by an angle of $(w_0t + \phi)$, the second rotates a point around the $x - axis$ by an angle Ωt and the last one again makes a rotation around the $z - axis$ by an angle of ϕ .

With these matrices one moves points of the sphere by controlling the parameters Ω , ϕ and t . It is important to notice that we can have different trajectories on the Bloch sphere when we choose different configurations of the latter parameters, although we have the same initial and final states.

To get the optimal trajectory under the action of the control Hamiltonian one can choose between the shortest time or the minimal trajectory. In the following section, we will show how some algorithms deal with the control.

1.2 Steering an state: the most common methods so far

In general, an optimal quantum control problem can be stated with the following ideas. One has a Hamiltonian H (acting on Hilbert space $\mathcal{H} = \mathbf{C}^N$) that describes the system which depends on some control parameters $u_j(t)$ with $j = 1, \dots, N_c$, where u'_j 's are in general time dependent (pulse shape) and N_c is the number of controls that one has or could implement. Thus, the main point of quantum control theory is to find the u'_j 's that extremize a given objective function \mathcal{F} , such as the system energy, the fidelity or entanglement. In most cases, it is necessary to start with an initial guess of values $u_j^0(t)$ and search for

updates or corrections until one arrives to the desired state with a certain error or to get to the optimal value for the objective function. In the following, we want to present the mostly used optimization algorithms.

1.3 GRAPE optimization

GRAPE stands for GRadient Ascent Pulse Engineering. It is used for optimizing pulse sequences for steering the dynamics of coupled nuclear spins (Khaneja et al. 2005). In the following, we want to describe the theory, the algorithm and some examples around GRAPE algorithm.

The method considers the problem of pulse design for polarization or coherence transfer in the absence of relaxation. Let $\rho(t)$ be the state of a spin system. Thus, its equation of motion is given by the Liouville-von Neumann equation:

$$\dot{\rho} = -i[(H_0 + \sum_{k=1}^m u_k(t)H_k), \rho], \quad (1.18)$$

where H_0 is the Hamiltonian of the system without perturbation, H_k are the control Hamiltonians and $u(t) = (u_1(t), u_2(t), \dots, u_m(t))$ are the amplitudes of the control fields.

We need to find the optimal amplitudes $u_k(t)$ of the radio frequency fields that steer a given initial density operator, the initial state, $\rho(0) = \rho_0$ during a specific time T to a density operator $\rho(T)$ with maximum overlap to some desired target density operator C , the final state.

The overlap function is given by the Hilbert-Schmidt scalar product. This product is defined on the C^* -algebra of bounded linear operators on \mathcal{H} , denoted by $\mathcal{B}(\mathcal{H})$. In our case, dealing with finite dimension, the $\mathcal{B}(\mathcal{H})$ is the algebra of all $n \times n$ complex matrices, with $\dim \mathcal{H} = n$. The product is given by,

$$\langle A, B \rangle = \text{Tr}(A^\dagger B), \quad (1.19)$$

where $A, B \in \mathcal{B}(\mathcal{H})$.

For GRAPE algorithm the overlap function is given by,

$$\Phi_0 = \langle C | \rho(T) \rangle = \text{Tr}(C^\dagger \rho(T)) \quad (1.20)$$

The method divides the time interval T into N equal parts,

$$\Delta t = T/N, \quad (1.21)$$

where u_k is constant, according to Fig. 1.1.

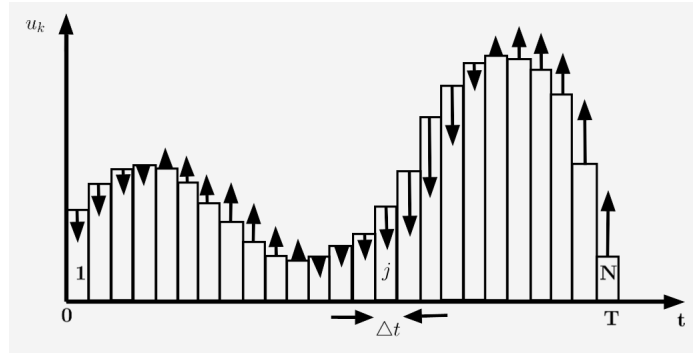


Figure 1.1: Schematic representation of a control amplitude $u_k(t)$, consisting of N steps of duration $\Delta t = T/N$. The arrows represent the gradients $\delta\Phi_0/\delta u_k(j)$ showing how each $u_k(j)$ might be modified in the next iteration to improve the performance of the overlap function Φ_0 . Image reproduced from (Khaneja et al. 2005)

The evolution operator at time j is given by,

$$U_j = e^{-i\Delta t(H_0 + \sum_{k=1}^m u_k(j)H_k)}. \quad (1.22)$$

Thus, the evolution of the state is given by

$$\rho(T) = U_N \dots U_1 \rho_0 U_1^\dagger \dots U_N^\dagger. \quad (1.23)$$

Expanding the overlap function,

$$\begin{aligned} \Phi_0 &= \langle C | U_N \dots U_1 \rho_0 U_1^\dagger \dots U_N^\dagger \rangle \\ &= \langle U_{j+1}^\dagger \dots U_N^\dagger C U_N \dots U_{j+1} | U_j \dots U_1 \rho_0 U_1^\dagger \dots U_j^\dagger \rangle. \end{aligned} \quad (1.24)$$

We can define

$$\lambda_j = U_{j+1}^\dagger \dots U_N^\dagger C U_N \dots U_{j+1}, \quad (1.25)$$

which is C backward propagated at $t = j\Delta t$, and

$$\rho_j = U_j \dots U_1 \rho_0 U_1^\dagger \dots U_j^\dagger, \quad (1.26)$$

which is ρ_0 propagated forwards at time $t = j\Delta t$.

We might ask: How does Φ_0 change when we perturb the control amplitude $u_k(j)$?

The perturbation of $u_k(j)$ is given by

$$u_k(j) \longrightarrow u_k(j) + \delta u_k(j). \quad (1.27)$$

Thus, using time-dependent perturbation theory, a change in U_j to the first order in $\delta u_k(j)$ is given by

$$\delta U_j = -i\Delta t \delta u_k(j) \overline{H_k} U_j, \quad (1.28)$$

with

$$\overline{H_k} \Delta t = \int_0^{\Delta t} U_j(\tau) H_k U_j(-\tau) d\tau, \quad (1.29)$$

and with

$$U_j(\tau) = \exp(-i\tau(H_0 + \sum_{k=1}^m u_k(j) H_k)). \quad (1.30)$$

For small Δt , which is $\Delta t \ll ||H_0 + \sum_{k=1}^m u_k(j) H_k||^{-1}$, we can assume $\overline{H_k} \approx H_k$. Thus, using (1.24) and (1.28),

$$\begin{aligned}
 \delta\Phi_0 &= \langle \lambda_j | \delta U_j \dots U_1 \rho_0 U_1^\dagger \dots U_j^\dagger + U_j \dots U_1 \rho_0 U_1^\dagger \dots \delta U_j^\dagger \rangle \\
 \frac{\delta\Phi_0}{\delta u_k(j)} &= \langle \lambda_j | \frac{\delta U_j}{\delta u_k(j)} (U_{j-1} \dots U_1 \rho_0 U_1^\dagger \dots U_j^\dagger) + U_j \dots U_1 \rho_0 U_1^\dagger \dots U_{j-1}^\dagger \frac{\delta U_j^\dagger}{\delta u_k(j)} \rangle \\
 &= \langle \lambda_j | -i\Delta t H_k \rho_j + i\Delta t \rho_j H_k \rangle.
 \end{aligned} \tag{1.31}$$

Thus,

$$\frac{\delta\Phi_0}{\delta u_k(j)} = -i\Delta t \langle \lambda_j | [H_k, \rho_j] \rangle. \tag{1.32}$$

Finally, we can increase the performance of Φ_0 updating $u_k(j)$,

$$u_k(j) \longrightarrow u'_k = u_k(j) + \epsilon \frac{\delta\Phi_0}{\delta u_k(j)}, \tag{1.33}$$

where ϵ is small.

1.3.1 GRAPE algorithm

If we want to build an algorithm to maximize the overlap function, the following will be useful:

1. Guess the initial $u_k(j)$
2. Starting from ρ_0 , calculate

$$\rho_j = U_j \dots U_1 \rho_0 U_1^\dagger \dots U_j^\dagger, \quad \forall j \leq N. \tag{1.34}$$

3. Starting from $\lambda_N = C$, calculate

$$\lambda_j = U_{j+1}^\dagger \dots U_N^\dagger C U_N \dots U_{j+1}, \quad \forall j \leq N \tag{1.35}$$

4. Evaluate $\frac{\delta\Phi_0}{\delta u_k(j)}$ and update the $m \times N$ control amplitudes $u_k(j)$ by $u'_k = u_k(j) + \epsilon \frac{\delta\Phi_0}{\delta u_k(j)}$ with ϵ a small number, $k = 1, \dots, m$ and $j = 1, \dots, N$. Evaluate the overlap function, if it has a higher value we are done, if not return to step 2.

1.3.2 GRAPE in action

As a demonstration of GRAPE, we want to steer the state $|0\rangle$ to $|x_+\rangle = \frac{1}{\sqrt{2}}(|0\rangle + |1\rangle)$. In a pictorial way, we want to go from the North pole $|0\rangle$ to one point in the Equator $|x_+\rangle$.

For this task, we can take

$$H_k = \{\sigma_x, \sigma_y, \sigma_z\}, \text{ and } H_0 = -\frac{1}{2}w_0\sigma_z \quad (1.36)$$

with w_0 the natural frequency of the system and the evolution operator is given by

$$U_j = I \cos(u_k(j)\Delta t) - iH_k \sin(u_k(j)\Delta t), \quad (1.37)$$

with $k = 0, \dots, 3$ and $u_0 = -\frac{w_0}{2}$.

The initial values for $u(t)$ are

$$u = \begin{bmatrix} 0 & 0 & 0 & 0 & 0 & 0 & 0 \\ -0.001 & -0.001 & 0 & 0 & 0.001 & 0.001 & 0.001 \\ w_0/2 & w_0/2 & w_0/2 & w_0/2 & w_0/2 & w_0/2 & w_0/2 \end{bmatrix}. \quad (1.38)$$

The number of rows are the pulses or fields that are controlling the system and the number of columns are the number of times that we divide the time ⁴.

With the above information, one produces the trajectory in Fig. 1.2.

Trying another initial state,

$$|\psi\rangle = \cos(\pi/8)|0\rangle + \sin(\pi/8)|1\rangle, \quad (1.39)$$

which is located in the meridian that joins $|0\rangle$ and $|x_+\rangle$ and we want to get to $|y+\rangle$ which is located in the Equator.

This time we want to use the GRAPE algorithm in Qutip (Johansson et al. 2013) which is a Python package about quantum mechanics and it has the GRAPE algorithm ready to

⁴The matrix u has been designed only as an illustrative example because in a real simulation there are more controlled fields and the time is divided more times.

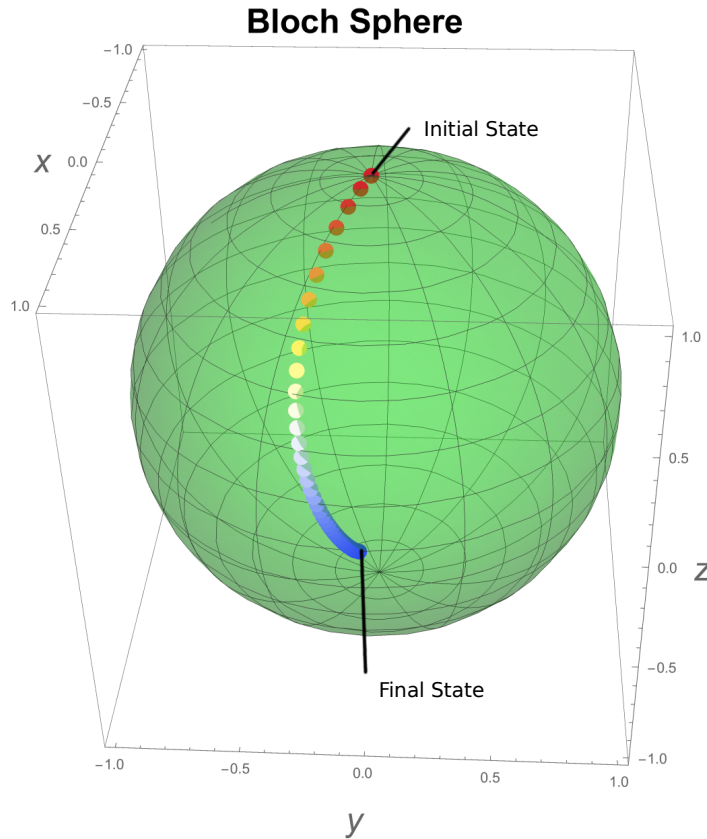


Figure 1.2: Transition from the initial state $|0\rangle$ to the final state $|x_+\rangle$. The red dot is the initial state and the blue is the final state. The trajectory on the Bloch sphere is given by GRAPE algorithm. The graph was made with Mathematica and following the algorithm with (1.38), $H_0 = \frac{-w_0}{2}\sigma_z$, $w_0 = 5$, $H_c = u_x\sigma_x + u_y\sigma_y + u_z\sigma_z$, $\epsilon = 0.4$, $N = 7$ and 45 iterations to arrive the final state and $\Phi_0 = 0.999944$.

use. We have the trajectory shown in Fig. 1.3 on the Bloch sphere using the the GRAPE algorithm. This graph is made using $H_0 = -\frac{w_0}{2}$, $H_c = u_x\sigma_x + u_y\sigma_y$ with u_x and u_y unknown constants and $j = 1, 2$, the total time of evolution is $T = 1$ and it is divided in $N = 100$ parts ($\Delta t = \frac{T}{N} = \frac{1}{100}$) and with an infidelity of around 1×10^{-5} .

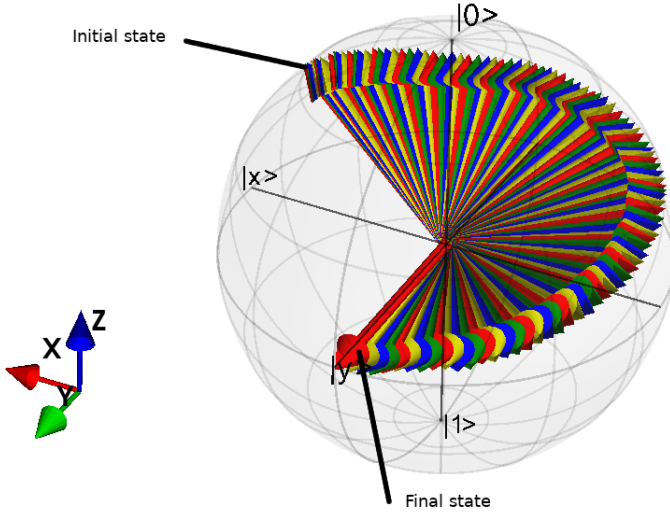


Figure 1.3: Transition from the initial state $|\psi\rangle = \cos(\pi/8)|0\rangle + \sin(\pi/8)|1\rangle$ to the final state $|y_+\rangle$, using Qutip package. The trajectory on the Bloch sphere is given by GRAPE algorithm. Every vector on the sphere shows the path with the optimize parameters for $H_0 = \frac{-w_0}{2}\sigma_z$, $H_c = u_x\sigma_x + u_y\sigma_y$, $w_0 = 5$, $T = 1$, $N = 100$ and the fidelity error $\times 10^{-5}$

1.4 CRAB Algorithm

CRAB takes the acronym from "Chopped RAndom Basis" technique. This optimization is based on the definition of a truncated randomized basis of functions for the control fields that transform the problem of a functional minimization to a multivariable function minimization that can be solved by a direct-search method (Caneva et al. 2011). In the case of state-state transition, the goal of CRAB algorithm is similar as before. Given a Hamiltonian H acting on a Hilbert space \mathcal{H} that depends on a set of time-dependent driving fields $\{\epsilon_j(t)\}$, search for the optimal transformation to drive, in time T , the initial state $|\psi_0\rangle \in \mathcal{H}$ into a target state $|\psi_G\rangle \in \mathcal{H}$ but minimizing the infidelity function which is

$$\mathcal{I}(T) = 1 - |\langle \psi(T) | \psi_G \rangle|^2. \quad (1.40)$$

1.4.1 CRAB in action

We want to present a state to state transitions using CRAB method. As well as GRAPE, CRAB is implemented in Qutip. We want to evolve the North pole given by

$$|\psi\rangle = |0\rangle, \quad (1.41)$$

to the state, $|y_+\rangle$, given by

$$|y_+\rangle = \frac{1}{\sqrt{2}}(|0\rangle + i|1\rangle). \quad (1.42)$$

The path given by this algorithm can be seen in Fig. 1.4. Each vector shows the trajectory of the initial state $|\psi\rangle$ to the final state.

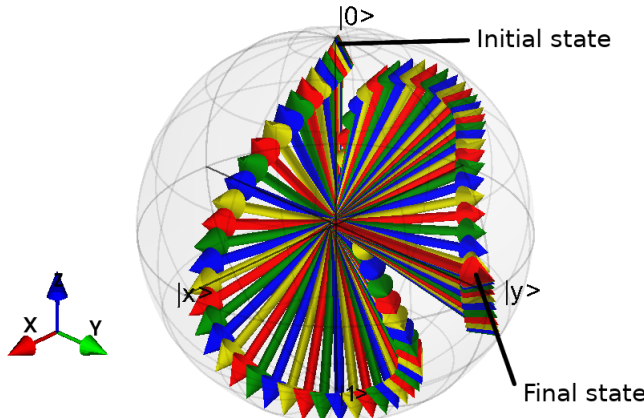


Figure 1.4: Transition from the initial state $|0\rangle$ to the final state $|y_+\rangle$. The trajectory on the Bloch sphere is given by the CRAB method of the Qutip package in Python. Every vector on the sphere shows the path that the initial state follows after the optimization. The graph corresponds to $H_0 = \frac{-w_0}{2}\sigma_z$, $w_0 = 5$, $H_c = \epsilon_x\sigma_x + \epsilon_y\sigma_y$, $T = 1$, $N = 100$ and the fidelity error $\times 10^{-3}$

1.5 Krotov's method

An improvement of GRAPE algorithm is the Krotov's method or simply Krotov. As we reviewed, GRAPE rely on forward propagation, backward propagation and update of

controls. In contrast, Krotov requires sequential updates and it does not need for a line search in the direction of the gradient (Goerz et al. 2019).

Krotov's method follows the same procedure as the general control method. The Hamiltonian $H(t)$ of the system depends on one or more control fields $\{\epsilon_l(t)\}$ and it is assumed that the dependence is linear

$$H(t) = H_0(t) + \epsilon_1(t)H_1 + \epsilon_2(t)H_2 + \dots \quad (1.43)$$

Krotov can be used to optimize the control fields $\{\epsilon_l(t)\}$ in a state to state transfer and to get the unitary operator of the evolution.

For state to state transition, the objective is to steer a known state $|\phi\rangle$ or a set of states $\{|\phi_k(t)\rangle\}$ at time zero to a target state $|\phi^{tgt}\rangle$ at time T . To achieve the objective, Krotov minimizes the following functional

$$J[\{|\phi_k^{(i)}(t)\rangle\}, \{\epsilon_l^{(i)}(t)\}] = J_T(\{|\phi_k^{(i)}(T)\rangle\}) + \sum_l \int_0^T g_a(\epsilon_l^{(i)}(t))dt + \int_0^T g_b(\{|\phi_k^{(i)}(t)\rangle\})dt, \quad (1.44)$$

where $\{\phi_k^{(i)}(T)\}$ are time evolved initial states $\{|\phi_k\rangle\}$ controlled by $\{\epsilon_k^{(i)}(t)\}$ of the i 'th iteration. If we want to transfer a single state, k is zero and for a single control field l is zero. Also for open quantum systems, the states $\{|\phi_k\rangle\}$ can be density matrices.

The main parts of the functional are the following:

- J_T called the final time functional, which for state to state transition $|\phi\rangle \rightarrow |\phi^{tgt}\rangle$ has the form

$$J_{T,ss} = 1 - |\langle \phi^{tgt} | \phi(T) \rangle|^2, \quad (1.45)$$

where $|\phi(T)\rangle$ is the evolution of $|\phi\rangle$ at time T . In general Krotov minimizes one minus the transition probability. The equation (1.45) is related with the term known as fidelity which we are going to review some of its properties in the following sections.

- g_a is the running cost on the control fields which helps the convergence of the algorithm and it depends on the shape of the update fields.

- g_b (optional) is the state dependent running cost. This encodes time dependent control targets or to penalize population in a subspace.

1.5.1 Krotov in action

The same as we did with GRAPE, we want to show some transitions. Using the Krotov package in Python, we want to evolve the initial state

$$|\psi\rangle = \cos(\pi/8)|0\rangle + \sin(\pi/8)|1\rangle, \quad (1.46)$$

to the state

$$|y_-\rangle = \frac{1}{\sqrt{2}}(|0\rangle - i|1\rangle). \quad (1.47)$$

The path can be seen in Fig. 1.5.

As another example, we have chosen the transition from the same $|\psi\rangle$ to

$$|x_-\rangle = \frac{1}{\sqrt{2}}(|0\rangle - |1\rangle). \quad (1.48)$$

The trajectory on the Bloch sphere is shown in the Fig. 1.6.

Looking into the algorithms and their graphs, one can see that every method maximize almost the same function which is the fidelity. Also, one can notice that every trajectory makes turns until they reach to the destiny instead of going directly to the final state. In contrast, our work aims to implement the geodesic of the density matrices manifold and maximize a function that concerns the geodesic and the evolution of the initial state. This is a completely different approach to solve the same problem. Before reviewing the geodesic and the objective function that has to be optimized, we want to introduce the geometry of Quantum states to settle the mathematics behind our methodology.

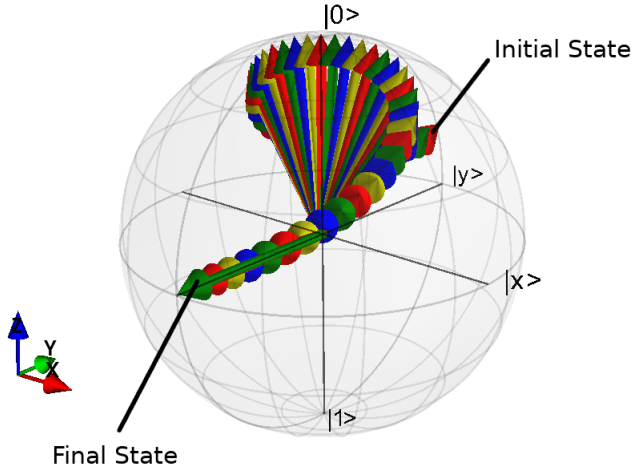


Figure 1.5: Transition from the initial state $|\psi\rangle = \cos(\pi/8)|0\rangle + \sin(\pi/8)|1\rangle$ to the final state $|y_-\rangle$. The trajectory on the Bloch sphere is given by the Krotov method. Every vector on the sphere shows the path that the initial state follows after the optimization. The graph was made using: $H_0 = -\frac{w_0}{2}\sigma_z$, $w_0 = 5$, $H_c = \epsilon_x\sigma_x + \epsilon_y\sigma_y$, the control parameters are modeled as Blackman functions with a constant amplitude of 0.2, with $t_star = 0$, $t_stop = 1$, $t_rise = 0.3$ and $T = 1$, $N = 50$ and the fidelity error of $\times 10^{-5}$.

1.6 Geometry of Quantum states

In this section, we want to present the mathematical framework that our work is based in order to study trajectories of the set of Quantum states.

1.6.1 States viewing from Physics and Maths

The definition of state in physics differs from the mathematical definition but both of them are related. In quantum mechanics, a state is a complete description of quantum system. From the mathematical point of view, a state is represented by a vector $|\psi\rangle$ and it is a ray in a Hilbert space \mathcal{H} . A ray is a subspace of the Hilbert space \mathcal{H} because physically, we can not distinguish between the state $|\psi\rangle$ from the state $c|\psi\rangle$ where $c \in \mathbf{C}$, thus we say that $c|\psi\rangle$ represents the same state as $|\psi\rangle$. The set of rays is the complex projective space

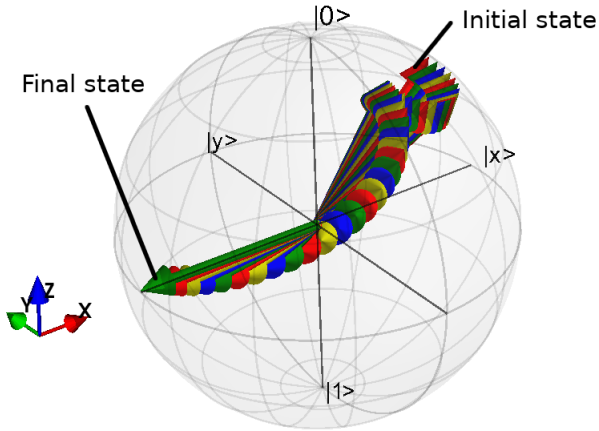


Figure 1.6: Transition from the initial state $|\psi\rangle = \cos(\pi/8)|0\rangle + \sin(\pi/8)|1\rangle$ to the final state $|x_-\rangle$. The trajectory on the Bloch sphere is given by the Krotov method. Every vector on the sphere shows the path that the initial state follows after the optimization. The graph was made using: $H_0 = -\frac{w_0}{2}\sigma_z$, $w_0 = 5$, $H_c = \epsilon_x\sigma_x + \epsilon_y\sigma_y$, the control parameters are modeled as Blackman functions with a constant amplitude of 0.2, with $t_star = 0$, $t_stop = 1$, $t_rise = 0.3$ and $T = 1$, $N = 50$ and the fidelity error of $\times 10^{-5}$.

denoted by \mathbf{CP}^{N-1} which has $2N - 2$ real dimensions. In summary, there is a one to one correspondence between physical states and rays in \mathcal{H} where a ray is an equivalent class of vectors that differ by a multiplication of a non zero complex scalar.

Being specific, rays are also called pure states and we will work with normalized states, $\langle\psi|\psi\rangle = 1$, and with finite dimensional Hilbert spaces of (complex) dimension N .

Pure states describe closed quantum systems but Nature prevent us for having purity. Working with open systems we are limited to study a part of a large system where states are not rays (Preskill 2020). Systems with two or more subsystems are called Composite Systems. For example, a bipartite system has two subsystems, A with Hilbert space \mathcal{H}_A and B with Hilbert space \mathcal{H}_B , thus the Hilbert space of the composite system AB is the tensor product $\mathcal{H}_A \otimes \mathcal{H}_B$. If the system A is prepared in the state $|\psi_A\rangle$ and the system B is prepared in the state $|\psi_B\rangle$, then the state that belongs to the composite system AB is

$$|\psi_A\rangle \otimes |\psi_B\rangle.$$

Composite systems are useful when we do not have access to a subsystem. For example, one can imagine that we have a system composed of two qubits. Qubit A which is in the laboratory and we can manipulate or observe it. On the other hand, qubit B is locked and we do not have access to it. In a general bipartite system, let $\{|i_A\rangle\}$ and $\{|j_A\rangle\}$ be orthogonal basis in \mathcal{H}_A and \mathcal{H}_B , respectively. Thus, a general pure state can be of the form

$$|\psi\rangle = \sum_{i,j} c_{ij} |i\rangle \otimes |j\rangle, \quad (1.49)$$

where we need $\sum_{i,j} |c_{ij}|^2 = 1$ in order to be normalized. We can introduce the reduce density matrix and the density matrix as

$$\rho_A = Tr_B \rho = Tr_B(|\psi\rangle \langle \psi|), \quad (1.50)$$

where $\rho = |\psi\rangle \langle \psi|$ is the density matrix and ρ_A is the reduce density matrix. In the last equation, we had traced the space B which we do not have access.

Density matrices has the following properties:

1. ρ_A is self-adjoint
2. ρ_A is positive
3. $Tr(\rho_A) = 1$
4. If the state of the subsystem is a ray, we say that the state is pure. Otherwise it is mixed.
5. For pure state $|\psi\rangle$, its density matrix $\rho_\psi = |\psi\rangle \langle \psi|$, has the property $\rho_\psi^2 = \rho_\psi$
6. Density matrices form a convex set. For any two density matrices ρ_1 and ρ_2 , we can construct another one by taking a convex combination of them:

$$\rho = p\rho_1 + (1-p)\rho_2, \quad 0 < p < 1. \quad (1.51)$$

As a notation, we call mixture states or mixed density matrices or mixed states.

7. Following the last idea, we can form a density matrix given an ensemble of a mixture of pure states. An ensemble is a set of pure states and probabilities: $\{|\psi_i\rangle, p_i\}_{i=1}^M$, such that $p_i \geq 0$ and $\sum_i p_i = 1$.
8. As a notation, the set of all density matrices ρ, σ, τ in a Hilbert space \mathcal{H} will be noted as $\mathcal{E}(\mathcal{H})$.

In summary, a state of a quantum system of Hilbert space \mathcal{H} is given by a density matrix ρ that is a non-negative operator defined on \mathcal{H} with the property $Tr\rho = 1$. In particular, pure states are the extreme points of the set $\mathcal{E}(\mathcal{H})$ and if $|\psi\rangle \in \mathcal{H}$

$$\rho_\psi = |\psi\rangle\langle\psi| \quad (1.52)$$

and $\|\psi\| = 1$

We want to finish this section with an important theorem of bipartite systems which is the Schmidt decomposition.

Theorem 1.6.1 (Schmidt decomposition). Any pure state $|\psi\rangle \in \mathcal{H}_A \otimes \mathcal{H}_B$ of a bipartite system admits a decomposition

$$|\psi\rangle = \sum_{i=1}^n \sqrt{\mu_i} |\alpha_i\rangle |\beta_i\rangle, \quad (1.53)$$

where $n = \min\{n_A, n_B\}$, $\mu_i \geq 0$, and $\{|\alpha_i\rangle\}_{i=1}^n$ and $\{|\beta_i\rangle\}_{i=1}^n$ are orthonormal families of \mathcal{H}_A and \mathcal{H}_B , respectively. μ_i and $|\alpha_i\rangle$ are eigenvalues and eigenvectors of the reduce state $\rho_A = Tr_B(|\psi\rangle\langle\psi|)$ and $|\beta_i\rangle$ are eigenvectors of the reduce state.

1.6.2 The Bures metric

Bures metric generalize the transition probability for pure states $|\langle\psi|\phi\rangle|^2$, where $|\psi\rangle$ and $|\phi\rangle$ are pure states, to mixed density matrices. This was done by using purifications (Ericsson 2007).

Definition 1.6.1 (Purifications). Let ρ be an arbitrary state on \mathcal{H} and \mathcal{K} be two Hilbert spaces. A pure state $|\psi\rangle \in \mathcal{H} \otimes \mathcal{K}$ such that $\rho = Tr_{\mathcal{K}}(|\psi\rangle \langle \psi|)$ is called a purification of ρ on $\mathcal{H} \otimes \mathcal{K}$.

In basic terms, we want to find a pure state $|\psi\rangle$ for a composite system such that the reduce density matrix of one of the subsystems is ρ . This is done by doing the following. Let $|\psi\rangle \in \mathcal{H} \otimes \mathcal{H}$ in Schmidt decomposition (Theorem 1.6.1)

$$|\psi\rangle = \sum_i c_i |i\rangle_A \otimes |u_i\rangle_B, \quad (1.54)$$

taking the trace respect to B , we get

$$\rho = Tr_B |\psi\rangle \langle \psi| = \sum_i c_i^2 |i\rangle_A \langle i|, \quad (1.55)$$

where this is possible if, and only if, $|i\rangle_A$ are eigenvectors of ρ and c_i are the square roots of the eigenvalues of ρ . Notice that we have certain liberty in choosing the basis $\{|u_i\rangle_B\}$ because it can be any basis of the form $\{U|u_i\rangle_B\}$, for some U unitary operator. This liberty will help us construct a fiber bundle in the following.

We can get an operator for every pure state $|\psi\rangle = \sum_{ij} c_{ij} |i\rangle_A |j\rangle_B$ by replacing the $|j\rangle_B$ with $_B \langle j|$, ending with $W = \sum_{ij} c_{ij} |i\rangle_A {}_B \langle j|$. This W is also a purification of the reduce state because

$$\rho = WW^\dagger, \quad (1.56)$$

but as we can see WU with U any unitary operator is also a purification of ρ . We end up with a kind of a fiber bundle⁵.

The W operators are called “amplitudes” and we can add a “phase” by applying a unitary operator WU . We need to add a constrain regarding the trace of density operators,

⁵A fiber bundle is a space that is locally a product space but globally can have a different topological structure.

$$TrWW^\dagger = 1. \quad (1.57)$$

The space where the operators W live is a subspace of the Hilbert Schmidt space which means that the set of W are finite rank operators with (1.57) and will be noted \mathcal{W}^k . In summary, a purification is a principal fiber bundle over the space of density operators $\mathcal{E}(\mathcal{H})$. Where the projection is given by,

$$\begin{aligned} \Pi : \quad & \mathcal{W}^k \rightarrow \mathcal{E}(\mathcal{H}) \\ & W \rightarrow \Pi(W) = WW^\dagger. \end{aligned} \quad (1.58)$$

The unitary operators of rank k in the Hilbert space \mathcal{H} noted as $U(k)$ being the symmetry group and $U(k)$ acts on the right by

$$R_U(W) = WU. \quad (1.59)$$

In the space \mathcal{W}^k where purifications live we define distances by

$$D^2(W_1, W_2) = Tr(W_1 - W_2)(W_1^\dagger - W_2^\dagger), \quad (1.60)$$

meanwhile in the base space $\mathcal{E}(\mathcal{H})$ distances between two density matrices ρ_1 and ρ_2 are defined as the length of the shortest path between the corresponding purifications

$$d_B^2(\rho_1, \rho_2) = \min_{U_1, U_2} D^2(W_1 U_1, W_2 U_2) = 2 - 2 \max_U Tr(W_1^\dagger W_2 U), \quad (1.61)$$

where $U = U_2 U_1^\dagger$.

In a practical sense, we need to use the polar decomposition⁶ such that $W = \sqrt{\rho}U$, where U is a unitary operator. Thus, if $W_1 = \sqrt{\rho_1}V$, for some V unitary operator,

$$(W_1^\dagger W_2 U)^2 = W_1^\dagger W_2 U U^\dagger W_2^\dagger W_1 = V^\dagger \sqrt{\rho_1} \rho_2 \sqrt{\rho_1} V, \quad (1.62)$$

taking the square root and then the trace,

⁶see Appendix: A.2

$$\max_U \text{Tr}(W_1^\dagger W_2 U) = \text{Tr} \sqrt{\sqrt{\rho_1} \rho_2 \sqrt{\rho_1}}. \quad (1.63)$$

The term $\sqrt{\sqrt{\rho_1} \rho_2 \sqrt{\rho_1}}$ was defined by (Uhlmann 1976) as the generalized “transition probablity” but it is more known as fidelity F after (Jozsa 1994). In terms of purifications,

$$F(\rho_1, \rho_2) = \max_{\text{purification}} |\langle \psi_1 | \psi_2 \rangle|^2 = \left(\text{Tr} \sqrt{\sqrt{\rho_1} \rho_2 \sqrt{\rho_1}} \right)^2. \quad (1.64)$$

Finally, the Bures distance is given by,

$$d_B^2(\rho_1, \rho_2) = 2 \left(1 - \text{Tr} \sqrt{\sqrt{\rho_1} \rho_2 \sqrt{\rho_1}} \right) = 2 \left(1 - \sqrt{F(\rho_1, \rho_2)} \right). \quad (1.65)$$

Working with square roots of matrices is not an easy task because we need to diagonalize the matrices before taking the root. However, if we are dealing with qubits, that is dimension 2, there is a trick which use only the trace and the determinant of the matrix (see theorem A.2.2 in Appendix A).

1.6.3 The Bures tensor metric

In this section we want to show that the Bures distance is Riemannain and determine its metric g_B . A Riemannian metric on $\mathcal{E}(\mathcal{H})$ is a map which associates to each $\rho \in \mathcal{E}(\mathcal{H})$ a scalar product g_ρ on the tangent space of $\mathcal{E}(\mathcal{H})$ at ρ . The tangent space can be identified with the (real) vector space of traceless density matrices by the mixture representation of a tangent vector (Fig. 1.7)(Andersson 2018; Spehner et al. 2017).

From any $\rho \in \mathcal{E}(\mathcal{H})$, we can extend it by a curve ρ_t in $\mathcal{E}(\mathcal{H})$ with velocity $\dot{\rho}$. The tangent vector $\dot{\rho}$ is identified with the operator $\rho^{(m)} \in \mathcal{B}_0^{s.a}$ by

$$\dot{\rho} = \dot{\rho}^{(m)} = \lim_{t \rightarrow 0} \frac{1}{t} (\rho_t - \rho) \quad (1.66)$$

Clarifying the derivative of a density matrix, we can continue with the Bures metric. To determine the Bures metric, we need to introduce a parameter $t \in \mathbb{R}$ such that,

$$d_B(\rho, \rho + t d\rho)^2 = 2 - 2\text{Tr}(A(t)), \quad \text{with } A(t) = (\sqrt{\rho}(\rho + t d\rho)\sqrt{\rho})^{1/2}. \quad (1.67)$$

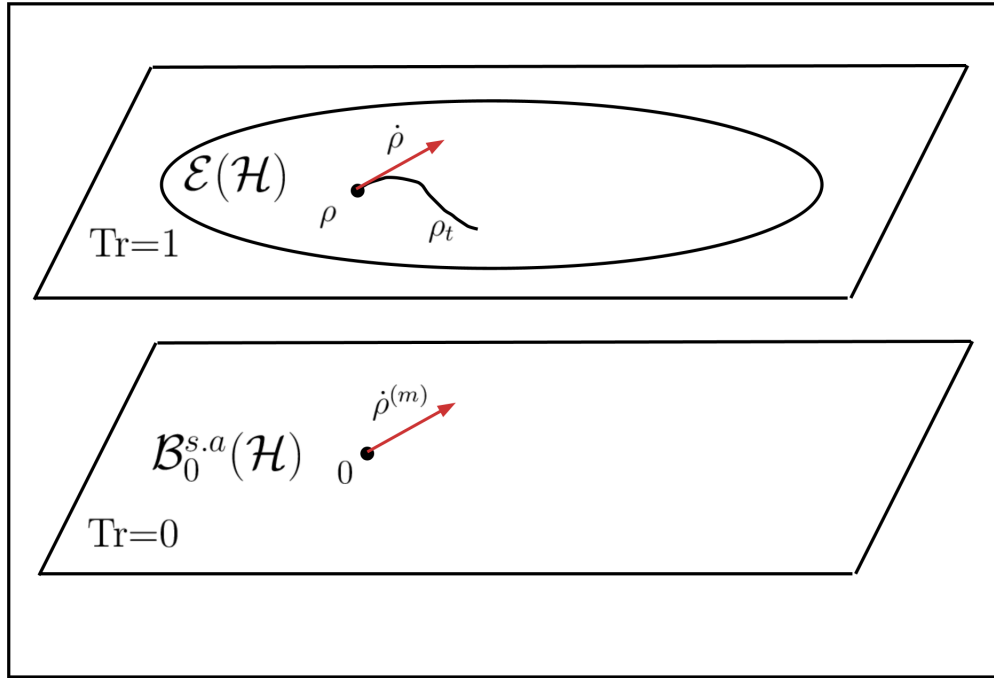


Figure 1.7: We can identify a tangent vector of a density operator in $\mathcal{E}(\mathcal{H})$ with a traceless density matrix which is in the space of bounded, traceless and self-adjoint operators, $\mathcal{B}_0^{s.a}$. This is done by “parallel transport” in the set $\mathcal{E}(\mathcal{H})$. This identification is called the mixture representation.

The scalar product will be given in terms of the eigenvectors $|k\rangle$ and eigenvalues p_k of ρ according to the spectral decomposition $\rho = \sum_k p_k |k\rangle \langle k|$. One can find,

$$\begin{aligned}\dot{A}(0)A(0) + AA(0)\dot{A}(0) &= \sqrt{\rho}d\rho\sqrt{\rho} \\ \ddot{A}(0)A(0) + 2\dot{A}(0)\dot{A}(0) + A(0)\ddot{A}(0) &= 0,\end{aligned}\tag{1.68}$$

From the first equation,

$$\langle k | \dot{A}(0) | l \rangle = \frac{\sqrt{p_l p_k}}{(p_l + p_k)} \langle k | d\rho | l \rangle .\tag{1.69}$$

In the second equation, multiplying by $A(0)^{-1}$ and taking the trace,

$$Tr(\ddot{A}(0)) = -Tr(\dot{A}(0)^2 A(0)^{-1}) = - \sum_{k,l=1}^n p_k^{-1} |\langle k | \dot{A}(0) | l \rangle|^2 = - \sum_{k,l=1} \frac{p_l |\langle k | d\rho | l \rangle|^2}{(p_k + p_l)^2},\tag{1.70}$$

where in the last step we have used (1.69).

With this results in mind, we return to the Bures distance and expand the term inside the trace until the second order, to get

$$d_B(\rho, \rho + t d\rho)^2 \approx 2 \left(1 - \text{Tr} \left(A(0) + \frac{t}{1!} \dot{A}(0) + \frac{t^2}{2!} \ddot{A}(0) + O[t^3] \right) \right). \quad (1.71)$$

We can see that

$$\begin{aligned} \text{Tr} A(0) &= \text{Tr} \rho = 1 \\ \text{Tr} \dot{A}(0) &= \text{Tr} d\rho = 0 \text{ because } d\rho \text{ is traceless.} \end{aligned} \quad (1.72)$$

In summary,

$$d_B(\rho, \rho + t d\rho)^2 = -\text{Tr}(\ddot{A}(0))t^2 + O[t^3]. \quad (1.73)$$

Thus, the tensor metric for a $A \in \mathcal{B}_0^{s.a}$,

$$(g_B)_\rho(A, A) = \frac{1}{2} \sum_{k,l} \frac{|\langle k | A | l \rangle|^2}{p_k + p_l}, \quad A \in \mathcal{B}_0^{s.a}, \rho > 0. \quad (1.74)$$

Using the polar identity we get the Riemannian inner product for A and B in $\mathcal{B}_0^{s.a}$,

$$\begin{aligned} (g_B)_\rho(A, B) &= \frac{1}{4} \left(g_\rho(A + B, A + B) - g_\rho(A - B, A - B) \right) && ; \text{ using polarization} \\ &= \frac{1}{8} \sum_{k,l} \frac{1}{p_l + p_k} \left(|\langle k | (A + B) | l \rangle|^2 - |\langle k | (A - B) | l \rangle|^2 \right) && ; \text{ from (1.74)} \\ &= \frac{1}{8} \sum_{k,l} \frac{1}{p_l + p_k} \left(4 \text{Re} \left(\overline{\langle k | A | l \rangle} \cdot \langle k | B | l \rangle \right) \right) && ; \text{ expanding factors} \\ &= \frac{1}{2} \text{Re} \left(\sum_{k,l} \frac{\overline{\langle k | A | l \rangle} \cdot \langle k | B | l \rangle}{p_l + p_k} \right) && ; \text{ changing } l \text{ for } k \\ (g_B)_\rho(A, B) &= \frac{1}{2} \sum_{k,l} \frac{\overline{\langle k | A | l \rangle} \cdot \langle k | B | l \rangle}{p_l + p_k}. && \end{aligned} \quad (1.75)$$

This inner product or the Bures inner product is very important in this work because this inner product will guide an initial state to a final one with the help of the geodesic between this two states.

1.6.4 Geodesic of the density matrices set

Geodesics in the set of density matrices comes from purifications. Being more explicit, if there is a geodesic between any pair of density matrices in $\mathcal{E}(\mathcal{H})$ there is a corresponding preimage in the Hilbert-Schmidt space \mathcal{W}^k , having the same length. We know that geodesics in \mathcal{W}^k are great circles then the geodesics in $\mathcal{E}(\mathcal{H})$ are projections of great circles.

Turning into a formula, the geodesic of density matrices ρ and σ in $\mathcal{E}(\mathcal{H})$ is given by (Howard N. Barnum 1998; Ericsson 2005, 2007):

$$\begin{aligned}\gamma(t) = & \left(\cos(t\theta_0) - \frac{\sin(t\theta_0)}{\tan(\theta_0)} \right)^2 \rho + \frac{\sin^2(t\theta_0)}{\sin^2 \theta_0} \sigma + \frac{\sin(t\theta_0)}{\sin \theta_0} \times \\ & \left(\cos(t\theta_0) - \frac{\sin(t\theta_0)}{\tan \theta_0} \right) \left(\sigma^{-1/2} (\sqrt{\sigma} \rho \sqrt{\sigma})^{1/2} \sigma^{1/2} + hc \right),\end{aligned}\quad (1.76)$$

where $\cos \theta_0 = \sqrt{F(\rho, \sigma)}$, hc is the transpose conjugate operation, $F(\rho, \sigma)$ is the fidelity (Spehner 2014; Jozsa 1994; Ericsson 2005), and t is a parameter between 0 and 1. The details of how this equation appears is not an easy task for an introduction, thus the reader can see appendix B.

Chapter 2

Methodology

In general terms, our methodology of steering an initial state is similar as methods like GRAPE, Krotov and CRAB. However, our function, as we will see in this chapter, that we want to maximize is the cosine of the angle between the time derivative of the geodesic $\dot{\gamma}(t)$ and the time evolution of a density matrix given by the Liouville-von Neumann equation. Keeping this general idea in mind our methodology stated as follows.

First, we need to select a Hamiltonian H or a set of Hamiltonians that will evolve the initial state ρ to the final one σ . The Hamiltonian H will depend on some real parameters $\{n_1, n_2, n_3, \dots\}$ which may depend or may not in time. These parameters will be chosen in order to maximize a function. Second, the function is the cosine of α given by the Bures inner product (1.75):

$$\cos(\alpha) = \frac{g_B(\dot{\gamma}(0), \dot{\rho}(0))}{\|\dot{\gamma}(0)\| \times \|\dot{\rho}(0)\|}, \quad (2.1)$$

where $\dot{\gamma}(t)$ is the derivative of the geodesic, $\dot{\rho}(t) = -i[H; \rho]$ is the Liouville-von Neumann equation. The norm $\|\cdot\|$ is the square root of the Bures inner product. Every term in the equation is evaluated at $t = 0$, thus $\rho(0) = \rho$ the initial state. We set the optimization at $t = 0$ because we need to be sure that both vectors be at the same point on the sphere.

Third, having the parameters $\{n_1, n_2, n_3, \dots\}$ that maximize $\cos \alpha$, these will be introduced into the evolution operator U which will evolve our initial state ρ for a small time Δt . The evolution operator will be given by the Hamiltonian H . Then, we have a new

initial state ρ' , this will be the new initial state to proceed to a new maximization of $\cos \alpha$ with new parameters $\{n_1, n_2, n_3, \dots\}$, as we can see in Fig. 2.1. Finally, when we are close to the desired state we finish the optimization algorithm.

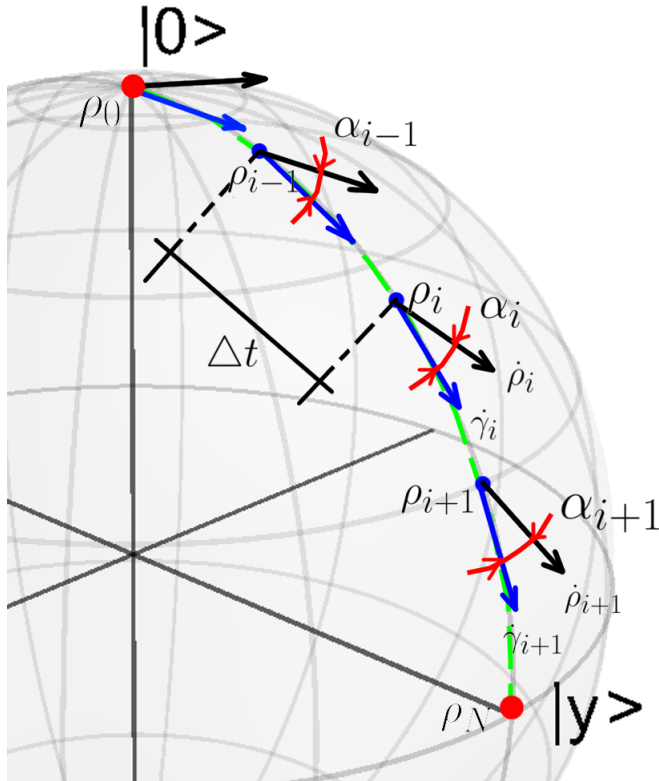


Figure 2.1: Schematic representation of our methodology. In the graph, we represent the step i of our method where $\dot{\gamma}_i$ is the time derivative of the geodesic, $\dot{\rho}_i$ is the evolution of the state ρ_i given by the Liouville-von Neumann equation, α_i is the angle that we want to optimize in order to find the direction of the final state given by $|\phi_2\rangle$, $|\psi_i\rangle = U(n_x, n_y, \dots, \Delta t) |\psi_{i-1}\rangle$, $\rho_0 = |\psi_1\rangle \langle \psi_1|$ is the initial state given as an input, $\rho_N = |\psi_N\rangle \langle \psi_N|$ is the final state given by our methodology. $|0\rangle$ represents the north pole and $|y\rangle$ is $|y_+\rangle$ on the Bloch sphere, and are plotted just for reference.

As we will see in the following, there are some subtleties that we need to address in order to accomplish the methodology.

2.1 Model

Following (Wagh & Rakhecha 2001; Cong 2014), we have chosen the form of the Hamiltonian as a linear combination of Pauli matrices, like

$$H = -\frac{w_0}{2}\sigma_z + \frac{n_x}{2}\sigma_x + \frac{n_y}{2}\sigma_y + \frac{n_z}{2}\sigma_z, \quad (2.2)$$

where $\hbar = 1$, n_x , n_y , n_z are real coefficients, in general are time dependent, that one has to tune in order to get the final state and σ_i with $i = x, y, z$ are Pauli matrices. However, we can set $n_z = 0$ having in mind that an universal quantum gates set can be given by σ_x , σ_y for a single qubit. Also from the experimental view, adding another control field can lead to a greater error in the fidelity function. Thus, we can work with

$$H = -\frac{w_0}{2}\sigma_z + \frac{n_x}{2}\sigma_x + \frac{n_y}{2}\sigma_y, \quad (2.3)$$

At first, we started working with the Hamiltonian given by (Cong 2014) where,

$$\begin{aligned} \frac{n_x}{2} &= -\frac{\hbar\Omega}{2} \cos(wt + \beta) \\ \frac{n_y}{2} &= \frac{\hbar\Omega}{2} \sin(wt + \beta). \end{aligned} \quad (2.4)$$

This was done because we have already a defined evolution operator, given by (1.17) with $\hbar = 1$ and at resonance $w = w_0$:

$$U(t) = \begin{bmatrix} e^{i\frac{tw_0}{2}} \cos\left(\frac{\Omega t}{2}\right) & ie^{i\frac{tw_0+2\beta}{2}} \sin\left(\frac{\Omega t}{2}\right) \\ ie^{-i\frac{(w_0t+2\beta)}{2}} \sin\left(\frac{\Omega t}{2}\right) & e^{-i\frac{tw_0}{2}} \cos\left(\frac{\Omega t}{2}\right) \end{bmatrix} \quad (2.5)$$

However, as we are working with Pauli matrices, we can use (2.2) with n_x , n_y and n_z (here we “turn on” the control field in z -axis and gain another control parameter) being constant and using Pauli matrices exponentiation given by,

$$e^{ia(\hat{n} \cdot \vec{\sigma})} = I \cos(a) + i(\hat{n} \cdot \vec{\sigma}) \sin(a), \quad (2.6)$$

for $\vec{a} = a\hat{n}$ and $|\hat{n}| = 1$. Thus, using (2.3), we find that

$$\begin{aligned} a &= tb = t\sqrt{\frac{(-w_0 + n_z)^2}{4} + \frac{n_x^2}{4} + \frac{n_y^2}{4}} \\ \hat{n} \cdot \vec{\sigma} &= \frac{1}{b} \left(\frac{-w_0 + n_z}{2} \sigma_z + \frac{n_x}{2} \sigma_x + \frac{n_y}{2} \sigma_y \right), \end{aligned} \quad (2.7)$$

with $b = \sqrt{\frac{(-w_0 + n_z)^2}{4} + \frac{n_x^2}{4} + \frac{n_y^2}{4}}$ and also we need to change the sign of the i in (2.6) by $-i$.

It is important to notice that all the reckons we are going to show were made with (2.4), but we are going to present results from both Hamiltonians, using (2.4) and (2.3). Another term which we need is the time derivative of the geodesic (1.76) which is straightforward,

$$\begin{aligned} \dot{\gamma}(t) &= \theta_0 \csc^2(\theta_0) \left(\left(\sigma^{-1/2} (\sqrt{\sigma} \rho \sqrt{\sigma})^{1/2} \sigma^{1/2} + hc \right) \times \sin((1 - 2t)\theta_0) \right. \\ &\quad \left. + \rho \sin(2(-1 + t)\theta_0) + \sigma \sin(2t\theta_0) \right). \end{aligned} \quad (2.8)$$

Next, we need to focus on the states. As we know there are two types: pure and mixed states. In the following, we are going to focus on pure states because the procedure for mixed is simpler regarding the reckons but the procedure is the same.

For pure states we have to make some modifications in the geodesic equation and in its derivative. Pure states are rank one matrices which are not invertible and we need invertible matrices in (1.76) and (2.8). To solve this problem, we need to use the polar decomposition.

Let be $\rho_\psi = |\psi\rangle\langle\psi|$ and $\sigma_\phi = |\phi\rangle\langle\phi|$ pure states. Then $\sqrt{\sigma_\phi} = \sigma_\phi = \sigma_\phi^2 = |\phi\rangle\langle\phi|$ and the same for $\sqrt{\rho_\psi} = \rho_\psi$. Setting $\rho_\psi = \rho$ and $\sigma_\phi = \sigma$, here comes the trick using polar decomposition.

We need to check if the following term is correct,

$$\sigma^{-1/2} (\sqrt{\sigma} \rho \sqrt{\sigma})^{1/2} \sqrt{\sigma} = \sqrt{\rho} U \sqrt{\sigma} \quad (2.9)$$

where U is a unitary matrix.

From the polar decomposition and taking the adjoint, we can get

$$\sqrt{\rho} \sqrt{\sigma} = U |\sqrt{\rho} \sqrt{\sigma}| \Rightarrow \sqrt{\sigma} \sqrt{\rho} = |\sqrt{\rho} \sqrt{\sigma}| U^* \quad (2.10)$$

then the last equation can be modified as

$$\begin{aligned}
 |\sqrt{\rho}\sqrt{\sigma}| &= \sqrt{(\sqrt{\rho}\sqrt{\sigma})^*(\sqrt{\rho}\sqrt{\sigma})} && ; \text{definition of } |A| = \sqrt{A^*A} \\
 &= \sqrt{\sqrt{\sigma}\rho\sqrt{\sigma}} \\
 &= \sqrt{(|\phi\rangle\langle\phi|)|\psi\rangle\langle\psi|(|\phi\rangle\langle\phi|)} && ; \text{pure states } \rho \text{ and } \sigma \\
 &= |\langle\phi|\psi\rangle||\phi\rangle\langle\phi|
 \end{aligned} \tag{2.11}$$

Now, we replace pure states and the last equation in (2.10) and pull out the term $U|\phi\rangle$ to get

$$\begin{aligned}
 |\psi\rangle\langle\psi||\phi\rangle\langle\phi| &= |\langle\phi|\psi\rangle|U|\phi\rangle\langle\phi| && ; \text{factor out the desired term} \\
 U|\phi\rangle &= \frac{\langle\psi|\phi\rangle}{|\langle\psi|\phi\rangle|}|\psi\rangle && ; \text{with } \langle\psi|\phi\rangle \neq 0
 \end{aligned} \tag{2.12}$$

Also from the first equation of (2.10), we notice that we can have

$$\begin{aligned}
 \sqrt{\sigma}\sqrt{\rho}U &= \sqrt{\sqrt{\sigma}\rho\sqrt{\sigma}} && ; \text{multiplying from the left by } \sigma^{-1/2} \text{ and from the right by } \sigma^{1/2} \\
 \sqrt{\rho}U\sqrt{\sigma} &= \sigma^{-1/2}\sqrt{\sqrt{\sigma}\rho\sqrt{\sigma}}\sqrt{\sigma} && ; \text{we arrived at (2.9).}
 \end{aligned} \tag{2.13}$$

Thus, now we can work with pure states which are not invertibles. With this in mind,

$$\begin{aligned}
 \sigma^{-1/2}\sqrt{\sqrt{\sigma}\rho\sqrt{\sigma}}\sqrt{\sigma} &= \sqrt{\rho}U\sqrt{\sigma} && ; \text{from last result} \\
 &= |\psi\rangle\langle\psi|U|\phi\rangle\langle\phi| && ; \text{replace (2.12)} \\
 &= \frac{\langle\psi|\phi\rangle}{|\langle\psi|\phi\rangle|}|\psi\rangle\langle\phi| && ; \text{with } \langle\psi|\phi\rangle \neq 0
 \end{aligned} \tag{2.14}$$

Finally, the geodesic in the case for pure states is given by:

$$\gamma(t) = \left(\cos\theta_0 t - \frac{\sin\theta_0 t}{\tan\theta_0} \right)^2 |\psi\rangle\langle\psi| + \frac{\sin^2\theta_0 t}{\sin^2\theta_0} |\phi\rangle\langle\phi| + \frac{\sin\theta_0 t}{\sin\theta_0} \left(\cos\theta_0 t - \frac{\sin\theta_0 t}{\tan\theta_0} \right) \left(\frac{\langle\psi|\phi\rangle}{|\langle\psi|\phi\rangle|} |\psi\rangle\langle\phi| + hc \right), \tag{2.15}$$

notice that $\langle\psi|\phi\rangle$ gives a phase factor $e^{i\delta}$ with $\delta = \text{Arg } \langle\psi|\phi\rangle$ and if $t = 0$, we get the initial state $|\psi\rangle\langle\psi|$ and at $t = 1$, we get the final state $|\phi\rangle\langle\phi|$. An important property of the last equation is that $\gamma(t)$ is a pure state, since

$$\begin{aligned}
 \gamma(t)^2 &= |\psi\rangle\langle\psi| (A^4 + 2|\langle\psi|\phi\rangle| A^3 B + B^2 A^2) \\
 &\quad + |\phi\rangle\langle\phi| (B^4 + 2|\langle\psi|\phi\rangle| AB^3 + B^2 A^2) \\
 &\quad + |\psi\rangle\langle\phi| (2A^2 B^2 \langle\psi|\phi\rangle + A^3 B \frac{\langle\psi|\phi\rangle}{|\langle\psi|\phi\rangle|} + AB^3 \frac{\langle\psi|\phi\rangle}{|\langle\psi|\phi\rangle|} + B^2 A^2 \langle\psi|\phi\rangle) \\
 &\quad + |\phi\rangle\langle\psi| (2A^2 B^2 \langle\phi|\psi\rangle + AB^3 \frac{\langle\phi|\psi\rangle}{|\langle\phi|\psi\rangle|} + AB^3 \frac{\langle\phi|\psi\rangle}{|\langle\phi|\psi\rangle|} + B^2 A^2 \langle\phi|\psi\rangle) \\
 &= A^2 |\psi\rangle\langle\psi| + B^2 |\phi\rangle\langle\phi| + \frac{AB}{|\langle\psi|\phi\rangle|} \left(\langle\psi|\phi\rangle |\psi\rangle\langle\phi| + \langle\phi|\psi\rangle |\phi\rangle\langle\psi| \right) \\
 &= \gamma(t),
 \end{aligned} \tag{2.16}$$

with

$$A = \left(\cos \theta_0 t - \frac{\sin \theta_0 t}{\tan \theta_0} \right) \quad \text{and} \quad B = \frac{\sin \theta_0 t}{\sin \theta_0}. \tag{2.17}$$

Then from (2.15), the derivative is given by,

$$\begin{aligned}
 \dot{\gamma}(t) &= \theta_0 \csc^2 \theta_0 \left(\left(\frac{\langle\psi|\phi\rangle}{|\langle\psi|\phi\rangle|} |\psi\rangle\langle\phi| + hc \right) \times \sin(1-2t)\theta_0 \right. \\
 &\quad \left. + |\psi\rangle\langle\psi| \sin(2(-1+t)\theta_0) + |\phi\rangle\langle\phi| \sin(2t\theta_0) \right)
 \end{aligned} \tag{2.18}$$

If $t = 0$, we get one of the important equations of this work,

$$\dot{\gamma}(0) = \theta_0 \csc^2 \theta_0 \left(\left(\frac{\langle\psi|\phi\rangle}{|\langle\psi|\phi\rangle|} |\psi\rangle\langle\phi| + hc \right) \times \sin \theta_0 - |\psi\rangle\langle\psi| \sin(2\theta_0) \right), \tag{2.19}$$

where $|\psi\rangle$ is the initial state, $|\phi\rangle$ is the final one and θ_0 is related to the fidelity of the states.

Notice that for mixed states (2.8) is correct and we just need to plug the term in the inner product.

Another term that we need to look in detail is the inner product between the time derivative of the geodesic given by the equation (2.19) and time evolution of a state given by the Liouville-von Neumann equation given by $\dot{\rho}(0) = -i[H, \rho(0)]$. In the following reckons we will not yet introduce our Hamiltonian. Let $\{|\psi_l\rangle, l = 0, 1, \dots\}$ be

an orthonormal basis of the Hilbert space such that $|\psi_0\rangle = |\psi\rangle$, then

$$\begin{aligned}
 g_B(\gamma(0), \rho(0)) &= \frac{1}{2} \sum_{k,l} \frac{\overline{\langle k | \gamma(0) | l \rangle} \langle k | \rho(0) | l \rangle}{p_k + p_l}; \text{ with } p_k + p_l > 0 \\
 &= \frac{i}{2} \sum_{\substack{k, l \\ p_k + p_l > 0}} \frac{\overline{\langle k | \gamma(0) | l \rangle} \langle k | H(0) | l \rangle (p_k - p_l)}{p_k + p_l} \\
 &= \frac{i}{2} \left(\sum_{l>1} \overline{\langle \psi | \gamma(0) | \psi_l \rangle} \langle \psi | H(0) | \psi_l \rangle (1) + \sum_{k>1} \overline{\langle \psi_k | \gamma(0) | \psi \rangle} \langle \psi_k | H(0) | \psi \rangle (-1) \right) \\
 &= \frac{i}{2} \left(\sum_{l>1} \overline{\langle \psi | \gamma(0) | \psi_l \rangle} \langle \psi | H(0) | \psi_l \rangle - \sum_{l>1} \overline{\langle \psi | \gamma(0) | \psi_l \rangle} \langle \psi | H(0) | \psi_l \rangle \right) \\
 &= -Im \left(\sum_{l>1} \overline{\langle \psi | \gamma(0) | \psi_l \rangle} \langle \psi | H(0) | \psi_l \rangle \right) \\
 &= -Im \left(\sum_{l>1} \langle \psi | H(0) | \psi_l \rangle \langle \psi_l | \gamma(0) | \psi \rangle \right) \\
 &= -Im \left(\langle \psi | H(0) \left(I - |\psi\rangle\langle\psi| \right) \gamma(0) | \psi \rangle \right) \\
 &= -Im \left(\langle \psi | H(0) \gamma(0) | \psi \rangle - \langle \psi | H(0) | \psi \rangle \langle \psi | \gamma(0) | \psi \rangle \right) \\
 &= -Im \left(\langle \psi | H(0) \gamma(0) | \psi \rangle \right),
 \end{aligned} \tag{2.20}$$

in these last reckons we used the following: the Liouville-von Neumann quantum equation $\dot{\rho} = -i[H, \rho]$, knowing that $|l\rangle$ and $|k\rangle$ are eigenvectors of ρ we get the factor $(p_l - p_k)$, we have expanded both \sum in two parts, one that has $|\psi\rangle$ as eigenvector with eigenvalue different from zero (it is equal to 1) and $|\psi_l\rangle$ as eigenvectors with eigenvalues equal to zero (we can do this because ρ is a pure state) but we need to be careful with the condition $p_k + p_l > 0$ which makes that one term does not contribute in each \sum , also we use $|\psi\rangle\langle\psi| + \sum |\psi_l\rangle\langle\psi_l| = I$ and finally the term $\langle\psi | H(0) | \psi \rangle \langle \psi | \gamma(0) | \psi \rangle$ vanish due to the fact that it belongs to \mathbb{R} and we want the imaginary part.

Finally, the last factor can be achieved using (2.19),

$$\langle \psi | H(0) \dot{\gamma}(0) | \psi \rangle = \theta_0 \csc^2(\theta_0) \left(\left(|\langle \psi | \phi \rangle| \langle \psi | H | \psi \rangle + \frac{\overline{\langle \psi | \phi \rangle}}{|\langle \psi | \phi \rangle|} \langle \psi | H | \phi \rangle \right) \sin \theta_0 - \langle \psi | H | \psi \rangle \sin 2\theta_0 \right), \quad (2.21)$$

replacing this in (2.20) and noting that $\langle \psi | H | \psi \rangle$ vanish when we take the imaginary part, we finally get

$$g_B(\dot{\gamma}(0), \dot{\rho}(0)) = \frac{-\theta_0}{|\langle \psi | \phi \rangle| \sin \theta_0} \operatorname{Im} \left(\langle \psi | H | \phi \rangle \overline{\langle \psi | \phi \rangle} \right). \quad (2.22)$$

With this result we are almost ready to get the maximum of our objective function.

2.1.1 The objective function $\cos \alpha$ and its maximum

In the above section, we have arrived to some parts of our objective function but there are some missing details to fix until we finish and proceed to present our algorithm of state to state transfer. As we can see our main goal in this section is to maximize

$$\cos(\alpha) = \frac{g_B(\dot{\gamma}(0), \dot{\rho}(0))}{\|\dot{\gamma}(0)\| \times \|\dot{\rho}(0)\|} \quad (2.23)$$

where $\gamma(0)$ is the geodesic of the quantum states, ρ is a density matrices, $\dot{\gamma}(0)$ is the time derivative of the geodesic and it is a vector of the tangent space of $\mathcal{B}(\mathcal{H})$, $\dot{\rho}(0) = -i[H(0), \rho(0)]$, $\cos(\alpha)$ is the angle between the two vectors as we can see in Fig. 2.1, g_B is the Bures inner product and $\|\cdot\|$ is the norm given by the same inner product. In the following, we want to use general pure states and get the results for each term in the objective function $\cos \alpha$. We will start with the reckon of $g_B(\dot{\gamma}(0), \dot{\rho}(0))$ next the terms in the denominator of the objective function.

We want to calculate the inner product g_B using the most general states. Given two states: initial and final states, $|\psi_1\rangle$ and $|\phi_2\rangle$, respectively. The subindices 1 and 2 are just for denoting which is the initial state “1” and the final state “2”,

$$\begin{aligned} |\psi_1\rangle &= \cos\left(\frac{\theta_1}{2}\right) |0\rangle + \sin\left(\frac{\theta_1}{2}\right) e^{i\phi_1} |1\rangle \\ |\phi_2\rangle &= \cos\left(\frac{\theta_2}{2}\right) |0\rangle + \sin\left(\frac{\theta_2}{2}\right) e^{i\phi_2} |1\rangle \end{aligned} \quad (2.24)$$

Also, we want to use a general Hamiltonian¹ for the system which is composed of two parts, the controlled or free Hamiltonian H_0 and the control Hamiltonian H_c , given by equation (2.3) with (2.4).

With this information, we want to solve the inner product (2.22) which is in the numerator of (2.23); thus, we need the following terms

$$\begin{aligned} \langle \phi_2 | \psi_1 \rangle &= \cos(\theta_1/2) \cos(\theta_2/2) + e^{i(\phi_1 - \phi_2)} \sin(\theta_1/2) \sin(\theta_2/2) \\ \langle \psi_1 | H(0) | \phi_2 \rangle &= \frac{1}{2} e^{-i(\beta + \phi_1)} \left(-\sin(\theta_1/2) \left(\Omega \cos(\theta_2/2) - e^{i(\beta + \phi_2)} w_0 \sin(\theta_2/2) \right) \right. \\ &\quad \left. - e^{i(\beta + \phi_1)} \cos(\theta_1/2) \left(w_0 \cos(\theta_2/2) + e^{i(\beta + \phi_2)} \Omega \sin(\theta_2/2) \right) \right). \end{aligned} \quad (2.25)$$

Now, θ_0 is related to the fidelity of the states $\cos \theta_0 = \sqrt{|\langle \psi_1 | \phi_2 \rangle|^2}$,

$$\cos \theta_0 = |\langle \psi_1 | \phi_2 \rangle| = \sqrt{\frac{1}{2} \left(1 + \cos \theta_1 \cos \theta_2 + \cos(\phi_1 - \phi_2) \sin \theta_1 \sin \theta_2 \right)}, \quad (2.26)$$

and

$$\sin \theta_0 = |\langle \psi_{1\perp} | \phi_2 \rangle| = \sqrt{\frac{1}{2} \left(1 - \cos \theta_1 \cos \theta_2 - \cos(\phi_1 - \phi_2) \sin \theta_1 \sin \theta_2 \right)}, \quad (2.27)$$

this last equation comes from the Pythagorean's theorem and $\cos \theta_0$, then we recognize that the result of $\sin \theta_0$ is the same as $|\langle \psi_{1\perp} | \phi_2 \rangle|$, where $|\psi_{1\perp}\rangle$ is given by

$$|\psi_{1\perp}\rangle = \sin(\theta_1/2) |0\rangle - e^{i\phi_1} \cos(\theta_1/2) |1\rangle. \quad (2.28)$$

Thus, for the inner product g_B we have

$$g_B(\dot{\gamma}(0), \dot{\rho}(0)) = \frac{-\theta_0}{\cos \theta_0 \sin \theta_0} \text{Im} \left(\langle \psi_1 | H | \phi_2 \rangle \langle \phi_2 | \psi_1 \rangle \right), \quad (2.29)$$

where we need to take the imaginary part of the product $\langle \psi_1 | H | \phi_2 \rangle$ and $\langle \phi_2 | \psi_1 \rangle$ given by (2.25). We have the numerator part of our objective function.

¹We follow (Cong 2014) but the reckons can be done by (2.3)

Another term is the norm of $\dot{\gamma}(0)$ given by,

$$\|\dot{\gamma}(0)\|^2 = g_B(\dot{\gamma}(0), \dot{\gamma}(0)) = \frac{1}{2} \sum_{k,l} \frac{|\langle k | \dot{\gamma}(0) | l \rangle|^2}{p_k + p_l}, \quad (2.30)$$

in terms of the eigenvalues and vectors of $\gamma(0) = |\psi_1\rangle\langle\psi_1|$, which are: $p_1 = 1$ and its eigenvector $|\psi_1\rangle$ and $p_2 = 0$ and its eigenvector $|\psi_{1\perp}\rangle$ given by (2.28),

$$\begin{aligned} \frac{1}{2} \sum_{k,l} \frac{|\langle k | \dot{\gamma}(0) | l \rangle|^2}{p_k + p_l} &= \frac{1}{2} \left(\sum_k \frac{|\langle k | \dot{\gamma}(0) | \psi_1 \rangle|^2}{p_k + 1} + \sum_k \frac{|\langle k | \dot{\gamma}(0) | \psi_{1\perp} \rangle|^2}{p_k} \right); \text{ with } p_1 + p_{1\perp} \neq 0 \\ &= \frac{1}{2} \left(\frac{|\langle \psi_1 | \dot{\gamma}(0) | \psi_1 \rangle|^2}{2} + 2 |\langle \psi_{1\perp} | \dot{\gamma}(0) | \psi_1 \rangle|^2 \right), \end{aligned} \quad (2.31)$$

to solve the last equation we need the following results

$$\begin{aligned} \langle \psi_1 | \psi_1 \rangle \langle \phi_2 | \psi_1 \rangle &= \langle \phi_2 | \psi_1 \rangle \\ \langle \psi_1 | \phi_2 \rangle \langle \psi_1 | \psi_1 \rangle &= \langle \psi_1 | \phi_2 \rangle \\ \langle \psi_1 | \psi_1 \rangle \langle \psi_1 | \psi_1 \rangle &= 1 \\ \langle \psi_{1\perp} | \psi_1 \rangle \langle \phi_2 | \psi_1 \rangle &= 0 \\ \langle \psi_{1\perp} | \phi_2 \rangle \langle \psi_1 | \psi_1 \rangle &= \langle \psi_{1\perp} | \phi_2 \rangle \\ \langle \psi_{1\perp} | \psi_1 \rangle \langle \psi_1 | \psi_1 \rangle &= 0, \end{aligned} \quad (2.32)$$

replacing $\dot{\gamma}(0)$ given by (2.19) in (2.31), we need again the following results

$$\begin{aligned} \langle \psi_1 | \dot{\gamma}(0) | \psi_1 \rangle &= \theta_0 \csc^2 \theta_0 \left(2 |\langle \psi_1 | \phi_2 \rangle| \sin \theta_0 - \sin(2\theta_0) \right) \\ &= \theta_0 \csc^2 \theta_0 \left(2 \cos \theta_0 \sin \theta_0 - \sin(2\theta_0) \right); \text{ using the } \cos \theta_0 = \sqrt{F(|\psi_1, \phi_2\rangle)} \\ &= 0; \text{ the term in parenthesis is zero} \\ \langle \psi_{1\perp} | \dot{\gamma}(0) | \psi_1 \rangle &= \theta_0 \csc^2 \theta_0 \left(\frac{\langle \phi_2 | \psi_1 \rangle}{|\langle \psi_1 | \phi_2 \rangle|} \langle \psi_{1\perp} | \phi_2 \rangle \right) \sin \theta_0. \end{aligned} \quad (2.33)$$

Now, replacing the last results in (2.31),

$$\begin{aligned} \frac{1}{2} \sum_{k,l} \frac{|\langle k | \dot{\gamma}(0) | l \rangle|^2}{p_k + p_l} &= \frac{1}{4} \theta_0^2 \csc^4 \theta_0 \frac{|\langle \phi_2 | \psi_1 \rangle|^2 |\langle \psi_{1\perp} | \phi_2 \rangle|^2 \sin^2 \theta_0}{|\langle \psi_1 | \phi_2 \rangle|^2} \\ \|\dot{\gamma}(0)\|^2 &= \theta_0^2; \text{ simplifying and } |\langle \psi_{1\perp} | \phi_2 \rangle| = \sin \theta_0. \end{aligned} \quad (2.34)$$

The last term that we need is $\|\dot{\rho}(0)\|$, which is given by

$$\begin{aligned}
 \|\dot{\rho}(0)\|^2 &= \frac{1}{2} \sum_{k,l} \frac{|\langle k | \dot{\rho}(0) | l \rangle|^2}{p_k + p_l} \\
 &= \frac{1}{2} \sum_k \frac{|\langle k | \dot{\rho}(0) | \psi_1 \rangle|^2}{p_k + 1} + \sum_k \frac{|\langle k | \dot{\psi}(0) | \psi_{1\perp} \rangle|^2}{p_k} \\
 &= \frac{1}{2} \left(\frac{|\langle \psi_1 | \dot{\rho}(0) | \psi_1 \rangle|^2}{2} + |\langle \psi_{1\perp} | \dot{\rho}(0) | \psi_1 \rangle|^2 + |\langle \psi_1 | \dot{\rho}(0) | \psi_{1\perp} \rangle|^2 \right) \\
 &= \frac{1}{2} \left(\frac{|\langle \psi_1 | \dot{\rho}(0) | \psi_1 \rangle|^2}{2} + 2 |\langle \psi_1 | \dot{\rho}(0) | \psi_{1\perp} \rangle|^2 \right).
 \end{aligned} \tag{2.35}$$

Now, notice that

$$\langle \psi_1 | -i[H(0), \dot{\rho}(0)] | \psi_1 \rangle = 0, \tag{2.36}$$

thus

$$\begin{aligned}
 \|\dot{\rho}(0)\|^2 &= |\langle \psi_1 | \dot{\rho}(0) | \psi_{1\perp} \rangle|^2 \\
 &= \frac{1}{4} \left((\Omega \cos \theta_1 \cos(\beta + \phi_1) - w_0 \sin \theta_1)^2 + \Omega^2 \sin^2(\beta + \phi_1) \right)
 \end{aligned} \tag{2.37}$$

In summary,

- The objective function is given by,

$$\frac{g_B(\dot{\psi}(0), \dot{\rho}(0))}{\|\dot{\psi}(0)\| \times \|\dot{\rho}(0)\|} = \frac{-\text{Im} \left(\langle \psi_1 | H(0) | \phi_2 \rangle \langle \phi_2 | \psi_1 \rangle \right)}{\frac{\cos \theta_0 \sin \theta_0}{2} \sqrt{\left((\Omega \cos \theta_1 \cos(\beta + \phi_1) - w_0 \sin \theta_1)^2 + \Omega^2 \sin^2(\beta + \phi_1) \right)}}, \tag{2.38}$$

with

$$\begin{aligned}
 \langle \phi_2 | \psi_1 \rangle &= \cos(\theta_1/2) \cos(\theta_2/2) + e^{i(\phi_1 - \phi_2)} \sin(\theta_1/2) \sin(\theta_2/2) \\
 \langle \psi_1 | H(0) | \phi_2 \rangle &= \frac{1}{2} e^{-i(\beta + \phi_1)} \left(-\sin(\theta_1/2) \left(\Omega \cos(\theta_2/2) - e^{i(\beta + \phi_2)} w_0 \sin(\theta_2/2) \right) \right. \\
 &\quad \left. - e^{i(\beta + \phi_1)} \cos(\theta_1/2) \left(w_0 \cos(\theta_2/2) + e^{i(\beta + \phi_2)} \Omega \sin(\theta_2/2) \right) \right).
 \end{aligned} \tag{2.39}$$

and

$$\cos \theta_0 = |\langle \psi_1 | \phi_2 \rangle| = \sqrt{\frac{1}{2} \left(1 + \cos \theta_1 \cos \theta_2 + \cos(\phi_1 - \phi_2) \sin \theta_1 \sin \theta_2 \right)}, \tag{2.40}$$

and

$$\sin \theta_0 = |\langle \psi_{1\perp} | \phi_2 \rangle| = \sqrt{\frac{1}{2} \left(1 - \cos \theta_1 \cos \theta_2 - \cos(\phi_1 - \phi_2) \sin \theta_1 \sin \theta_2 \right)}, \quad (2.41)$$

We summarized what we want and all the equations in the following diagram

We want to maximize: $\cos(\alpha) = \frac{g_B(\dot{\gamma}(0), \dot{\rho}(0))}{\|\dot{\gamma}(0)\| \times \|\dot{\rho}(0)\|}$

Where γ is the geodesic and ρ is the density matrix of the Liouville-von Neumann equation g_B is the metric of the tangent space of the density matrices

What we know

$$|\psi_1\rangle = \cos\left(\frac{\theta_1}{2}\right)|0\rangle + \sin\left(\frac{\theta_1}{2}\right)e^{i\phi_1}|1\rangle$$

Initial state: θ_1 and ϕ_1 are given

$$|\phi_2\rangle = \cos\left(\frac{\theta_2}{2}\right)|0\rangle + \sin\left(\frac{\theta_2}{2}\right)e^{i\phi_2}|1\rangle$$

Final state: θ_2 and ϕ_2 are given

A Hamiltonian is given: σ_i are Pauli matrices and w_0 natural frequency

$$H(t) = H_0 + H_c(t) = -\frac{\hbar w_0}{2}\sigma_z - \frac{\hbar\Omega}{2}\cos(w_0t + \beta)\sigma_x + \frac{\hbar\Omega}{2}\sin(w_0t + \beta)\sigma_y$$

$$U(t) = \begin{bmatrix} e^{i\frac{tw_0}{2}}\cos\left(\frac{\Omega t}{2}\right) & ie^{i\frac{tw_0+2\beta}{2}}\sin\left(\frac{\Omega t}{2}\right) \\ ie^{-i\frac{(w_0t+2\beta)}{2}}\sin\left(\frac{\Omega t}{2}\right) & e^{-i\frac{tw_0}{2}}\cos\left(\frac{\Omega t}{2}\right) \end{bmatrix}$$

The evolution operator associated to the Hamiltonian

$$\frac{g_B(\dot{\gamma}(0), \dot{\rho}(0))}{\|\dot{\gamma}(0)\| \times \|\dot{\rho}(0)\|} = \frac{-Im\left(\langle\psi_1|H(0)|\phi_2\rangle\langle\phi_2|\psi_1\rangle\right)}{\frac{\cos\theta_0\sin\theta_0}{2}\sqrt{\left((\Omega\cos\theta_1\cos(\beta+\phi_1) - w_0\sin\theta_1)^2 + \Omega\sin^2(\beta+\phi_1)\right)}},$$

The objective function

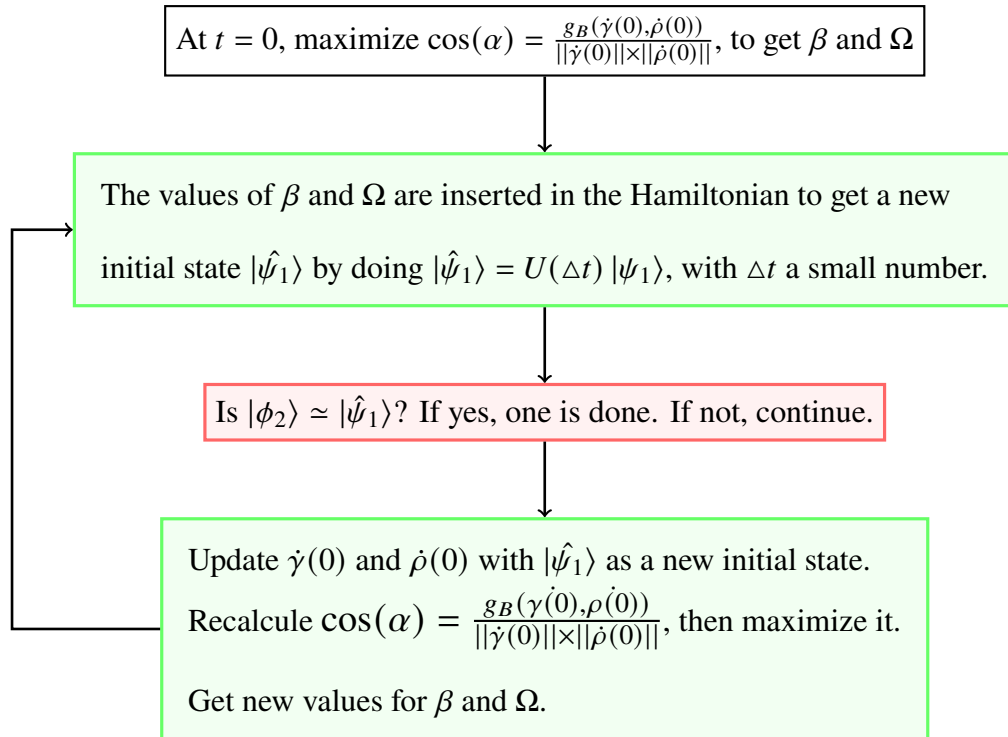
$$\begin{aligned} \cos\theta_0 &= |\langle\psi_1|\phi_2\rangle| \\ \sin\theta_0 &= |\langle\psi_{1\perp}|\phi_2\rangle| \end{aligned}$$

What we do not know:
 β and Ω

The variables in the Hamiltonian β and Ω are given by the control field or control Hamiltonian H_c

2.1.2 State to state transfer: pure states procedure

The following diagram is our methodology or algorithm of steering a given initial pure state to a given final pure state:



We are going to follow (Khaneja et al. 2005) to set Δt in terms of w_0 the natural frequency of the system. If w_0 is 1 Hz, Δt is in the order of 0.0025s. We finish the algorithm when

$$1 - |\langle \hat{\psi}_1 | \phi_2 \rangle| < 0.01, \quad (2.42)$$

which is very conservative value due to the fact that the methods reviewed in the introduction can achieve values less than $\times 10^{-5}$.

Finally, we need to add an experimental constrain in the control amplitude parameters in order to preserve the two level quantum system (Abraham et al. 2019). In the case using (2.4), this constrain is given by,

$$-w_0 \leq \Omega \leq w_0, \quad (2.43)$$

this prevents that the system will be exited to other greater levels like, $|2\rangle$ or $|3\rangle$, etc. In the case for (2.2),

$$-w_0 \leq n_x \leq w_0, -w_0 \leq n_y \leq w_0, -w_0 \leq n_z \leq w_0. \quad (2.44)$$

2.1.3 State to state transfer for mixed states

As we mentioned early, the procedure for mixed states is not difficult; however, we need to present the details for this procedure. At first, we need to prepare out the initial and final states. In order to do this, we need a convex sum using pure states. Thus, the following set of pure states will help us to get our mixed states

$$\left\{ \begin{array}{l} |0\rangle\langle 0| = \begin{bmatrix} 1 & 0 \\ 0 & 0 \end{bmatrix}, |1\rangle\langle 1| = \begin{bmatrix} 0 & 0 \\ 0 & 1 \end{bmatrix}, |x_+\rangle\langle x_+| = \frac{1}{2} \begin{bmatrix} 1 & 1 \\ 1 & 1 \end{bmatrix}, \\ |x_-\rangle\langle x_-| = \frac{1}{2} \begin{bmatrix} 1 & -1 \\ -1 & 1 \end{bmatrix}, |y_+\rangle\langle y_+| = \frac{1}{2} \begin{bmatrix} 1 & -i \\ i & 1 \end{bmatrix}, |y_-\rangle\langle y_-| = \frac{1}{2} \begin{bmatrix} 1 & i \\ -i & 1 \end{bmatrix} \end{array} \right\}. \quad (2.45)$$

The initial ρ_1 and final σ_2 states are given by a convex sum of this set.

As you remember, we need to deal with root squares of matrices. Fortunately, there is a relation for a root square of matrix that deals with trace and the determinant of the matrix. Thus, the root of a 2×2 matrix, is given by²

$$\sqrt{A} = \frac{1}{\tau} \left(A + I \det^{1/2}(A) \right) \quad (2.46)$$

with

$$\tau = \left(\text{Tr}(A) + 2 \det^{1/2}(A) \right)^{1/2}. \quad (2.47)$$

Thus, the term that we need to address is the following

$$(\sqrt{\sigma_2} \rho_1 \sqrt{\sigma_2})^{1/2} = \frac{1}{\hat{\tau}} (\sqrt{\sigma_2} \rho_1 \sqrt{\sigma_2} + \det^{1/2}(\rho_1) \det^{1/2}(\sigma_2)), \quad (2.48)$$

²for details see A and A.2.2

with

$$\hat{\tau} = (Tr\rho_1\sigma_2 + 2det^{1/2}(\rho_1)det^{1/2}(\sigma_2))^{1/2}. \quad (2.49)$$

As we did before, we want to present a diagram summarizing what we are searching for and what do we have,

We want to maximize: $\cos(\alpha) = \frac{g_B(\dot{\gamma}(0), \dot{\rho}(0))}{\|\dot{\gamma}(0)\| \times \|\dot{\rho}(0)\|}$
 In this case for mixed density matrices

Where γ is the geodesic and $\dot{\rho}$ is the density matrix of the Liouville-von Neumann equation g_B is the metric of the tangent space of the density matrices manifold.

What we know

Initial state ρ_1 and final state σ_2
 given by a convex combination of pure density matrices

A general Hamiltonian is given: σ_i are Pauli matrices and w_0 natural frequency

$$H(t) = H_0 + H_c(t) = -\frac{\hbar w_0}{2} \sigma_z - \frac{\hbar \Omega}{2} \cos(w_0 t + \beta) \sigma_x + \frac{\hbar \Omega}{2} \sin(w_0 t + \beta) \sigma_y$$

$$U(t) = \begin{bmatrix} e^{i \frac{t w_0}{2}} \cos\left(\frac{\Omega t}{2}\right) & i e^{i \frac{t w_0 + 2\beta}{2}} \sin\left(\frac{\Omega t}{2}\right) \\ i e^{-i \frac{(w_0 t + 2\beta)}{2}} \sin\left(\frac{\Omega t}{2}\right) & e^{-i \frac{t w_0}{2}} \cos\left(\frac{\Omega t}{2}\right) \end{bmatrix}$$

The evolution operator
 associated to the Hamiltonian

$$g_B(\dot{\gamma}(0), \dot{\rho}(0)) = \frac{1}{2} \sum_k \sum_l \frac{\overline{\langle k | \dot{\rho}(0) | l \rangle} \langle k | \dot{\gamma}(0) | l \rangle}{p_k + p_l}$$

The inner product

$$\dot{\gamma}(0) = \theta_0 \csc^2(\theta_0) \left(\left(\sigma_2^{-1/2} (\sqrt{\sigma_2} \rho_1 \sqrt{\sigma_2})^{1/2} \sigma_2^{1/2} + hc \right) \times \sin(\theta_0) + \rho_1 \sin(-2\theta_0) \right)$$

Geodesic in the case of mixed density matrices

$$F(\rho_1, \sigma_2) = \text{Tr}(\rho_1 \sigma_2) + 2\sqrt{\det \rho_1 \det \sigma_2}; \text{ from (Jozsa 1994)}$$

$$\theta_0 = \arccos(\sqrt{F(\rho_1, \sigma_2)}); \text{ from Ericsson (2005)}$$

The Fidelity and θ_0

$$\dot{\rho}(0) = -i[H(0), \rho(0)] \text{ with } \rho(0) = \rho_1$$

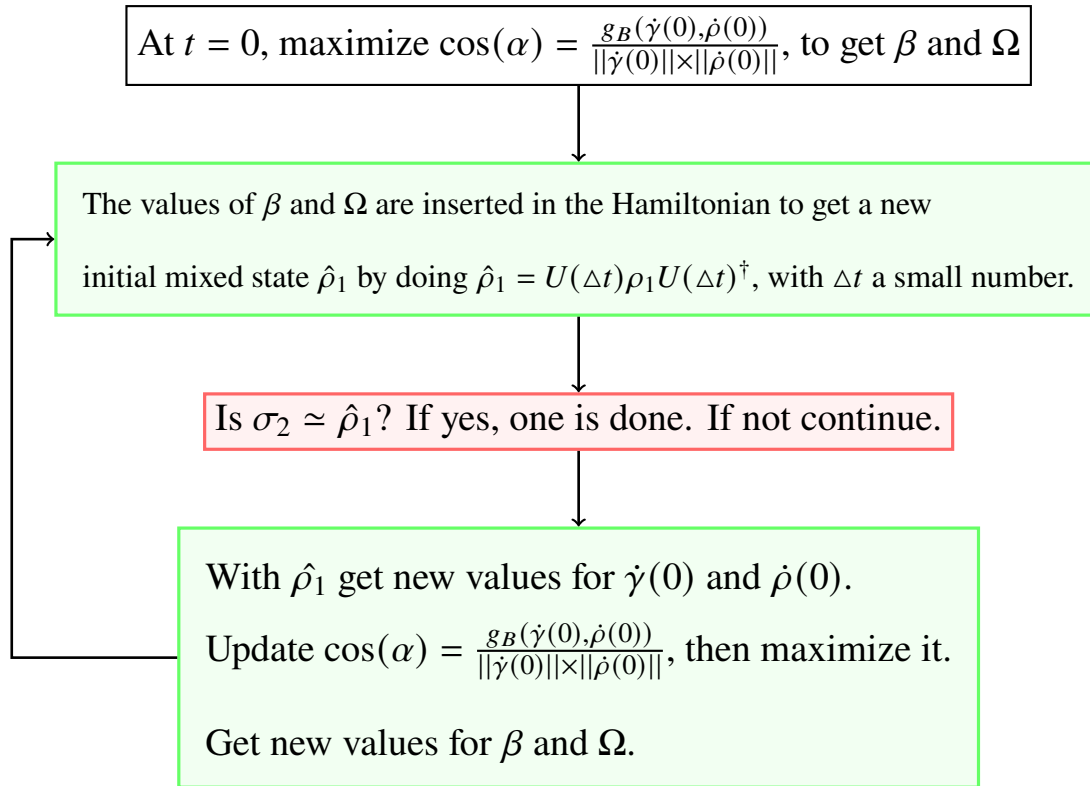
The Liouville-von Neumann equation

What we do not know: β and Ω

The variables in the Hamiltonian β and Ω are given by the control field or control Hamiltonian H_c

2.1.4 State to state transfer: mixed states procedure

The algorithm for state to state transfer for mixed states is very similar as for pure states and it is given by



We chose Δt as before, if w_0 is 1 Hz, Δt is in the order or 0.0025s. We finish the algorithm when

$$1 - F(\rho_1, \sigma_2) < 0.01 \quad (2.50)$$

2.2 Using a most general Hamiltonian

Trying another Hamiltonian and we follow the same procedure as before. We only need to change the Hamiltonian and the evolution operator.

The Hamiltonian that we want to try is the following,

$$H(t) = H_0 + H_c = -\frac{w_0}{2}\sigma_z + \frac{n_x}{2}\sigma_x + \frac{n_y}{2}\sigma_y, \quad (2.51)$$

with $\hbar = 1$ and which gives the following unitary operator

$$U(t) = e^{-\frac{i}{\hbar}Ht} = \cos(nt)I - i(\hat{n} \cdot \vec{\sigma}) \sin(nt), \quad (2.52)$$

where we have used $n = \sqrt{\frac{w_0^2}{4} + \frac{n_x^2}{4} + \frac{n_y^2}{4}}$ and

$$\vec{n} = \begin{bmatrix} \frac{n_x}{2} \\ \frac{n_y}{2} \\ \frac{w_0}{2} \end{bmatrix}, \quad (2.53)$$

and $\vec{\sigma}$ are the Pauli matrices. The diagram that summarize all the equations is the same as before with some changes in the Hamiltonian and the Unitary operator. Also, the procedure to maximize the objective function is the same as the case of mixed states.

We want to maximize: $\cos(\alpha) = \frac{g_B(\dot{\gamma}(0), \dot{\rho}(0))}{\|\dot{\gamma}(0)\| \times \|\dot{\rho}(0)\|}$
 Using mixed density matrices

Where γ is the geodesic and $\dot{\rho}$ is the density matrix of the Liouville-von Neumann equation g_B is the metric of the tangent space of the density matrices

What we know

Initial ρ_1 and final σ_2 states are given by a convex sum

A general Hamiltonian is given: σ_i are Pauli matrices and w_0 natural frequency

$$H(t) = H_0 + H_c = -\frac{\hbar w_0}{2} \sigma_z + \frac{n_x}{2} \sigma_x + \frac{n_y}{2} \sigma_y, \text{ where } n_x \text{ and } n_y \text{ are constants}$$

The evolution operator

$$U(t) = e^{-iHt} = \cos(nt)I - i(\hat{n} \cdot \vec{\sigma}) \sin(nt), n = \sqrt{\frac{w_0^2}{4} + \frac{n_x^2}{4} + \frac{n_y^2}{4}}$$

$$g_B(\dot{\gamma}(0), \dot{\rho}(0)) = \frac{1}{2} \sum_k \sum_l \frac{\langle k | \dot{\rho}(0) | l \rangle \langle k | \dot{\gamma}(0) | l \rangle}{p_k + p_l}$$

The inner product

$$\dot{\gamma}(0) = \theta_0 \csc^2(\theta_0) \left(\left(\sigma_2^{-1/2} (\sqrt{\sigma_2} \rho_1 \sqrt{\sigma_2})^{1/2} \sigma_2^{1/2} + hc \right) \times \sin(\theta_0) + \rho_1 \sin(-2\theta_0) \right)$$

Geodesic in the case of mixed density matrices

$$F(\rho_1, \sigma_2) = Tr(\rho_1 \sigma_2) + 2\sqrt{\det \rho_1 \det \sigma_2}; \text{ from (Jozsa 1994)}$$

$$\theta_0 = \arccos(\sqrt{F(\rho_1, \sigma_2)}); \text{ from (Ericsson 2005)}$$

The Fidelity and θ_0

$$\dot{\rho}(0) = -i[H(0), \rho(0)] \text{ with } \rho(0) = \rho_1 \quad \text{The Liouville-von Neumann equation}$$

What we do not know:

n_x and n_y

The variables in the Hamiltonian n_x and n_y are given by the control field or control Hamiltonian H_c

In the next chapter we want to show the results of some state to state transfers. The results will be given by the trajectories that follows the initial to state to the final graphs of the Bloch sphere

Chapter 3

Results and discussion

In § 2, we derived a methodology to transfer an initial quantum state ρ_1 to a final one σ_2 based on the geodesic $\gamma(t)$ of the density matrices manifold, the evolution of a density matrix $\mathcal{E}(\mathcal{H})$ given by the Liouville-von Neumann equation, $\dot{\rho}(t) = -i[H(t), \rho(t)]$ and the Bures metric g_B which is Riemannian in $\mathcal{E}(\mathcal{H})$. The methodology consists in a sequence of optimizations of some parameters $\{n_x, n_y\}$, given by the Hamiltonian, that maximize the cosine of the angle α between the time derivative of the geodesics vector $\dot{\gamma}(t)$ and the evolution of the initial state $\rho_1(t)$. The evolution of the initial state is given by a Hamiltonian that is a linear combination of Pauli matrices and the parameters $\{n_x, n_y\}$. The mentioned methodology was made for pure and mixed states. However, we needed to adequate the equations for pure states due to the fact that this states do not admit an inverse matrix. In this chapter, we show how our model behaves steering states on the Bloch sphere using the Hamiltonian which depends of the trigonometric functions sin and cos and the other one which consisted in n_x and n_y .

3.1 Experiments for pure states

In this section, there are some numerical experiments based on the previous method. In all the following experiments, we have used $\hbar = 1$ and the constant $w_0 = 5$ which are

considered values to observe the trajectory of the state transfer on the Bloch sphere. In the following experiments we have used the Hamiltonian given by¹ (2.4)

$$H(t) = H_0 + H_c(t) = -\frac{\hbar w_0}{2} \sigma_z - \frac{\hbar \Omega}{2} \cos(w_0 t + \beta) \sigma_x + \frac{\hbar \Omega}{2} \sin(w_0 t + \beta) \sigma_y. \quad (3.1)$$

The initial and final states were chosen without any distinction in particular. However, the time that runs the simulation, which will be called computational time, is longer when the initial state is in the North and South pole than on other initial states, we will discuss this issue at the end of the section.

- From the initial state $|\psi_1\rangle = \cos \frac{\pi}{8} |0\rangle + \sin \frac{\pi}{8} |1\rangle$, ($\theta_1 = \pi/4, \phi_1 = 0$) to the final state $|\phi_2\rangle = |x_+\rangle = \frac{1}{\sqrt{2}} |0\rangle + \frac{1}{\sqrt{2}} |1\rangle$, ($\theta_2 = \pi/2, \phi_2 = 0$). For this evolution, we have used $\Delta t = 0.004$ and 20 steps to reach the final state.

Fig. 3.1 shows the trajectory of our method which are the dots in rainbow colors and the geodesic which is black line. In the plot, the red point is the initial state and the purple one is the final. In this experiment, if we give another step which is the 21th, the last dot (related to the last step) will not get close enough to the final state in order to accomplish our requirement of 0.01 for the infidelity. Thus, the step 20 is the best approximation to the final state.

- From the initial state $|\psi_1\rangle = \cos \frac{\pi}{8} |0\rangle + \sin \frac{\pi}{8} |1\rangle$, ($\theta_1 = \pi/4, \phi_1 = 0$) to the final state $|\phi_2\rangle = |y_+\rangle = \frac{1}{\sqrt{2}} |0\rangle + i \frac{1}{\sqrt{2}} |1\rangle$, ($\theta_2 = \pi/2, \phi_2 = \pi/2$). For this evolution, we have used $\Delta t = 0.05$ and 24 steps to reach the final state. The result is presented in Fig. 3.2. According to this Fig., the control fields make the motion of the initial state, given by the red dot, counter clock wise. This makes that the evolution of the initial state does not follow the geodesic path; however, the method reaches to the final state.

¹keep in mind we can extend the results with (2.3) where n_x and n_y are unknowns

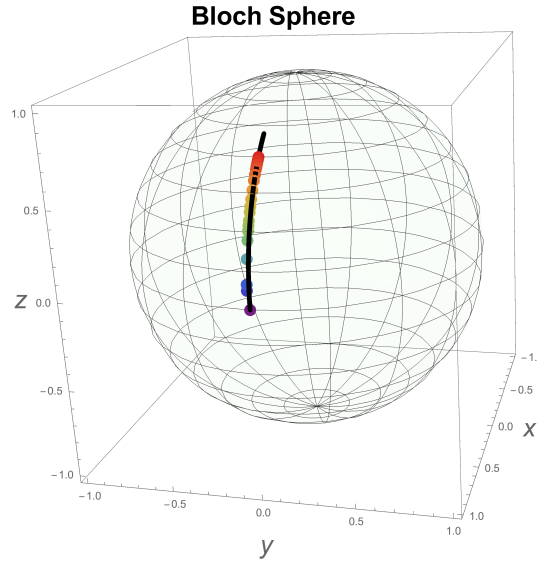


Figure 3.1: The red dot is the initial state and the purple is the final state. This evolution is over a meridian, from $|\psi_1\rangle = \cos \frac{\pi}{8} |0\rangle + \sin \frac{\pi}{8} |1\rangle$ to $|\phi_2\rangle = \frac{1}{\sqrt{2}} |0\rangle + \frac{1}{\sqrt{2}} |1\rangle$ with $w_0 = 5$ and using (3.1). The Black line is the geodesic between the initial and final states.

3. In this case we swap the initial and final states of the previous experiment. From the initial state $|\psi_1\rangle = |y_+\rangle = \frac{1}{\sqrt{2}} |0\rangle + i \frac{1}{\sqrt{2}} |1\rangle$, $(\theta_1 = \pi/2, \phi_1 = \pi/2)$ to the final state $|\phi_2\rangle = \cos \frac{\pi}{8} |0\rangle + \sin \frac{\pi}{8} |1\rangle$, $(\theta_2 = \pi/4, \phi_2 = 0)$. For this evolution, we have used $\Delta t = 0.03$ and 10 steps to reach the final state. The result is presented in Fig. 3.3 where the purple point is the initial and the red is the final state, respectively. The exchange of the states gives a trajectory in a good relation with the geodesic; however, as we will see the trajectory that follows the geodesic depends on the values of Δt and the Hamiltonian.
4. From the initial state $|\psi_1\rangle = \cos \frac{\pi}{8} |0\rangle + \sin \frac{\pi}{8} |1\rangle$, $(\theta_1 = \pi/4, \phi_1 = 0)$ to the final state $|\phi_2\rangle = |y_-\rangle = \sqrt{\frac{1}{2}}(|0\rangle - i|1\rangle)$, $(\theta_2 = \pi/2, \phi_2 = 3/2\pi)$. For this evolution, we have used $\Delta t = 0.02$ and 15 steps to reach the final state. The result is presented in Fig. 3.4 where the initial state is the red dot and the final state is the purple. Viewing this Fig., we find that the trajectory is very similar as the trajectory of the geodesic in black which means that our Hamiltonian is good enough to replicate the path of

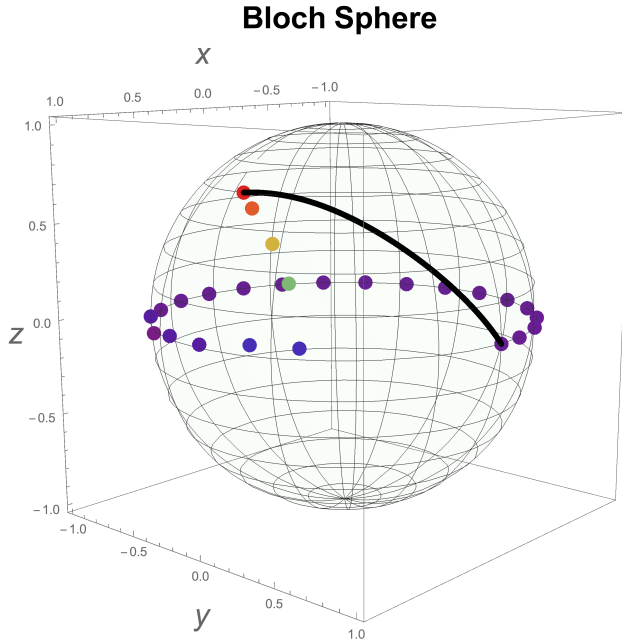


Figure 3.2: This transition is from $|\psi_1\rangle = \cos \frac{\pi}{8} |0\rangle + \sin \frac{\pi}{8} |1\rangle$ to $|\phi_2\rangle = |y_+\rangle = \frac{1}{\sqrt{2}} |0\rangle + i \frac{1}{\sqrt{2}} |1\rangle$ with $w_0 = 5$ and using (3.1). The red dot is the initial state and the purple (at the end of the geodesic) is the final state. The evolution is going counter clock-wise and in some steps it follows the Equator until it reaches to the final state. The Black line is the geodesic between the initial and final states.

the Hamiltonian for this case given the infidelity of 0.01.

5. From the initial state $|\psi_1\rangle = |0\rangle$, $(\theta_1 = 0, \phi_1 = 0)$ to the final state $|\phi_2\rangle = |x_+\rangle = \sqrt{\frac{1}{2}}(|0\rangle + |1\rangle)$, $(\theta_2 = \pi/2, \phi_2 = 0)$. For this evolution, we have used $\Delta t = 0.008$ and 105 steps to reach the final state. The result is presented in Fig. 3.5, where the initial red dot in the initial state and the purple dot is the final state. The computational time of this plot was greater than the others. This is because the evolution of the initial state is very small in contrast to the other experiments.

In every experiment we worked with (3.1) and for every value of β and Ω , we have achieved the maximization of the objective function $\cos \alpha$ with value 1, even in the second experiment which does not follow the geodesic. This means that we are getting the right

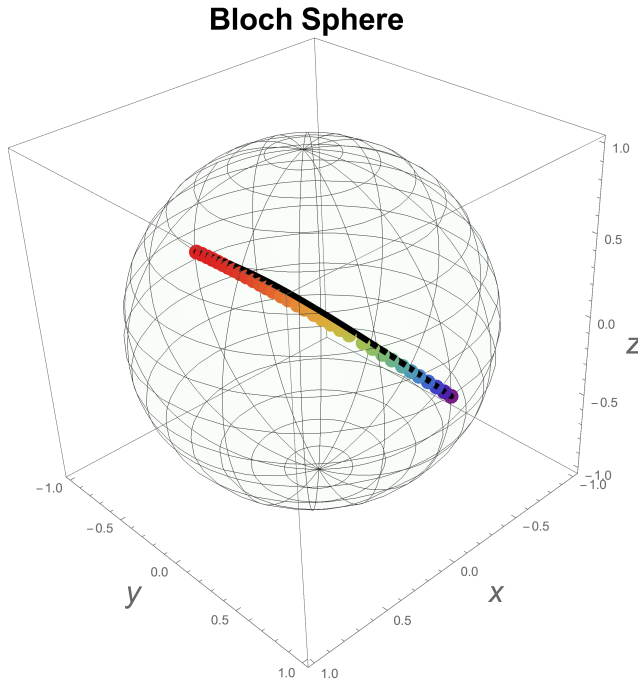


Figure 3.3: This evolution is from $|\phi_1\rangle = |y_+\rangle = \frac{1}{\sqrt{2}}|0\rangle + i\frac{1}{\sqrt{2}}|1\rangle$ to $|\psi_2\rangle = \cos \frac{\pi}{8}|0\rangle + \sin \frac{\pi}{8}|1\rangle$ with $w_0 = 5$ and using (3.1). The purple dot is the initial state and the red is the final state. The evolution given by the Hamiltonian (3.1) depends of the direction of the final state. The Black line is the geodesic between the initial and final states.

direction in each step. Also, it is important to notice that we always get to the final state which is one of our goals, even when the trajectory does not follow the geodesic such as the second experiment. We have to say that for small Δt we get smooth trajectories but this turns out in more computational time to wait until the trajectory of our methodology reach the final state.

In the second experiment with Fig. 3.2, we see that the trajectory of our methodology does not follow the geodesic but if we use a Δt small in the order of 0.001 we follow it, as we can see in Fig. 3.6. However as we mentioned early, if we use smaller Δt the computational time that it takes to get to the final state is longer and in some cases it will take minutes with a normal portable computer which is ours.

From the experiments, if the evolution of the steering follows a counterclockwise

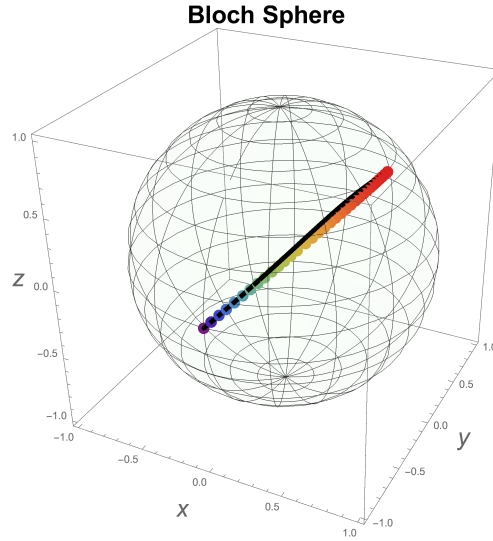


Figure 3.4: This evolution is from $|\psi_1\rangle = \cos \frac{\pi}{8} |0\rangle + \sin \frac{\pi}{8} |1\rangle$ to $|\phi_2\rangle = |y_-\rangle$ with $w_0 = 5$ and using (3.1). The red dot is the initial state and the purple is the final state. In this experiment the Hamiltonian given by (3.1) replicates the geodesic, the black line, given the infidelity of 0.01.

direction we can set Δt greater values in contrast to the clockwise direction where we need small Δt in order that the new state in each iteration does not deviate from the geodesic, as we can see in Fig 3.6. This has to be with the rotation orientation of Pauli matrices, which in the form that we are working ², give a counterclockwise rotation.

A similar issue, we have with the fifth experiment in Fig. 3.5, where we need a small Δt to reach to the final state $|x_+\rangle$. In this type of transition, we have a liberty at the initial state³ $|0\rangle$ which is the angle ϕ where we set 0 but we could chose any value ϕ . This liberty in ϕ makes that our method lose the geodesic trajectory at the beginning of the optimization of the objective function $\cos \alpha$, but with small values of Δt we can keep the trajectory close to the geodesic.

²The form of Pauli matrices that we are using: $\sigma_x = \begin{bmatrix} 0 & 1 \\ 1 & 0 \end{bmatrix}$, $\sigma_y = \begin{bmatrix} 0 & -i \\ i & 0 \end{bmatrix}$ and $\sigma_z = \begin{bmatrix} 1 & 0 \\ 0 & -1 \end{bmatrix}$

³the ket $|0\rangle$ can be made by using $\theta = 0$ and any value of the angle ϕ because, $|0\rangle = \cos(\frac{\theta}{2}) |0\rangle + e^{i\phi} \sin(\frac{\theta}{2}) |1\rangle = 1 |0\rangle + 0 |1\rangle$

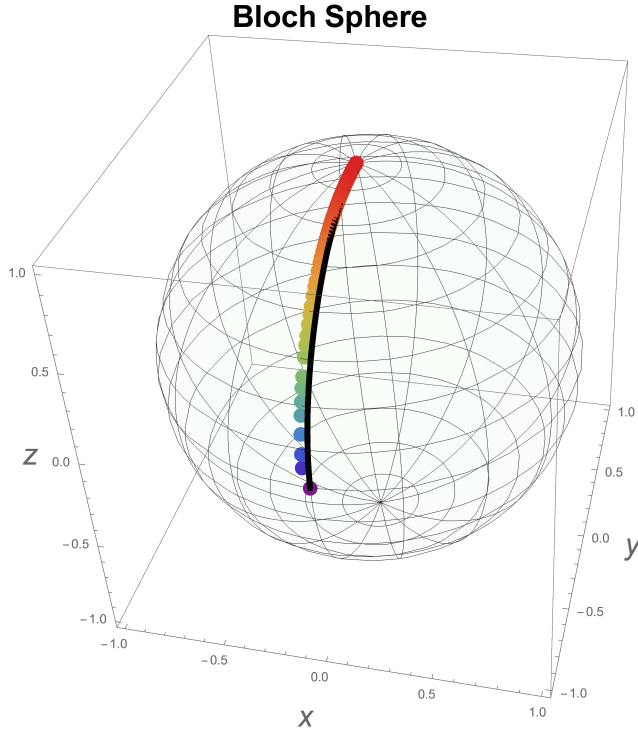


Figure 3.5: Evolution from $|\psi_1\rangle = |0\rangle$ to $|\phi_2\rangle = |x_+\rangle$ with $w_0 = 5$ and using (3.1). The red dot is the initial state and the blue is the final state. The Black line is the geodesic between the initial and final states.

3.2 Experiments for pure states with a general Hamiltonian

In this section we want to change our Hamiltonian for another more general given by (2.3)

$$H = -\frac{w_0}{2}\sigma_z + \frac{n_x}{2}\sigma_x + \frac{n_y}{2}\sigma_y, \quad (3.2)$$

with constants n_x and n_y instead of the function sin and cos. In general terms, the methodology is the same but we need to use the unitary operator given by (2.52) for the evolution of the initial state.

In the following, we show some transitions using the Hamiltonian proposed above.

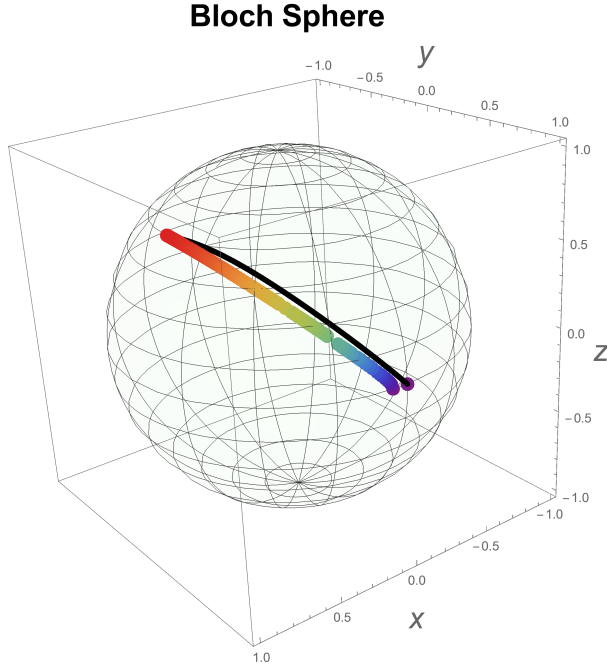


Figure 3.6: The transition from $|\psi_1\rangle = \cos \frac{\pi}{8} |0\rangle + \sin \frac{\pi}{8} |1\rangle$ to $|\phi_2\rangle = |y_+\rangle = \frac{1}{\sqrt{2}} |0\rangle + i \frac{1}{\sqrt{2}} |1\rangle$ makes a clockwise rotation. We need $\Delta t = 0.003$ in order to have a small deviation from the geodesic.

1. From the initial state $|\psi_1\rangle = \cos \frac{\pi}{8} |0\rangle + \sin \frac{\pi}{8} |1\rangle$, ($\theta_1 = \pi/4, \phi_1 = 0$) to the final state $|\phi_2\rangle = |x_+\rangle = \frac{1}{\sqrt{2}} |0\rangle + \frac{1}{\sqrt{2}} |1\rangle$, ($\theta_2 = \pi/2, \phi_2 = 0$). For this evolution, we have used $\Delta t = 0.001$ and 5 steps to reach the final state.

The result is in Fig. 3.7, where the red dot is the initial state and the purple is the final. As before, if we give another step, the last dot (related to the last step) will be located far from our final state. Thus, the step 5 is the best approximation to the final state. Our methodology with the Hamiltonian given by (2.3) gives less computational time which means less points and we keep our infidelity under 0.01.

2. From the initial state $|\psi_1\rangle = \cos \frac{\pi}{8} |0\rangle + \sin \frac{\pi}{8} |1\rangle$, ($\theta_1 = \pi/4, \phi_1 = 0$) to the final state $|\phi_2\rangle = |y_+\rangle = \frac{1}{\sqrt{2}} |0\rangle + i \frac{1}{\sqrt{2}} |1\rangle$, ($\theta_2 = \pi/2, \phi_2 = \pi/2$). For this evolution, we have used $\Delta t = 0.00029$ and 22 steps to reach the final state. The result is presented in Fig. 3.8, where the initial state is the red dot and the purple is the final state. As we can see, the Hamiltonian given by (2.3) follows the geodesic path in a better way

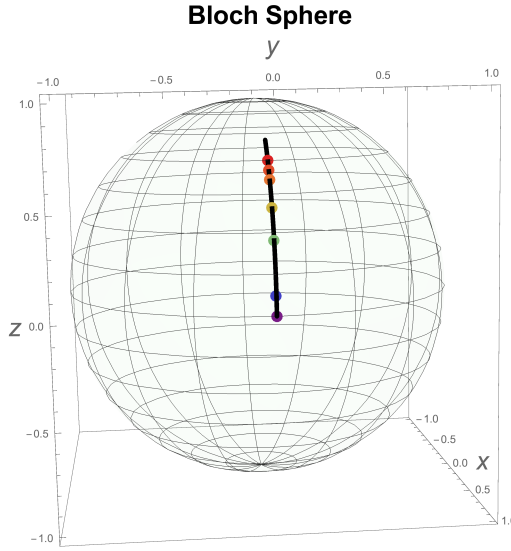


Figure 3.7: Transition from: $|\psi_1\rangle = \cos \frac{\pi}{8} |0\rangle + \sin \frac{\pi}{8} |1\rangle$ to $|x_+\rangle$ using the Hamiltonian (2.3) with n_x and n_y constants. The red dot is the initial state and the purple is the final state. The blue dot is the best approximation of the final state according to our method. The Black line is the geodesic between the initial and final states. Our methodology with this Hamiltonian gives less steps.

than the Hamiltonian with cos and sin functions.

3. From the initial state $|\psi_1\rangle = \cos \frac{\pi}{8} |0\rangle + \sin \frac{\pi}{8} |1\rangle$, $(\theta_1 = \pi/4, \phi_1 = 0)$ to the final state $|\phi_2\rangle = |y_-\rangle = \sqrt{\frac{1}{2}}(|0\rangle - i|1\rangle)$, $(\theta_2 = \pi/2, \phi_2 = 3/2\pi)$. For this evolution, we have used $\Delta t = 0.0008$ and 17 steps to reach the final state. The result is presented in Fig. 3.9, where the red dot is the initial state and the purple is the final state. Viewing the plot, our method with (2.3) follows almost in an identical way the path of the geodesic.
4. From the initial state $|\psi_1\rangle = |0\rangle$, $(\theta_1 = 0, \phi_1 = 0)$ to the final state $|\phi_2\rangle = |x_+\rangle = \sqrt{\frac{1}{2}}(|0\rangle + |1\rangle)$, $(\theta_2 = \pi/2, \phi_2 = 0)$. For this evolution, we have used $\Delta t = 0.001$ and 71 steps to reach the final state. The result is presented in Fig. 3.10, where the red dot is the initial state and the final state is the blue dot. The purple dot is best approximation we got with our method.

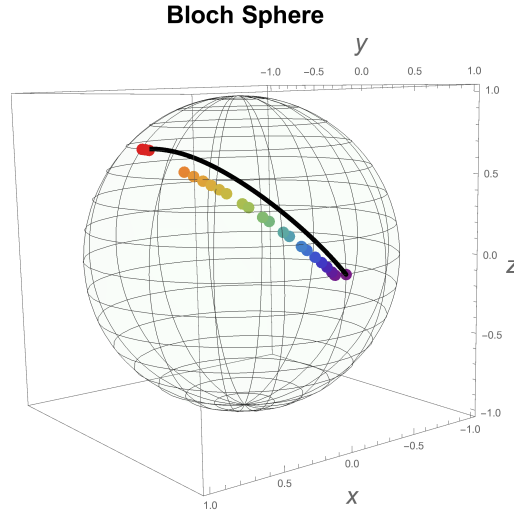


Figure 3.8: This evolution is from: $|\psi_1\rangle = \cos \frac{\pi}{8} |0\rangle + \sin \frac{\pi}{8} |1\rangle$ to $|\phi_2\rangle = |y_+\rangle$ where the red dot is the initial state and the purple (at the end of the geodesic) is the final state. The driven Hamiltonian is given by (2.3), with n_x and n_y unknowns constants. The Black line is the geodesic between the initial and final states.

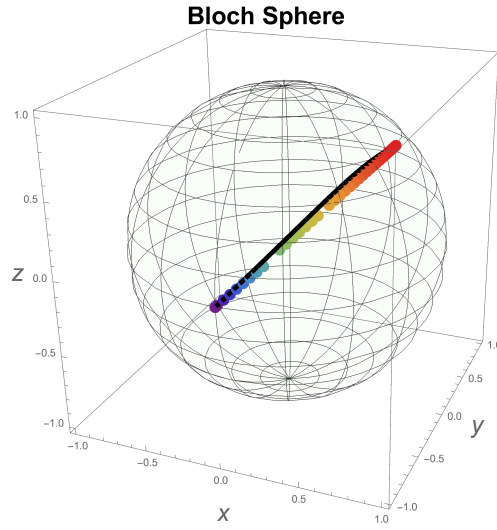


Figure 3.9: This evolution is from $|\psi_1\rangle = \cos \frac{\pi}{8} |0\rangle + \sin \frac{\pi}{8} |1\rangle$ to $|\phi_2\rangle = |y-\rangle$. The red dot is the initial state and the purple is the final state. The driven Hamiltonian is given by (2.3), with n_x and n_y unknowns constants. The Black line is the geodesic between the initial and final states.

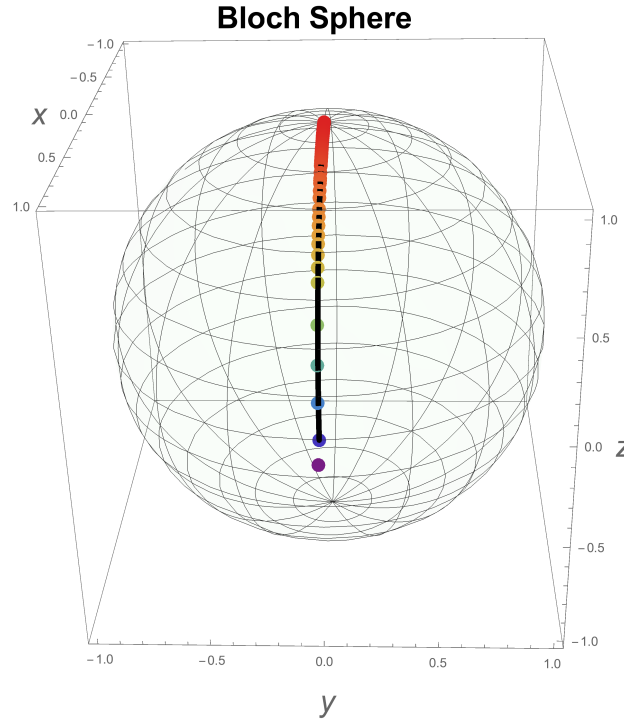


Figure 3.10: Evolution from $|\psi_1\rangle = |0\rangle$ to $|\phi_2\rangle = |x_+\rangle$. The red dot is the initial state and the blue is the final state. The purple point is the most accurate final state according to our methodology. The driven Hamiltonian is given by (2.3), with n_x and n_y unknowns. The Black line is the geodesic between the initial and final states.

Using (2.3) with n_x and n_y unknown constants, our method used less steps than before which means it is more computational fast. However, our method with this Hamiltonian keeps the infidelity in the same value for 0.01. Thus, we have not gained in accuracy. Also, we still have some disagreements respect with the geodesic as we can see with Fig. 3.8 but in every experiment the maximum for the objective function was 1 which means that we are always in the direction of the final state. In summary, this Hamiltonian has improved the efficiency of our methodology while keeping the accuracy.

3.3 Experiments with mixed states

In the last section, we see that we had better results with the Hamiltonian 2.3, with n_x and n_y unknown constants, than the one with cos and sin. Thus, the following experiments with mixed states are going to be developed with the Hamiltonian with n_x and n_y .

Dealing with mixed states, we require a convex sum of (2.45) to get the initial and final states.

- We had chosen the following convex sum for the first state:

$$\rho_1 = \frac{1}{10} |1\rangle\langle 1| + \frac{8}{10} |x_-\rangle\langle x_-| + \frac{1}{10} |y_-\rangle\langle y_-| \quad (3.3)$$

and for the final state

$$\sigma_2 = \frac{1}{5} |0\rangle\langle 0| + \frac{1}{5} |x_+\rangle\langle x_+| + \frac{3}{5} |y_+\rangle\langle y_+|. \quad (3.4)$$

The trajectory of the transition is given by the Fig. 3.11, where the blue dot is the initial state and the red is the final state. Also, in the left we can appreciate the top view and the right is the front view. For this figure, we have used 21 steps and $\Delta t = 0.02$. From the top view, we can see that the last step the red dot is the best approximation of our method, as always with infidelity less than 0.01.

- The second experiment with mixed states, we have chosen the following states.

From the initial state given by

$$\rho_1 = \frac{1}{5} |0\rangle\langle 0| + \frac{3}{5} |x_-\rangle\langle x_-| + \frac{1}{5} |y_-\rangle\langle y_-| \quad (3.5)$$

and the final state

$$\sigma_2 = \frac{1}{3} |1\rangle\langle 1| + \frac{2}{3} |x_+\rangle\langle x_+|. \quad (3.6)$$

The trajectory of the transition is in Fig. 3.12, where the red dot is the initial state and the purple the final state. The blue dot is the best approximation of our method. For this figure we have used 24 steps and $\Delta t = 0.0008$.

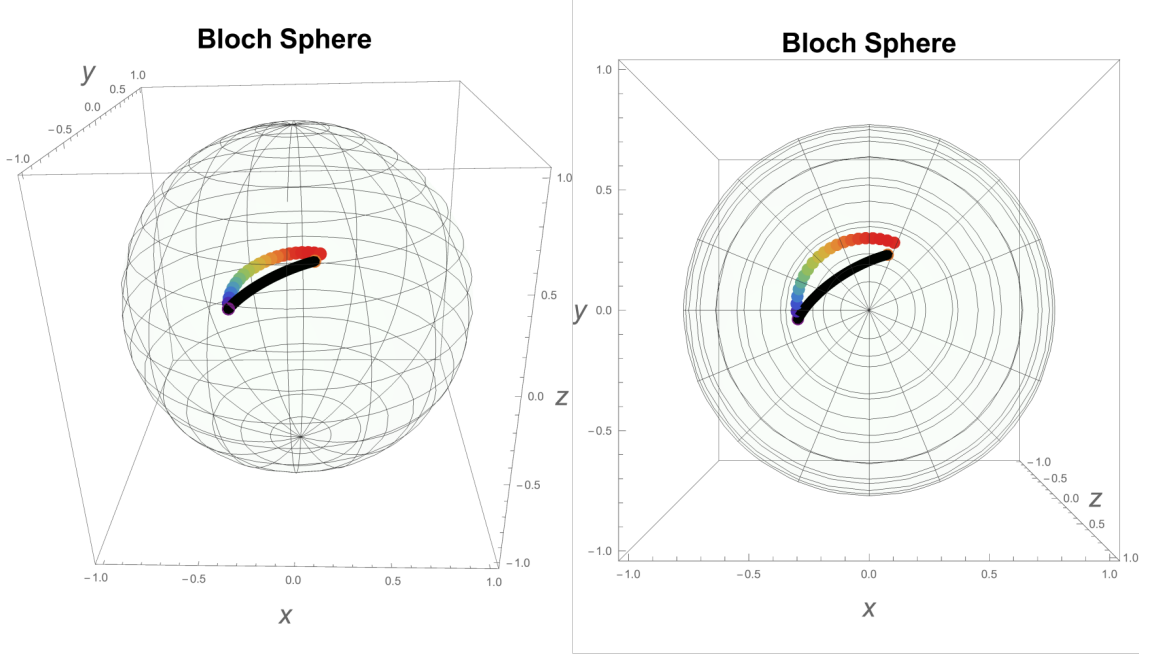


Figure 3.11: Evolution from ρ_1 to σ_2 , two mixed states. The blue dot is the initial state and the orange is the final state. The Black line is the geodesic between the initial and final states.

In these experiments for mixed states, we have used the Hamiltonian with n_x and n_y unknowns constants⁴. In our results, we got that the maximum of the objective function is in the range from 0.6 to 0.8. This shows that in each step we are not getting the exactly the right direction for the evolution, comparing with pure states that always we get 1. Also for mixed states, our method decreases the accuracy to arrive to the final state because for the infidelity we have a value of 0.02, comparing with pure states which it was 0.01.

3.4 Improvements

At the moment with our algorithm, we can control the direction of evolution of the state on the Bloch sphere by the coefficients n_x, n_y using the Hamiltonian given by (2.3); however we do not have control on the forward evolution which is given by Δt in every

⁴If we use the Hamiltonian with sin and cos functions we arrived to almost the same results

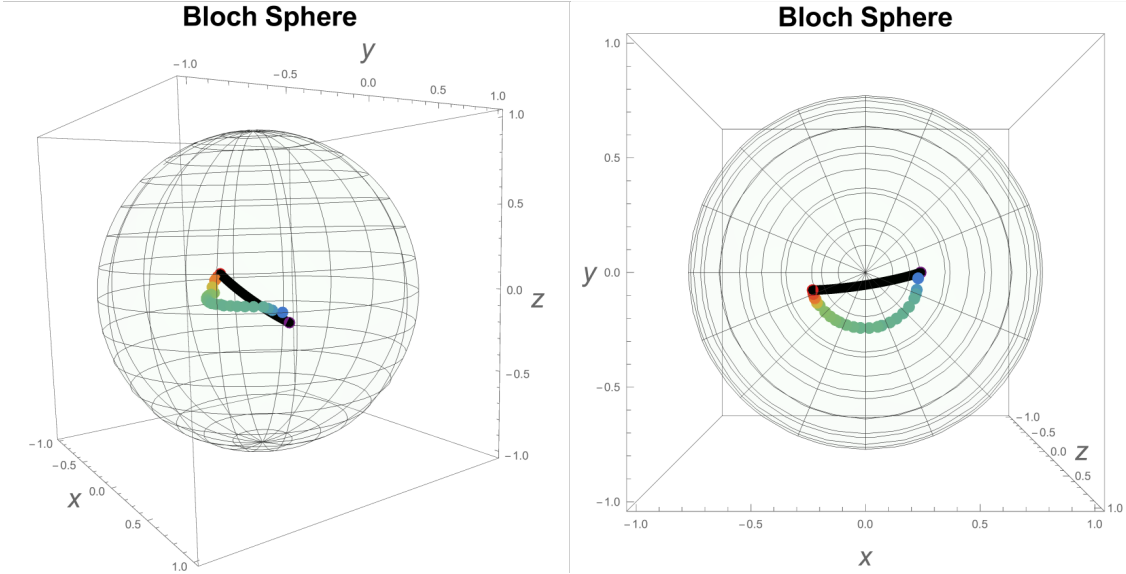


Figure 3.12: Evolution from ρ_1 to σ_2 , two mixed states. The red dot is the initial state and the purple is the final state. The Black line is the geodesic between the initial and final states. The blue point is the best approximation of the final state given by our method.

step, also we can see this on Fig. 2.1. This produces a poor convergence to the final state; thus a greater infidelity. Take in mind that Δt is a fixed value based on other algorithms reviewed before. Also, we are not satisfied with the trajectory given in Fig. 3.2 and we want to improve it by adding another control field parameter or coefficient.

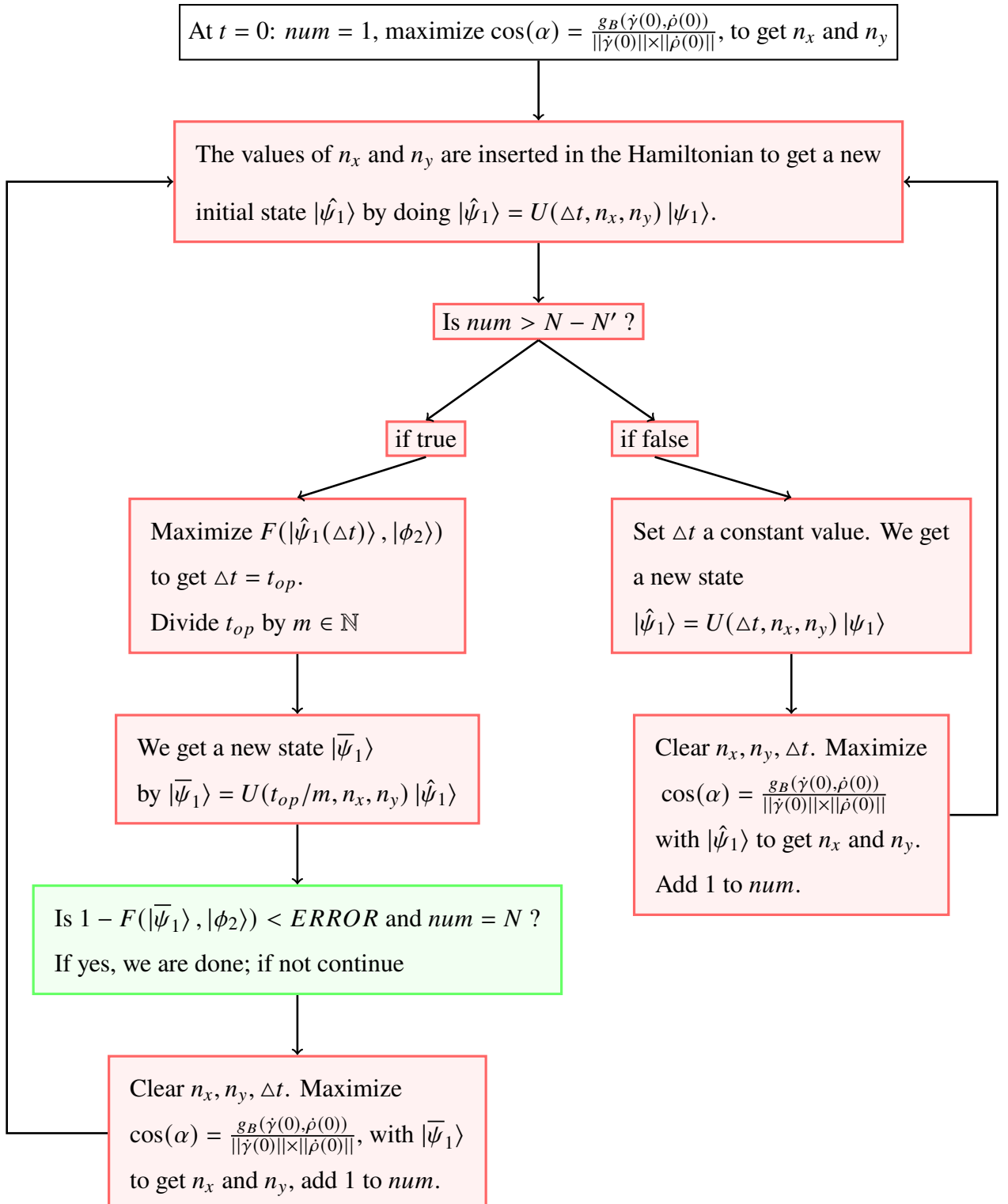
A feasible idea that we can use to improve the infidelity⁵ is by introducing an optimization function that depends on time. For example, we can use the fidelity equation between the simulated evolved state with the coefficients n_x, n_y and with the final state, the state that we want to reach. The key point here is that we leave the time Δt as an unknown variable. Then, what we need to search is the time $\Delta t = t_{op}$ at which the fidelity is maximize. This will help to control the evolution in time and the maximization of the fidelity; however, this time $\Delta t = t_{op}$ must be taken as an approximation of the real time to reach to the final state because the maximization of the fidelity is not always 1. Then, we can take a fraction of t_{op} and evolve the state. Combining this idea with our previous methodology, we can set a

⁵We want to get lower values of the infidelity which will give us a better final state.

certain amount of steps denoted by N' at the end of the hole previous algorithm that will be using this optimization in the fidelity function. We can call this idea a “hybrid algorithm” and we can explain it in the following:

1. We need to set an error constant given by $ERROR$ which will be the threshold that one search for in the Fidelity function. In reality we want, $1 - F(|\psi_N\rangle, |\phi_2\rangle) < ERROR$, where $|\psi_N\rangle$ is the final state given by our methodology and $|\phi_2\rangle$ is the final state that we want to arrive.
2. We have to define the total number of steps N , that will steer to initial state to the final one. This N are the number of dots (and steps in our algorithm) that will be located on the Bloch sphere.
3. Also, we need to set a number of steps N' that will lead to the accuracy in the Fidelity function that one wants. Notice that N' and N are related to the total time of the evolution T of the initial state $|\psi_1\rangle$, given by $T = (N - N') \times \Delta t + \sum_{i=1}^{N'} t_{op}/m$, with $m \in \mathbb{N}$. This T will give us the physical time that our algorithm will take in order to reach to the final state.
4. In order to explain this hybrid model, we set a counter of steps given by num , which will goes form 1 to N .

In the following chart, we want to present our hybrid algorithm:



In the following, we present the performance of the hybrid algorithm with a transition

from $|\psi_1\rangle = \cos \frac{\pi}{8} |0\rangle + \sin \frac{\pi}{8} |1\rangle$ to $|\phi_2\rangle = |y-\rangle$ using (2.3) with n_x, n_y unknowns constants. This transition is similar as Fig. 3.9 and we can see it on the Bloch sphere in Fig. 3.13. For this experiment, we got an infidelity of 3.5×10^{-5} which is a better result comparing with 0.01 that we got with our previous model in the same transition. Also, we got a total time of evolution of $T = 0.29$ which is a value of reference according to the geodesic time. Being specific, the geodesic equation starting from the initial state arrives to the final state in $T = 1$. In this transition, our model arrives to the final state faster than the geodesic equation.

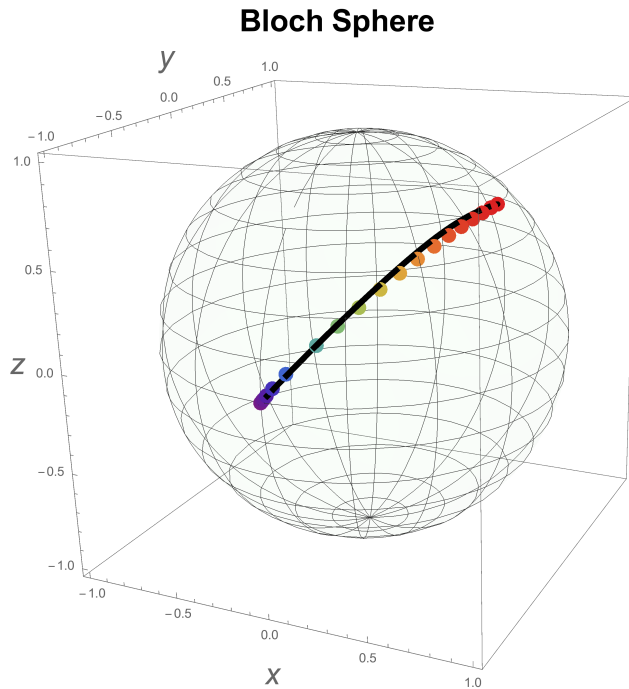


Figure 3.13: The hybrid algorithm: evolution from $|\psi_1\rangle = \cos \frac{\pi}{8} |0\rangle + \sin \frac{\pi}{8} |1\rangle$ to $|\phi_2\rangle = |y-\rangle$. The red dot is the initial state and the purple is the final state. The driven Hamiltonian is given by (2.3), with n_x and n_y unknowns constants. The Black line is the geodesic between the initial and final states. For this experiment, we have used $ERROR = 1 \times 10^{-3}$, $m = 2$, $N = 17$, $\Delta t = 0.2$, $N' = 5$ and we got an infidelity of 3.5×10^{-5} and $T = 0.29$.

Focusing on the trajectory given by the Fig. 3.2, where we showed that with small values of Δt our methodology can follow the geodesic in a better form than when using

large values of Δt . An improvement for this issue will be by adding another control parameter in the z direction. This can be done by setting the control field variable $n_z \neq 0$ on our proposed Hamiltonian (2.3). Thus,

$$H = \frac{-w_0 + n_z}{2} \sigma_z + \frac{n_x}{2} \sigma_x + \frac{n_y}{2} \sigma_y, \quad (3.7)$$

where n_z is the new control field parameter and n_x and n_y are the unknown control field parameters that we were working with and also taking in mind that $w_0 = 5$ is the natural frequency of the system⁶; thus is a fixed value. Applying this new feature to the transition $|\psi_1\rangle = \cos \frac{\pi}{8} |0\rangle + \sin \frac{\pi}{8} |1\rangle$ to $|\phi_2\rangle = |y+\rangle$, we ended up with an infidelity of 7.5×10^{-5} as one can see the result on Fig. 3.14. Also for this experiment, we used $N = 34$ steps, $\Delta t = 0.035$ and we set a constrain⁷ in the control fields of $-w_0 \leq n_z \leq w_0$, $-w_0 \leq n_x \leq w_0$, $-w_0 \leq n_y \leq w_0$.

Joining both ideas, that is adding in the hybrid algorithm another control parameter in the n_z and applying to the transition $|\psi_1\rangle = \cos \frac{\pi}{8} |0\rangle + \sin \frac{\pi}{8} |1\rangle$ to $|y_+\rangle$, with $ERROR = \times 10^{-5}$, $N = 28$, $N' = 8$ and $m = 2$, one can see our result in Fig. 3.15. For this transition, we got an infidelity of 8.7×10^{-6} which is a value that is in range with the algorithms reviewed before. In addition with this new improvements with more steps, one can improve the value of the infidelity even more.

A fact or probably a drawback is that we noticed that the trajectories with our algorithm has an orientation of rotation. For instance, if we want to go from the $|x_+\rangle$ to $|y_+\rangle$ which is a trajectory in the Ecuadorian plane, our methodology does not follow the smallest trajectory instead it follows the largest as we can see in the right of Fig. 3.16. This experiments have been made with the Hamiltonian given by (3.7) and using $m = 2$ to divide t_{op} (the hybrid algorithm).

⁶According to Abraham et al. (2019), the transmon qubit of IBM Quantum has a natural frequency of $5MHz$

⁷The constrain is due to fact that the transition frequencies must be bounded by the energy difference between the $|1\rangle$ and $|0\rangle$ states. Higher amplitudes of the control fields can lead to other unwanted excitation levels .

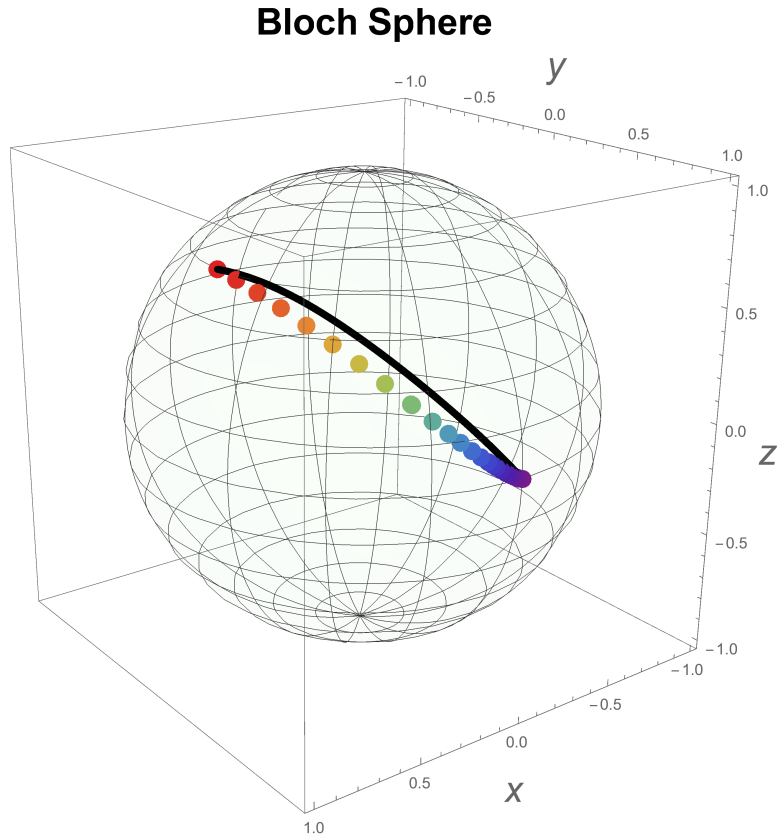


Figure 3.14: This transition is from $|\psi_1\rangle = \cos \frac{\pi}{8} |0\rangle + \sin \frac{\pi}{8} |1\rangle$ to $|\phi_2\rangle = |y_+\rangle$. The red dot is the initial state and the purple is the final state. Here, we have added a new control coefficient n_z in the direction of the $z - axis$. The black line is the geodesic.

This issue is due to the fact that the term $\frac{-w_0}{2}\sigma_z$ in the Hamiltonian (2.3) makes always a counterclockwise rotation in the $z - axis$. A practical solution might be changing the sign of the term $\frac{-w_0}{2}\sigma_z$ which gives a solution for this problem. This can be done by applying a σ_x to the Hamiltonian H_0 given a new Hamiltonian H'_0 ,

$$H'_0 = \sigma_x^\dagger H_0 \sigma_x = \frac{w_0}{2} \sigma_z. \quad (3.8)$$

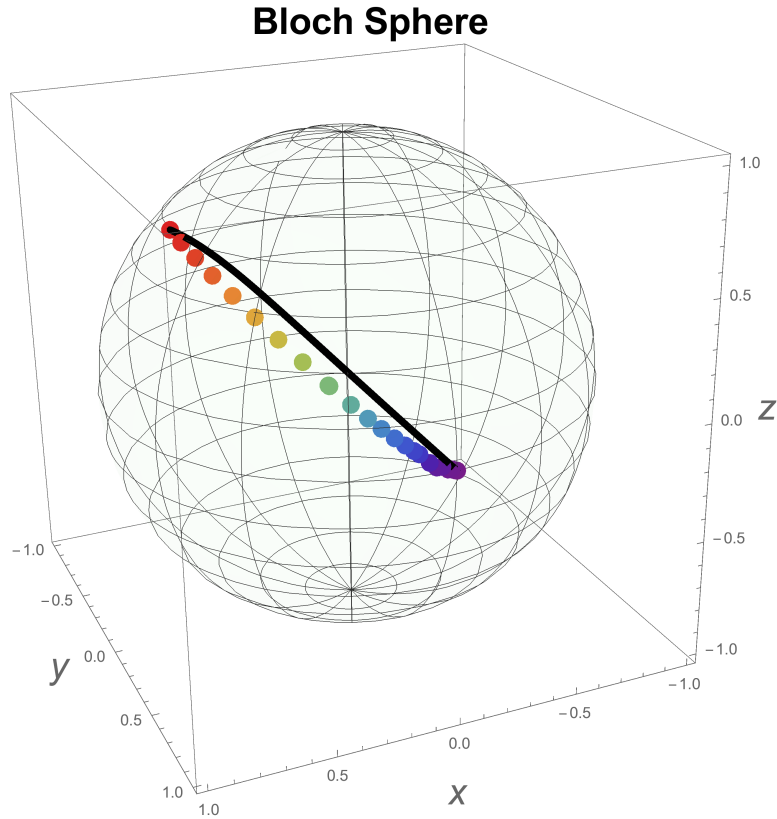


Figure 3.15: This transition is from $|\psi_1\rangle = \cos \frac{\pi}{8} |0\rangle + \sin \frac{\pi}{8} |1\rangle$ to $|\phi_2\rangle = |y_+\rangle$. The red dot is the initial state and the purple is the final state. Here, we have added a new control coefficient n_z in the direction of the z -axis. Also, we have implemented an optimization in the Fidelity equation to get a better time parameter Δt . The black line is the geodesic. For this figure, $N = 28$, $N' = 8$, $ERROR = \times 10^{-5}$, $m = 2$ and we got an infidelity of 8.7×10^{-6} and $T = 1.36$

3.5 Analysis and comparison with other models

At first, our methodology of state to state transition for mixed and pure states based on geometrical equations of the density matrices manifold in general gives trajectories that follows the geodesic between the two states. For the case of pure states, we have found that the chosen Hamiltonians, the one that depends on sin and cos functions and the one with n_x , n_y unknown constants, follow the geodesic almost in every experiment. Even in the worst scenario like Fig. 3.2, where we proved that with small Δt and more steps we can get

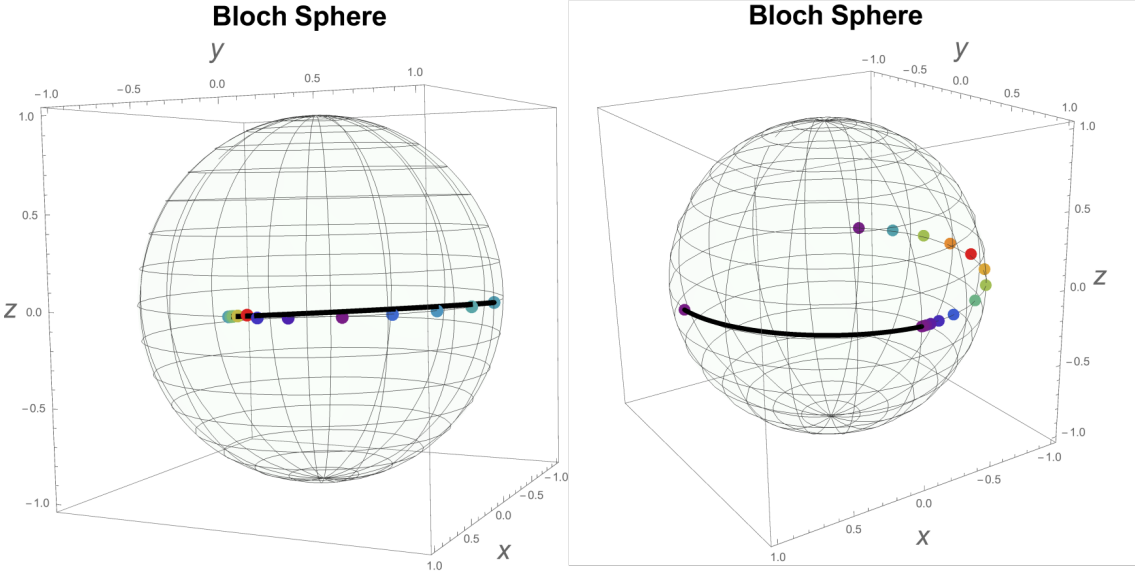


Figure 3.16: Left: Transition from $|y_+\rangle$ to $|x_+\rangle$. The dark green dot on the right is the initial state and the light green is the final state. Right: Transition from $|x_+\rangle$ to $|y_+\rangle$. The purple dot on the left is the initial state and the final state is in the cluster of purple dots. The Black line is the geodesic between the initial and final states. These figures show that our algorithm follows a counterclockwise rotation with (3.7) and does not follow the geodesic, which is the black line, in the case of figure on the right.

the final state as we can see in Fig. 3.6. Also for pure states using both Hamiltonians, we got the same results for the infidelity given by the equation $1 - F(\rho_1, \sigma_2)$ and with value 0.01. We have to say that an infidelity of our value is not in the range of models presented before like CRAB, GRAPE and Krotov where one can find values of infidelity in the order of 10^{-5} and 10^{-6} .

To solve the issue of high value of infidelity in our methodology, we have came up with a “hybrid model” that joins the optimization of $\cos \alpha$ which gives the “direction” of where the final state is located and the optimization of $F(|\psi_1\rangle, |\phi_2\rangle)$ which gives the evolution in time to arrive at the final state. Keeping this hybrid model in mind, we can show that the performance of our model is better against CRAB and GRAPE algorithms when one needs few steps to arrive to the final state. The term “few” is 10- 30 steps to arrive to the

final state. To show this, we set the following experiment.

At first, one needs to know that CRAB and GRAPE receive the following data: the initial and final states $|\phi_1\rangle$ and $|\phi_2\rangle$ respectively, the total time of the evolution T , the number of time slots given by N (which gives the number of points on the Bloch sphere and also gives $\Delta t = T/N$), the Hamiltonian of the system H_0 , the control Hamiltonian H_c and the error in the infidelity. With this, we have planned the following: we set the initial state given by the North pole, $|0\rangle$ and the final state $|y-\rangle$, $T = 0.6$, $N = 22$, $H_0 = -\frac{w_0}{2}\sigma_z$, $H_c = \frac{n_x}{2}\sigma_x + \frac{n_y}{2}\sigma_y + \frac{n_z}{2}\sigma_z$ with n_x, n_y, n_z unknown real variables and the infidelity 10^{-5} . One can see the results using CRAB in Fig. 3.17, using GRAPE in Fig. 3.18 and using our model Fig. 3.19.

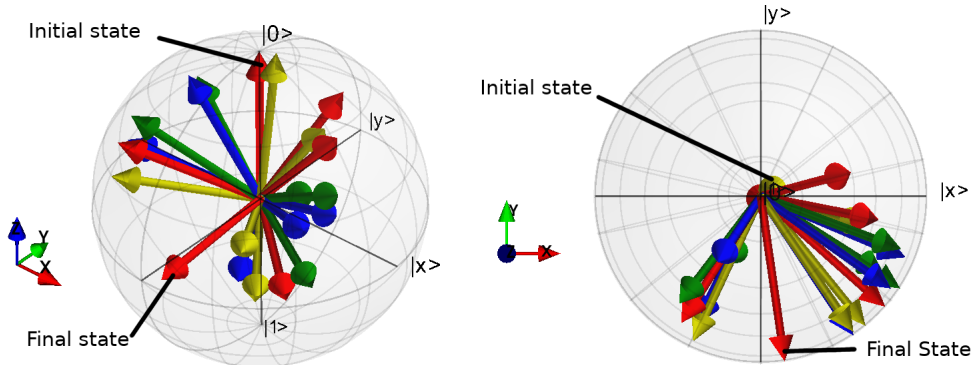


Figure 3.17: Transition from $|\psi_1\rangle = |0\rangle$ to $|\phi_2\rangle = |y-\rangle$ using CRAB algorithm with 22 steps. In both figures, the vectors represent the evolution of the initial state after the optimization. The left figure is a plot in 3d meanwhile the right figure is a projection in the $x - y$ plane. On the right, we see that the red vector called final state is the best approximation of CRAB. For this figures we used: $H_0 = -\frac{w_0}{2}$, $H_c = n_x/2\sigma_x + n_y/2\sigma_y + n_z/2\sigma_z$, $w_0 = 5$, $N = 22$, $T = 0.6$, $fid_err_targ = 10^{-5}$, $amp_lbound = -w_0$, $amp_ubound = w_0$. The infidelity for this experiment using CRAB is 7.84×10^{-6} .

The infidelity of CRAB for this transition is 7.84×10^{-6} and for the GRAPE is 3.47×10^{-7} , meanwhile our hybrid model gives 3.05×10^{-8} . For this specific transition where we fix the amount of steps in the transition, our algorithm outperforms CRAB and GRAPE.

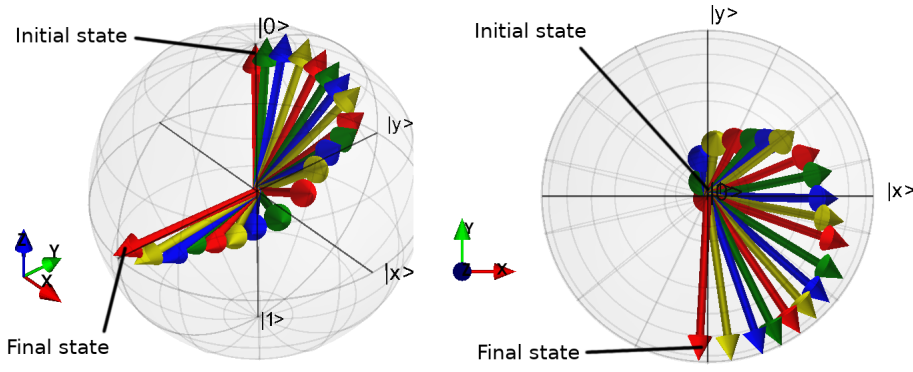


Figure 3.18: Transition from $|\psi_1\rangle = |0\rangle$ to $|\phi_2\rangle = |y_-\rangle$ using GRAPE algorithm with 22 steps. In both figures, the vectors represent the evolution of the initial state after the optimization. The left figure is a plot in 3d meanwhile the right figure is a projection in the $x - y$ plane. On the right, we see that the red vector called final state is the best approximation of GRAPE. For this figures we used: $H_0 = \frac{-w_0}{2}\sigma_z$, $H_c = n_x/2\sigma_x + n_y/2\sigma_y + n_z/2\sigma_z$, $w_0 = 5$, $N = 22$, $T = 0.6$, $fid_err_targ = 10^{-5}$, $amp_lbound = -w_0$, $amp_ubound = w_0$. The infidelity for this experiment using GRAPE is 3.47×10^{-7} .

Thus, this result is very promising⁸ because with simple optimization functions inside a simple algorithm we are capable of getting infidelity values which are in range of powerful and well established models in the quantum control community which are CRAB, GRAPE and Krotov. Also, one can see on the Bloch sphere that our model reach to the final state in a better way than GRAPE and CRAB. We have to admit that Krotov model is better in every simulation even with a small amount of values of steps.

In particular comparing with GRAPE algorithm, the initial state of our methodology advance always forward in time, it is sequential, and we do not need to give initial “guess” values for control fields parameters. In GRAPE algorithm, the evolution in every step is forward and backward propagated in order to find and update the control coefficients. This can be seen in equations (1.34) and in (1.35). Also, if one wants to program the GRAPE

⁸However, applying these improvements in our algorithm with mixed states we did not get better results. We are not sure the source for this issue, however we think that we need to add the term that generates the geometric phases in the Hamiltonian.

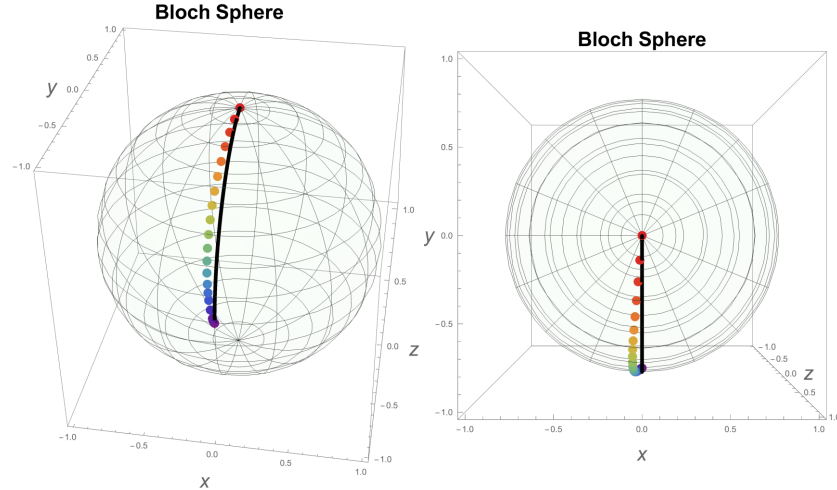


Figure 3.19: Transition from $|\psi_1\rangle = |0\rangle$ to $|\phi_2\rangle = |y_-\rangle$ using the Hybrid algorithm with 22 steps. In both figures, the dots represent the evolution of the initial state given by our methodology. The left figure is a plot in 3d meanwhile the right figure is a projection in the $x - y$ plane. The black line is the trajectory of the geodesic. For this figure, $H_0 = -\frac{1}{2}w_0\sigma_z$, $H_c = \frac{n_x}{2}\sigma_x + \frac{n_y}{2}\sigma_y + \frac{n_z}{2}\sigma_z$, $N = 22$, $N' = 3$, $ERROR = \times 10^{-5}$, $m = 2$ and $T = 0.6$. With this data, we got an infidelity of 3.05×10^{-8} .

algorithm by oneself, at first the algorithm is not a laborious task; however giving the initial “guess” values of the control coefficients, as we did it in (1.38), is not straightforward⁹. Even more, if one does not have an educated decision for the guess initial parameters, the algorithm does not converge. These issues in GRAPE algorithm make our methodology a better choice.

3.6 Future activities

In the future, we want to address some important facts that the other models have and the misbehavior of our algorithm in the case of mixed states in order to have a better

⁹One does not have this issue with the Qutip package. The GRAPE Qutip package is a modification of the GRAPE algorithm presented in the introduction where the initial guess values are random numbers and the algorithm has a monotonic convergence.

transition control algorithm. At first, we need to add interactions with the environment. Second, the possibility to add more qubits or the scaling to a great number of qubits. A third, we need to find an improvement for mixed states in our methodology.

The first can be feasible by the Lindblad master equation which is a generalization of the Liouville-von Neumann equation (Sarandy & Lidar 2005). This master equation uses a set of damping operators which simulate the environment. The second issue is really important to have because entanglement is a key point in every quantum communication protocol, for example.

An idea to fix the issue with mixed states might be by adding the term $(\gamma \times \dot{\gamma})$ in the set of Hamiltonians given by (1.1), which gives the adiabatic phase. This idea came from (Fasihi et al. 2012), where they used the Lewis - Reisenfeld Invariant (LRI) to control mixed states of a two-level quantum system. This method is an improvement in time from adiatic quantum control methods (Sarandy et al. 2011). This suggests that we need to recover the Hamiltonian terms that produces geometrical phases in order to control mixed states.

Chapter 4

Conclusions

Finally, after presented the methodology and some experiments of transferring quantum pure and mixed states, we want to present the conclusions of this work.

- For a single qubit, we have found a set of Hamiltonians H given as a linear combination of Pauli matrices $\{\sigma_x, \sigma_y, \sigma_z\}$ and with unknown real constants $\{n_x, n_y, n_z, \Delta t\}$ that follows the geodesic of the density matrix manifold, in the transitions presented in this work. We found some disagreements in the case for mixed states; however for pure states, our model performed well in transferring these types of states. Even, we ended with an improved idea called “hybrid model” that maximize the objective function given by $\cos \alpha$ in (2.23) and the fidelity function between the initial and final state. At the moment, the constrain that our model has, it is in the control field parameters that in general are bounded by the natural frequency of the system, $-w_0 \leq n_x \leq w_0$, $-w_0 \leq n_y \leq w_0$, $-w_0 \leq n_z \leq w_0$, with w_0 the natural frequency of the system; thus making our model plenty room for developing and improving in the future.
- We have reviewed and simulated well known algorithms in quantum control theory which are CRAB, GRAPE and Krotov. In general terms, all these models maximize

the fidelity function or minimize the infidelity given by

$$I(|\psi_1\rangle, |\phi_2\rangle) = 1 - F(|\psi_1\rangle, |\phi_2\rangle), \quad (4.1)$$

where $|\psi_1\rangle$ and $|\phi_2\rangle$ are the initial and final pure states and F is the fidelity given by $F(|\psi_1\rangle, |\phi_2\rangle) = \sqrt{|\langle\psi_1|\phi_2\rangle|}$. We presented Python simulations of these models and we found a scenario where our model outperforms these models. We got an infidelity in the order of 10^{-8} which is superior against CRAB and GRAPE for the same number of steps in the time evolution. The scenario that we got this result was in the transition from the initial state, the North pole $|0\rangle$ to the final state given by $|y_-\rangle$ using $H_0 = -\frac{1}{2}w_0\sigma_z$ as the system Hamiltonian, $H_c = \frac{n_x}{2}\sigma_x + \frac{n_y}{2}\sigma_y + \frac{n_z}{2}\sigma_z$ as the control Hamiltonian with n_x, n_y, n_z real variables and a total time evolution of $T = 0.6$, $N = 22$ the number of time slots.

- In this work, we have reviewed and used concepts of geometry of the set of density matrices. For instance, the geodesic of density matrices is a key point in this work and it comes from purifications of density matrices. Geometrically, purifications are principal fiber bundles over the set of density matrices. In the case of pure states, we have changed the geodesic equation such that it is well defined for not invertible matrices. Also, we have used the tensor metric given by the Bures distance, which generalize Fubiny-Study distance for pure states, defined between two density matrices. This tensor metric helps us to define the direction, given by $\{n_x, n_y, n_z\}$ in H_c , of where the final state is located.
- There are some challenges that we need to address in order to have a complete state to state transition algorithm. One issue is the interaction between the environment. Another is the scaling to a bunch of qubits. Finally, we have found that our methodology does not follow adequately the geodesic in the case for mixed states. We have an insight given by (Fashihi et al. 2012) that we need to add the term $(\gamma \times \dot{\gamma})$ in (1.1) in order to improve our methodology. However this final fact, can be an starting point for a future research.

Bibliography

Abraham H., et al., 2019, Qiskit: An Open-source Framework for Quantum Computing, doi:10.5281/zenodo.2562110

Aguiar Pinto A., Moutinho M., Thomaz M., 2009, Brazilian Journal of Physics, 39, 326

Andersson O., 2018, PhD thesis, Stockholm University

Bohm A., Mostafazadeh A., Koizumi H., Niu Q., Zwanziger J., 2003, The Geometric Phase in Quantum Systems, 1 edn. Theoretical and Mathematical Physics, Springer-Verlag Berlin Heidelberg, doi:10.1007/978-3-662-10333-3

Brif C., Chakrabarti R., Rabitz H., 2010, New Journal of Physics, 12, 075008

Caneva T., Calarco T., Montangero S., 2011, Phys. Rev. A, 84, 022326

Cong S., 2014, Control of Quantum Systems: Theory and Methods

Ericsson , 2005, Journal of Physics A: Mathematical and General, 38, L725–L730

Ericsson Å., 2007, PhD thesis, Stockholm University, Department of Physics

Fasihi M.-A., Wan Y., Nakahara M., 2012, Journal of the Physical Society of Japan, 81, 024007

Goerz M., Basilewitsch D., Gago-Encinas F., Krauss M. G., Horn K. P., Reich D. M., Koch C., 2019, SciPost Physics, 7

BIBLIOGRAPHY

- Howardf N. Barnum I., 1998, Phd thesis, New Mexico, <http://citeseerx.ist.psu.edu/viewdoc/download?doi=10.1.1.139.2448&rep=rep1&type=pdf>
- Johansson J., Nation P., Nori F., 2013, Computer Physics Communications, 184, 1234
- Jozsa R., 1994, Journal of Modern Optics, 41, 2315
- Khaneja N., Reiss T., Kehlet C., Schulte-Herbrüggen T., Glaser S. J., 2005, Journal of Magnetic Resonance, 172, 296
- Machnes S., Assémat E., Tannor D., Wilhelm F. K., 2018, Phys. Rev. Lett., 120, 150401
- Preskill J., 2020, Quantum Information and Computation. <http://theory.caltech.edu/~preskill/ph219/index.html#lecture>
- Sarandy M. S., Lidar D. A., 2005, Phys. Rev. Lett., 95, 250503
- Sarandy M., Duzzioni E., Serra R., 2011, Physics Letters A, 375, 3343
- Spehner D., 2014, Journal of Mathematical Physics, 55, 075211
- Spehner D., Illuminati F., Orszag M., Roga W., 2017, Geometric measures of quantum correlations with Bures and Hellinger distances ([arXiv:1611.03449](https://arxiv.org/abs/1611.03449))
- Uhlmann A., 1976, Reports on Mathematical Physics, 9, 273
- Wagh A. G., Chand Rakhecha V., 1990, Physics Letters A, 148, 17
- Wagh A. G., Rakhecha V. C., 1993, Phys. Rev. A, 48, R1729
- Wagh A. G., Rakhecha V. C., 2001, Pramana, 56, 305
- Wagh A. G., et al., 1997, Phys. Rev. Lett., 78, 755

Appendix A

Mathematical aid

In this chapter, one can find useful properties and theorems of some basic definitions like positive operators, SVD, polar decomposition, reshaping and vectorization operations. These algebraic tools, as quantum information theorists call them, are basics bricks to manipulate and understand quantum information in a mathematical way.

The notation is the following. $\mathbb{M}_{m,n}$ will be set of $m \times n$ matrices over \mathbb{C} . The set of square matrices is denoted by \mathbb{M}_n .

A.1 Singular Value Decomposition *SVD*

Theorem A.1.1 (Singular Value Decomposition). Let $A \in \mathbb{M}_{m,n}$ with rank $k \leq m$ then there are $U \in \mathbb{M}_m$ and $V \in \mathbb{M}_n$ unitary matrices such that

$$A = U\Sigma V^\dagger, \quad (\text{A.1})$$

where $\Sigma = \{\sigma_{ij}\} \in \mathbb{M}_{m,n}$ such that

$$\sigma_{ij} = 0, \quad \text{for } i \neq j, \quad (\text{A.2})$$

and

$$\sigma_{11} \geq \sigma_{22} \geq \dots \geq \sigma_{kk} \geq \sigma_{k+1,k+1} = \dots = \sigma_{qq} = 0, \quad (\text{A.3})$$

with $q = \min\{m, n\}$.

The numbers $\sigma_{ii} \equiv \sigma_i$ are singular values ¹, the columns of U are eigenvectors of AA^\dagger and the columns of V are eigenvectors of $A^\dagger A$.

A.2 Polar decomposition

Definition A.2.1 (Modulus of a matrix). The modulus of $A \in \mathbb{M}_{m,n}$ is a positive semidefinite matrix $|A| = (A^\dagger A)^{1/2} \in \mathbb{M}_n$.

Theorem A.2.1 (How to get $|A|$). Let $A \in M_{m,n}$ be nonzero, $\text{rank } A = r \geq 1$, and let the Singular Value Decomposition (SVD), $A = U\Sigma V^\dagger$ where $\Sigma_r = \text{diag}(\sigma_1, \dots, \sigma_r)$ are positive singular values of A such that $\sigma_1 \geq \sigma_2 \dots \geq \sigma_r \geq 0$. For any integer $k \geq r$, defines $\Sigma_k = \Sigma_r \oplus 0_{k-r} \in \mathbb{M}_k$. Then

$$|A| = V\Sigma_n V^\dagger \quad \text{and} \quad |A^\dagger| = U\Sigma_n U^\dagger \quad (\text{A.4})$$

Definition A.2.2 (Polar decomposition). Let $A \in \mathbb{M}_{m,n}$ and suppose that $\text{rank } A = r \geq 1$. Let the SVD, $A = V\Sigma W^\dagger$.

1. if $m \geq n$, let $U = V_n W^\dagger$, in which $V = [V_n V']$ and $V_n \in \mathbb{M}_{m,n}$
2. if $m \leq n$, let $U = V W_m^\dagger$, in which $W = [W_m W']$ and $W_m \in \mathbb{M}_{n,m}$
3. if $m = n$, let $U = V W^\dagger$.

then $U \in \mathbb{M}_{m,n}$ has orthonormal column (if $m \geq n$) or orthonormal rows (if $m \leq n$) and

$$A = U|A| = |A^\dagger|U \quad (\text{A.5})$$

Definition A.2.3 (Positive semidefinite square root). If $A \in M_n$ is positive semidefinite, the unique positive semidefinite matrix $A^{1/2}$ such that $(A^{1/2})^2 = A$ is called the positive semidefinite square root of A . If A is positive definite, we define $(A^{1/2})^{-1} = A^{-1/2}$.

¹non-negative square roots of the eigenvalues of AA^\dagger

Theorem A.2.2. let $A \in \mathbb{M}_2$ be a semidefinite positive and nonzero, and let

$$\tau = (TrA + 2\det(A)^{1/2})^{1/2},$$

then $\tau > 0$ and

$$A^{1/2} = \frac{1}{\tau}(A + (\det A)^{1/2}I) \quad (\text{A.6})$$

Appendix B

Physical aid

Here are some reckons that explain more this work.

B.1 Index and relative states

We can construct a *maximally entangled pure state* from a extended quantum system. Let \mathcal{H}_S be the Hilbert space of our system which has an orthonormal basis $|\alpha_k\rangle$ and $\dim\mathcal{H}_S = n$ and \mathcal{H}_E the Hilbert space of our environment with $|\beta_k\rangle$ an orthonormal basis with $\dim\mathcal{H}_E = n$. A maximally entangled pure state will be given by,

$$|\psi^{SE}\rangle = \frac{1}{\sqrt{n}} \sum_k |\alpha_k^S\rangle |\beta_k^E\rangle. \quad (\text{B.1})$$

It is practical to use non-normalized states,

$$|\tilde{\psi}^{SE}\rangle = \sqrt{n} |\psi^{SE}\rangle. \quad (\text{B.2})$$

Using (B.1) or (B.2), we can have a one-to-one correspondence between \mathcal{H}_S and \mathcal{H}_E . For every state $|b^E\rangle$ from the environment there is a unique state $|a^S\rangle$ in the system such that

$$\frac{1}{\sqrt{n}} |a^S\rangle = \langle b^E | \psi^{SE} \rangle \quad (\text{B.3})$$

$$|a^S\rangle = \langle b^E | \tilde{\psi}^{SE} \rangle. \quad (\text{B.4})$$

Definition B.1.1 (Index and Relative states). The state $|b^E\rangle$ is called *index state* in the environment that yields to $|a^S\rangle$ meanwhile the state $|a^S\rangle$ is called *relative state* in the system to $|b^E\rangle$.

Given a general state $|\phi^S\rangle$ of the system, the state $|\phi^{*E}\rangle$ such that $|\psi^S\rangle$ is the relative state to $|\phi^{*E}\rangle$ is called the index state of $|\phi^S\rangle$. The procedure to find $|\phi^{*E}\rangle$ from $|\phi^S\rangle$ will be, if we have

$$|\phi^S\rangle = \sum_k a_k |\alpha_k^S\rangle, \quad (\text{B.5})$$

then

$$|\phi^{*E}\rangle = \sum_k a_k^* |\beta_k^E\rangle. \quad (\text{B.6})$$

Actually,

$$\begin{aligned} \langle \phi^{*E} | \tilde{\psi}^{SE} \rangle &= \sum_{kl} a_k \langle \beta_k^E | \beta_l^E \rangle |\alpha_l^S\rangle \\ &= \sum_k a_k |\alpha_k^S\rangle \\ &= |\phi^S\rangle \end{aligned} \quad (\text{B.7})$$

B.2 Where does the geodesic of Quantum states come from ?

In our problem or let us say in our story, one of our main characters is the geodesic equation of quantum states. One must show where (1.76) comes from or at least a glance of the origin of this equation for the sake of the reader. For this, we are going to follow (Howardf N. Barnum 1998)

Let begin with $|\phi_1\rangle \in \mathcal{H}_A \otimes \mathcal{H}_B$ and $|\phi_2\rangle \in \mathcal{H}_A \otimes \mathcal{H}_B$, two pure states and λ_i and $\{|e_i^1\rangle\}$ are eigenvalues and eigenvectors of $Tr_B(|\phi_1\rangle\langle\phi_1|)$ and μ_i and $\{|e_i^2\rangle\}$ are eigenvalues and eigenvectors for $Tr_B(|\phi_2\rangle\langle\phi_2|)$, we will explain explicitly and better where all these eigenvalues and vectors come from.

Recall the Schmidt decomposition theorem (1.6.1), which states that any pure state, $|\phi_1\rangle$, of a bipartite systems admits the following decomposition,

$$|\phi_1\rangle = \sum_i \sqrt{\lambda_i} |e_i^1\rangle \otimes |f_i^1\rangle, \quad (\text{B.8})$$

where $\{|f_i^1\rangle\}$ is an orthonormal family (eigenvectors of $\rho_{1,B} = Tr_A |\phi_1\rangle\langle\phi_1|$) and λ_i are the eigenvalues of $\rho_{1,A} = \rho_1 = Tr_B |\phi_1\rangle\langle\phi_1|$. Thus, we have a similar result for $|\phi_2\rangle$ with $\rho_{2,A} = \rho_2 = Tr_B |\phi_2\rangle\langle\phi_2|$

$$|\phi_2\rangle = \sum_i \sqrt{\mu_i} |e_i^2\rangle \otimes |f_i^2\rangle. \quad (\text{B.9})$$

- Let define, V a unitary operator such that

$$\begin{aligned} V : \quad & \mathcal{H}_A \longrightarrow \mathcal{H}_A \\ & |e_i^1\rangle \longmapsto |e_i^2\rangle = V |e_i^1\rangle, \end{aligned} \quad (\text{B.10})$$

V changes basis in the space \mathcal{H}_A .

- Similar we can have, U_1 a unitary operator such that

$$\begin{aligned} U_1 : \quad & \mathcal{H}_A \longrightarrow \mathcal{H}_B \\ & |e_i^1\rangle \longmapsto |f_i^1\rangle = U_1 |e_i^1\rangle, \end{aligned} \quad (\text{B.11})$$

changes basis from \mathcal{H}_A to \mathcal{H}_B . U_1 is well defined according to (B.1), if we have a pure maximally state (which is $|\phi_1\rangle$ and also $|\phi_2\rangle$), there is one-to-one correspondence between states in \mathcal{H}_A and \mathcal{H}_B through the pure state.

- Finally,

$$\begin{aligned} U_2 : \quad & \mathcal{H}_B \longrightarrow \mathcal{H}_B \\ & |f_i^1\rangle \longmapsto |f_i^2\rangle = U_2 |f_i^1\rangle, \end{aligned} \quad (\text{B.12})$$

U_2 changes basis in \mathcal{H}_B .

- Then we can get,

$$|f_i^2\rangle = U_2 U_1 |e_i^1\rangle \quad (\text{B.13})$$

Also, we need a lemma

Lemma B.2.1 (Transpose Lemma (Jozsa 1994)). Let $\{|e_i\rangle\}, i = 1, \dots, n$, be an orthogonal basis of \mathcal{H} and let $|\psi\rangle \in \mathcal{H} \otimes \mathcal{H}$ be a vector,

$$|\psi\rangle = \sum_i |e_i\rangle \otimes |e_i\rangle, \quad (\text{B.14})$$

then for any operator A on \mathcal{H} ,

$$\begin{aligned} (A \otimes I) |\psi\rangle &= (I \otimes A^T) |\psi\rangle && , \text{ or} \\ \sum_i A |e_i\rangle \otimes |e_i\rangle &= \sum_i |e_i\rangle \otimes A^T |e_i\rangle. \end{aligned} \quad (\text{B.15})$$

The proof is quit easy. Remember that any vector is given by

$$|e_j\rangle = A |e_i\rangle = \sum_j a_{ji} |e_i\rangle \text{ with } a_{ji} = \langle e_j | A | e_i \rangle. \quad (\text{B.16})$$

Thus,

$$\begin{aligned} (A \otimes I) |\psi\rangle &= (A \otimes I) \sum_i |e_i\rangle \otimes |e_i\rangle \\ &= \sum_i \sum_k a_{ik} |e_k\rangle \otimes |e_i\rangle \\ &= \sum_{i,k} |e_k\rangle \otimes a_{ik} |e_i\rangle \\ &= \sum_k |e_k\rangle \otimes \sum_i a_{ki}^T |e_i\rangle \\ &= (I \otimes A^T) \sum_k |e_k\rangle \otimes |e_k\rangle \\ &= (I \otimes A^T) |\psi\rangle, \end{aligned} \quad (\text{B.17})$$

which is the end of the proof.

Using the above equations, the Transpose Lemma and $|\phi_1\rangle$,

$$\begin{aligned}
 |\phi_1\rangle &= \sum_i \sqrt{\lambda_i} |e_i^1\rangle \otimes |e_i^1\rangle \\
 &= \sqrt{\rho_1} \otimes U_1 |\psi\rangle \\
 &= (\sqrt{\rho_1} \otimes I)(U_1^T \otimes I) |\psi\rangle, \text{ by the Transpose Lemma,} \\
 |\phi_1\rangle &= \sum_i \sqrt{\rho_1} U_1^T |e_i^1\rangle \otimes |e_i^1\rangle
 \end{aligned} \tag{B.18}$$

also we used the fact that

$$\sqrt{\rho_1} = \sqrt{\text{Tr } |\phi_1\rangle \langle \phi_1|} = \sqrt{\sum_i \lambda_i |e_i^1\rangle \langle e_i^1|} = \sum_i \sqrt{\lambda_i} |e_i^1\rangle \langle e_i^1|. \tag{B.19}$$

The same with $|\phi_2\rangle$,

$$\begin{aligned}
 |\phi_2\rangle &= \sum_j \sqrt{\mu_j} V |e_j^1\rangle \otimes U_2 U_1 |e_j^1\rangle \\
 &= \sqrt{\rho_2} V \otimes U_2 U_1 |\psi\rangle \\
 &= \sqrt{\rho_2} V U_1^T U_2^T \otimes I |\psi\rangle \\
 &= \sum_j \sqrt{\rho_2} V U_1^T U_2^T |e_j^1\rangle \otimes |e_j^1\rangle
 \end{aligned} \tag{B.20}$$

Thus, we get

$$\begin{aligned}
 |\phi_1\rangle &= \sum_i \sqrt{\rho_1} U_1^T |e_i^1\rangle \otimes |e_i^1\rangle \\
 |\phi_2\rangle &= \sum_j \sqrt{\rho_2} V U_1^T U_2^T |e_j^1\rangle \otimes |e_j^1\rangle.
 \end{aligned} \tag{B.21}$$

The inner product of these two states,

$$\begin{aligned}
 \langle \phi_1 | \phi_2 \rangle &= \sum_{i,j} \langle e_i^1 | (U_1^T)^\dagger \sqrt{\rho_1} \sqrt{\rho_2} V U_1^T U_2^T | e_j^1 \rangle \langle e_i^1 | e_j^1 \rangle ; \text{ with } \langle e_i^1 | e_j^1 \rangle = \delta_{ij} \\
 &= \text{Tr} \left((U_1^T)^\dagger \sqrt{\rho_1} \sqrt{\rho_2} V U_1^T U_2^T \right) \\
 &= \text{Tr} \left(\sqrt{\rho_1} \sqrt{\rho_2} V U_1^T U_2^T (U_1^T)^\dagger \right)
 \end{aligned} \tag{B.22}$$

Taking the maximum of the absolute value,

$$\max_{|\phi_2\rangle} |\langle \phi_1 | \phi_2 \rangle| = \max_U |\text{Tr}(\sqrt{\rho_1} \sqrt{\rho_2} V U)|; \text{ with } U = V U_1^T U_2^T (U_1^T)^\dagger, \tag{B.23}$$

where the left maximum is taking over all state $|\phi_2\rangle$ such that $\rho_2 = Tr_B(|\phi_2\rangle\langle\phi_2|)$ and the right maximum is taken over U all unitary operators.

Now, we can use the following lemma,

Lemma B.2.2. If A is any operator, $u = \max_U |TrAU|$ (the maximum is taken over all unitary operators U) is reached when AU is positive and then $u = Tr|A|$.

Proof:

The proof could begin assuming that A is invertible and with polar decomposition $A = |A|U_0$. Then, we need to maximize $|Tr|A|V|$ over all unitary operators V . In the eigen basis of $|A|$ where $|A| = diag(\lambda_1, \dots, \lambda_n)$ with $\lambda_i \geq 0$, one has $|Tr|A|V| = |\sum_i \lambda_i V_{ii}|$. We know that V is unitary and for every i is true that $|V_{ii}| \leq 1$. Then the maximum is reached when $V = I$ and we have $|Tr|A|| = Tr|A|$, because $|A|$ is positive. If A is not invertible, we have to follow the same procedure in the orthogonal complement of the eigenvalue zero space.

Thus, the maximum is reached when

$$\sqrt{\rho_1}\sqrt{\rho_2}U = |\sqrt{\rho_2}\sqrt{\rho_1}| \iff U = \rho_2^{-1/2}\rho_1^{-1/2}|\sqrt{\rho_2}\sqrt{\rho_1}|, \quad (\text{B.24})$$

here we have used the polar decomposition $|A| = \sqrt{AA^\dagger}$ taken from (Howardf N. Barnum 1998) which is different from ours which is $|A^\dagger| = \sqrt{A^\dagger A}$ but at the end both polar decomposition give the same geodesic equation.

The correspond state $|\phi_2\rangle$ is, in view of (B.21),

$$\begin{aligned} |\phi_2^{opt}\rangle &= \sum_i \sqrt{\rho_2}VU_1^T U_2^T |e_i^1\rangle \otimes |e_i^1\rangle \\ &= \sum_i \rho_1^{-1/2}|\sqrt{\rho_2}\sqrt{\rho_1}|U_1^T |e_i^1\rangle \otimes |e_i^1\rangle \end{aligned} \quad (\text{B.25})$$

We are almost there, we can get the geodesic equation by the equation of the trigonometric circle on the hypersphere

$$|\phi_\tau\rangle = (\cos \tau - \frac{\sin \tau}{\tan \theta}) |\phi_1\rangle + \frac{\sin \tau}{\sin \theta} |\phi_2\rangle \quad (\text{B.26})$$

with $\tau \in [0, \theta]$ and θ is the Hilbert space distance between the two pure states. Finally, the geodesic equation is

$$\gamma(t) = \text{Tr}_B |\phi_\tau\rangle\langle\phi_\tau|. \quad (\text{B.27})$$

If we take a closer look to one of the terms in Tr_B ,

$$\begin{aligned} \text{Tr}_B |\phi_1\rangle\langle\phi_2^{opt}| &= \sum_i \sqrt{\rho_1} U_1^T |e_i^1\rangle\langle e_i^1| (U_1^T)^\dagger |\sqrt{\rho_2}\sqrt{\rho_1}| \rho_1^{-1/2} ; U_1^T |e_i^1\rangle\langle e_i^1| (U_1^T)^\dagger = |e_i^2\rangle\langle e_i^2| \\ &= \sqrt{\rho_1} |\sqrt{\rho_2}\sqrt{\rho_1}| \rho_1^{-1/2} ; \sum_i |e_i^2\rangle\langle e_i^2| = I \\ &= \sqrt{\rho_1} (\sqrt{\rho_1}\rho_2\sqrt{\rho_1})^{1/2} \rho_1^{-1/2} ; \text{ using polar decomposition.} \end{aligned} \quad (\text{B.28})$$

Now, we need to prove the following

$$\sqrt{\rho_1} (\sqrt{\rho_1}\rho_2\sqrt{\rho_1})^{1/2} \rho_1^{-1/2} = \rho_2^{-1/2} (\sqrt{\rho_2}\rho_1\sqrt{\rho_2})^{1/2} \rho_2^{1/2}. \quad (\text{B.29})$$

To prove this, we are going to use our definition of polar decomposition, $|A| = \sqrt{A^\dagger A}$,

$$\sqrt{\rho_1}\sqrt{\rho_2} = U |\sqrt{\rho_1}\sqrt{\rho_2}|, \text{ with } U \text{ unitary.} \quad (\text{B.30})$$

Thus,

$$|\sqrt{\rho_2}\sqrt{\rho_1}|^2 = \sqrt{\rho_1}\sqrt{\rho_2} (\sqrt{\rho_1}\sqrt{\rho_2})^\dagger = U |\sqrt{\rho_1}\sqrt{\rho_2}|^2 U^\dagger, \quad (\text{B.31})$$

then

$$|\sqrt{\rho_2}\sqrt{\rho_1}| = U |\sqrt{\rho_1}\sqrt{\rho_2}| U^\dagger. \quad (\text{B.32})$$

Multiplying by $\rho_1^{1/2}$ on the left and by $\rho_1^{-1/2}$ on the right, we get (B.28),

$$\begin{aligned} \rho_1^{1/2} |\sqrt{\rho_2}\sqrt{\rho_1}| \rho_1^{-1/2} &= \rho_1^{1/2} U |\sqrt{\rho_1}\sqrt{\rho_2}| U^\dagger \rho_1^{-1/2} \\ &= \rho_2^{-1/2} \sqrt{\rho_2}\sqrt{\rho_1} U |\sqrt{\rho_1}\sqrt{\rho_2}| U^\dagger \rho_1^{-1/2} \rho_2^{1/2}. \end{aligned} \quad (\text{B.33})$$

Now from (B.30)

$$(\sqrt{\rho_1}\sqrt{\rho_2})^{-1} = (U |\sqrt{\rho_1}\sqrt{\rho_2}|)^{-1}, \quad (\text{B.34})$$

which after applying the inverse and the transpose we get

$$\rho_1^{-1/2} \rho_2^{-1/2} = U |\sqrt{\rho_1}\sqrt{\rho_2}|^{-1}. \quad (\text{B.35})$$

Thus, replacing the last equation in (B.33),

$$\begin{aligned}\rho_1^{1/2}|\sqrt{\rho_2}\sqrt{\rho_1}|\rho_1^{-1/2} &= \rho_2^{-1/2}\sqrt{\rho_2}\sqrt{\rho_1}U|\sqrt{\rho_1}\sqrt{\rho_2}|U^\dagger U|\sqrt{\rho_1}\sqrt{\rho_2}|^{-1}\rho_2^{1/2} \\ &= \rho_2^{-1/2}\sqrt{\rho_2}\sqrt{\rho_1}U\rho_2^{1/2}.\end{aligned}\quad (\text{B.36})$$

Notice that

$$(\sqrt{\rho_1}\sqrt{\rho_2})^\dagger = (U|\sqrt{\rho_1}\sqrt{\rho_2}|)^\dagger, \quad (\text{B.37})$$

which leads us to

$$\sqrt{\rho_2}\sqrt{\rho_1} = |\sqrt{\rho_1}\sqrt{\rho_2}|U^\dagger. \quad (\text{B.38})$$

Hence, replacing in (B.36),

$$\rho_1^{1/2}|\sqrt{\rho_2}\sqrt{\rho_1}|\rho_1^{-1/2} = \rho_2^{-1/2}|\sqrt{\rho_1}\sqrt{\rho_2}|\rho_2^{1/2} = \rho_2^{-1/2}(\sqrt{\rho_2}\rho_1\sqrt{\rho_2})^{1/2}\rho_2^{1/2}, \quad (\text{B.39})$$

which is the awful term of (1.76).